DESIGNING COMBINATION DRUG REGIMENS TO IMPROVE GLIOBLASTOMA CHEMOTHERAPY: A PHARMACOKINETIC PHARMACODYNAMIC MODELING APPROACH

by

Saugat Adhikari

A Dissertation

Submitted to the Faculty of Purdue University

In Partial Fulfillment of the Requirements for the degree of

Doctor of Philosophy

Department of Pharmacy Practice

West Lafayette, Indiana

August 2021

THE PURDUE UNIVERSITY GRADUATE SCHOOL
STATEMENT OF COMMITTEE APPROVAL

Dr. Robert E. Stratford, Co-Chair
Division of Clinical Pharmacology-Indiana University

Dr. Brian R. Overholser, Co-Chair
Department of Pharmacy Practice

Dr. James E. Tisdale
Department of Pharmacy Practice

Dr. Kevin M. Sowinski
Department of Pharmacy Practice

Dr. Karen E. Pollok
Department of Pediatrics-Indiana University

Approved by:
Dr. Alan J. Zillich

Dedicated to my family
For their advice, their patience, and their faith,
Because they always understood.

ACKNOWLEDGMENTS

I would like to express my deep sense of gratitude to my major advisor Dr. Robert E. Stratford for his valuable guidance, suggestions, and continuous support during my PhD. I cannot thank him enough for making me the part of his research group and for his unconditional support towards achieving my professional and personal goals.

I owe a great deal of thanks to the other members of my committee. Dr. Karen Pollok has greatly contributed to my training by being a key collaborator and I would like to thank her for the education she provided me. Dr. Brian Overholser has served as a co-mentor and contributing to my pharmacokinetic training and providing me with all the help relating to the department. I would like to thank Dr. Jim Tisdale for his teachings in clinical pharmacology and for always having a kind word of encouragement. I would like to thank Dr. Kevin Sowinski for his role in my committee and his expertise with pharmacokinetic modeling has been of great assistance to me.

I would also like to thank Dr. Harlan Shannon for educating me on the project. My sincere thanks to the Indiana CTSI for providing me with financial support throughout the tenure of my study. Over these years in Indiana, I have come across many individuals for whom I have great regard. A special thank you to my friends and colleagues who have stood by me in all my efforts for successfully completing this work. My deepest gratitude goes to my family for their unflagging love and support throughout my life. I would like to thank all of you in making this project a worthy endeavor.

TABLE OF CONTENTS

LIST OF TABLES

LIST OF FIGURES

LIST OF ABBREVIATIONS

GBM	Glioblastoma
WHO	World Health Organization
IR	Irradiation
BBB	Blood-brain-barrier
SOC	Standard of Care
TMZ	Temozolomide
SMIs	Small Molecule Inhibitors
MDM2	Murine double minute 2
AKT	pro-survival protein kinase B
PI3K	phosphoinositide 3-kinase
CDK4/6	cyclin D1-Rb-p16/ink4a
PKPD	Pharmacokinetic Pharmacodynamic
TSC	Tumor Static Concentration
ACB	Abemaciclib
LOQ	Loss on Quantification
MS/MS	Tandem Mass Spectroscopy
PDX	Patient Derived Xenografts
K_a	Absorption rate constant
K_e	Elimination rate constant
F	Bioavailability
V	Volume of distribution
CL	Clearance
C	Concentration
Kap.o.	oral absorption
Kai.p.	intraperitoneal absorption
Fp.o.	oral bioavailability
Fi.p.	intraperitoneal biovailability
NSG	NOD.Cg-*Prkdc*^{scid} *Il2rg*^{tm1Wjl}/SzJ
U87	Uppsala 87 malignant Glioma
GBM 10	Glioblastoma10 cells

GBM 43	Glioblastoma 43 cells
GDC0068	Ipatasertib
RG7388	Idasanutlin
AIC	Akaike information criterion
CWRES	Conditional Weighted Residual
BSV	Between Subject Variability
p.o.	oral dose
VPCs	Visual Predictive Checks
pcVPCs	Prediction corrected Visual Predictive Checks
RSE	Relative Standard Error
TGI	Tumor Growth Inhibition
MTD	Maximum Tolerated Dose
DMSO	Di-methyl Sulfoxide
$kg_{, exp}$	Exponential tumor growth rate, temozolomide sensitive cells
$kg_{,lin}$	Linear tumor growth rate, temozolomide sensitive cells
kk	kinetics of cell death/kill rate/ transit rate
$kgR_{,exp}$	exponential tumor growth rate, temozolomide resistant cells
kgR, l_{in}	Linear tumor growth rate, temozolomide resistant cells
$k_{s\text{-}to\text{-}r}$	Conversion rate, temozolmide sensitive to resistant
V0	Initial tumor volume
b_{TMZ}	Temozolomide potency term
b_{RG7388}	Idasnutlin potenty term
b_{RG7112}	Rg7112 potency term
$b_{GDC0068}$	Ipatasertib potency term
PK	Pharmacokinetic
PD	Pharmacodynamic

ABSTRACT

Despite advancements in therapies, such as surgery, irradiation (IR) and chemotherapy, outcome for patients suffering from glioblastoma (GBM) remains fatal; the median survival time is only about 15 months. Even with novel therapeutic targets, networks and signaling pathways being discovered, monotherapy with such agents targeting such pathways has been disappointing in clinical trials. Poor prognosis for GBM can be attributed to several factors, including failure of drugs to cross the blood-brain-barrier (BBB), tumor heterogeneity, invasiveness, and angiogenesis. Development of tumor resistance, particularly to temozolomide (TMZ) and IR, creates a substantial clinical challenge.

The primary focus of the work described herein was to develop a modeling and simulation approach that could be applied to rationally develop novel combination therapies and dose regimens that mitigate resistance development. Specifically, TMZ was combined with small molecule inhibitors that are either currently in clinical trials or are approved drugs for other cancer types, and which target the disease at various resistance signaling pathways that are induced in response to TMZ monotherapy. To accomplish this objective, an integrated PKPD modeling approach was used. A PK model for each drug was first defined. PK models were subsequently linked to a PD model description of tumor growth dynamics in the presence of a single drug or combinations of drugs. A key outcome of these combined PKPD models was tumor static concentration (TSC) [1] curves of TMZ in combination with small molecule inhibitors that identify combination drug exposures predicted to arrest tumor growth. This approach was applied to TMZ in combination with abemaciclib (a dual CDK4/6 small molecule inhibitor) based on data from a published study [2] evaluating abemaciclib (ACB) efficacy in combination with TMZ in a U87 GBM xenograft model. TSC was also constructed for TMZ in combination with RG7388 (MDM2 inhibitor) based on the data from an in-vivo study that evaluated effects on tumor growth suppression of these small molecule inhibitors in combination with TMZ in GBM 10 patient derived xenografts.

In GBM 43 mouse xenografts, emergence of resistance to TMZ treatment was identified. Thus, a resistance integrated PKPD model was developed to predict tumor growth kinetics after treatment with TMZ in GBM 43 tumors. Population PK models in immune deficient NOD.Cg-

Prkdc^{scid} *Il2rg*^{tm1Wjl}/SzJ (NSG) mice for TMZ and small molecule inhibitors (GDC0068/RG7112) were developed based on a combination of data obtained from an in-vivo study and published sources. Subsequently, PK models were linked to tumor volume data obtained from GBM 43 subcutaneous xenografts. Model parameters quantifying tumor volume dynamics were precisely estimated (coefficient of variation < 40%) compared to a base tumor growth inhibition model in GBM 43 that did not incorporate resistance development. Graphical diagnostics of the resistance incorporated PKPD tumor growth inhibition model demonstrated a superior fit compared to the base model, and accurately captured the emergence of resistance to the TMZ monotherapy treatment observed in the GBM 43 patient derived xenograft model.

CHAPTER 1. INTRODUCTION

1.1 The Disease and the unmet need

Glioblastoma (GBM) is the most aggressive primary malignant brain tumor, classified as most malignant tumors (Grade IV) by the World Health Organization (WHO) [3], with an average age-adjusted incidence rate of 32 people per 1,000,000 [4]. Statistical reports published by the central brain tumor registry of United States between 2013 to 2017 reported that the GBM accounts for the 48.6% of the distribution of malignant primary brain and other CNS tumor by histology and 57.7% of the distribution of primary brain and other CNS gliomas by histology [5].

Despite advancements in therapies, such as surgery, irradiation (IR) and chemotherapy, outcome for patients suffering from GBM remains fatal. The poor prognosis and significant challenge for GBM can be attributed to the infiltrative nature of the tumor, failure of drugs to cross the blood-brain-barrier (BBB), tumor heterogeneity, invasive properties and angiogenesis, all of which contribute to tumor resistance development to standard of care (SOC) chemotherapy with TMZ [3, 6]. Indeed, surgical resection of the tumor to the maximal physical extent, followed by radiation and chemotherapy with TMZ is the current SOC for primary and recurrent GBM [7]. Despite novel therapeutic targets, networks and signaling pathways being discovered, monotherapy in general has failed in oncology clinical trials [8]. The combination of radiotherapy with adjunctive monotherapy with TMZ has increased the survival rate of patients with GBM, however the median survival time is only about 14.6 months [9].

1.2 Current therapeutic options and their impact

Surgery and radiation therapy in absence of TMZ shows median overall survival of 10 to 12 months in patients suffering from GBM, plus concomitant administration of standard of care therapy TMZ extends the overall survival by an additional three months only [10] . In 2017, the Food and Drug Administration approved the use of bevacizumab in addition to current line of therapy for newly diagnosed GBM, however therapeutic outcome still remains poor with median overall survival up to 18 months only [11] . The standard course of recurrent GBM therapy with TMZ consists of several 28-day cycles, each cycle that consists of administration of the maximum tolerated dose of 150 – 200 mg/m^2 administered only on the first five days to limit dose-limiting

toxicity. Several alternate regimens have been investigated for their potential to improve efficacy and/or reduce toxic side effects. These consist of low dose daily administration with no dose breaks (metronomic therapy, 25 – 50 mg/m^2), 7 days on/7 days off at 100 – 150 mg/m^2/day, and 21 days on/7 days off at 75 – 100 mg/m_2/day [12]. None of these alternate approaches has improved progression free survival and overall survival relative to the standard regimen [12]. No therapeutic benefits were detected from the dense TMZ dosing regimen of 75-100 mg/m2 days 1 to 21 every 28 days for 12 cycle maximum compared to conventional TMZ dosing regimen of 150-200 mg/m2 days 1 to 5 every 28 days for 12 cycle maximum indicating prolonged exposure to TMZ did not improve patient outcomes as measured by survival rate [13].

1.3 The standard of care drug: Temozolomide

1.3.1 Temozolomide metabolism and DNA damage

TMZ is a DNA alkylator and a second generation imidazotetrazine that readily crosses the BBB [6]. Median half-life in humans is 1.8 hours. TMZ is stable at acidic pH (<5) and labile at pH (>7) [14]. TMZ is a prodrug at physiologic pH of blood (ca. 7.4), undergoing spontaneous hydrolysis to reactive compound, 5-(3-methyltriazen-1-yl)-imidazole-4-carboxamide (MTIC). MTIC further liberates AIC and the active form methyl diazonium ion. This electrophilic ion transfers the methyl group to the negatively charged DNA creating DNA adducts. The cytotoxicity of TMZ is attributed to alkylation of DNA. Alkylation (methylation) occurs mainly at the N7 positions of guanine, N3 adenine and O6 guanine residues that mediates the cytotoxicity [15] .
The active metabolite, MTIC, has an even shorter half-life (ca. 30 minutes) than TMZ. With such a short half-life, effectively all of a TMZ dose and derived MTIC are eliminated before the next day when administered on a daily basis, which is the case for all of the above regimens. Where these regimens differ is with respect to the extent of DNA methylation from a given dose, which is expected to be dose dependent, and the number of successive days that methylation takes place. Describing the relationship between these differences and the timing of the tumor adaptive response is challenging, given genetic differences in tumors, and the numerous possible TMZ doses and dose durations. Development of tumor resistance, particularly to TMZ monotherapy, creates a substantial clinical challenge [16].

1.3.2 Mechanisms of Temozolomide resistance in GBM

The cytotoxicity of TMZ is primarily mediated through O6 guanine residues. During DNA replication, alkylation of the O6 site mispairs with thymine instead of cytosine, opposite the methyl guanine, and therefore triggers G2-M cell cycle arrest leading to cell death [17]. However, the DNA repair mechanisms counteract the DNA damage caused by TMZ. The most important repair mechanisms impacting the cytotoxicity of TMZ are enzyme methyl guanine-DNA methyl transferase (MGMT), DNA mismatch repair (MMR) and DNA base excision repair (BER). During DNA alkylation, MGMT directly facilitates repair by removing the methyl adduct, restoring guanine [18]. Hence MGMT protects cancer cells from chemotherapeutic agents like TMZ. The loss of function of DNA mismatch repair caused due to the microsatellite DNA instability makes O6 site thymine mispairs go unrecognized [18] and a cell continues to cycle and survive. Methylation at N7 and N3 sites are repaired by BER. DNA lesions generated by these sites are repaired by BER and become resistant to TMZ [18].

1.4 Rationale for combination therapy

Poor understanding of resistance development and tumor adaptive response timing to TMZ continues to lead to investigations of multiple chemotherapeutic agents that target the numerous pro-survival adaptations induced by TMZ. Thus far, their use as monotherapy in recurrent GBM has not been successful [19-23], but promise has been demonstrated upon combining these targeted agents with TMZ [24]. A combination therapy of two or more therapeutic agents has proven to be more effective than radiation and monotherapy, and currently several clinical trials aim to investigate combination drug regimens to exploit the underlying mechanism of oncogenesis and resistance development [6].

Based on the current understanding of therapeutic targets and signaling networks in GBM, it is hypothesized that combination drug regimens will mitigate resistance development by targeting the disease via TMZ-induced signaling pathways with brain penetrant small molecule inhibitors (SMIs), and that this approach will prolong survival time in GBM. One such pathway activated by TMZ therapy is the Murine double minute 2 (MDM2) / tumor protein p53 /p73 signaling pathway, wherein the MDM2 pathway functions as the treatment response modulator of the DNA damage response by regulating p53/p73 activation and DNA repair. Published data indicate sustained

activation of the TMZ induced p53/p73 pathway by MDM2 inhibition [25-27]. Inactivation of the TMZ-induced MDM2/p53/p73 pathway by an MDM2 inhibitor significantly improves efficacy and survival of recurrent GBM [28]. However, tumors adapt to this therapy over time and growth once again progresses. Another pathway that functions as a treatment response modulator and activated by TMZ therapy is the pro-survival protein kinase B (AKT)/phosphoinositide 3-kinase (PI3K)/mTOR signaling pathway. AKT directly phosphorylates MDM2 at Ser166, which leads to increased E3 ubiquitin ligase activity and thus activates MDM2-dependent inhibition of p53 to increase cell survival [9, 29]. Existence of a growth promoting link between MDM2 and AKT networks provides rationale for combination therapy by dual targeting of MDM2 and AKT pathways activated by TMZ [4, 9, 28]. Also, targeting the CDK4/6 cyclin D1-Rb-p16/ink4a pathway using a potent CDK4 and CDK6 kinase inhibitor alone or in combination has potential for treating CNS tumors such as GBM [2]. This strategic targeting of TMZ induced response surface networks is depicted in Figure 1.1. Data show that SOC therapy (TMZ) combined with MDM2, AKT and CDK4/6 kinase inhibitors (RG7388, GDC0068, and ACB, respectively) inhibits GBM cell growth in-vivo and increases survival in a GBM xenograft model [30].

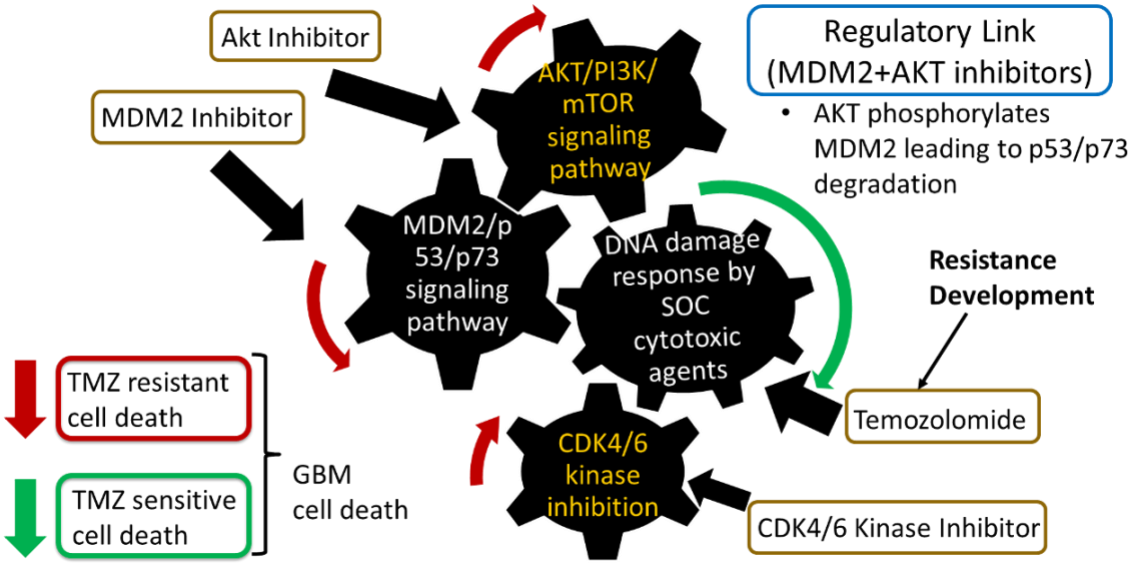

Figure 1.1: Strategic targeting of TMZ induced response surface networks. Induction of treatment response networks by TMZ or radiotherapy provide the rationale to potentiate DNA damage by strategic targeting of TMZ induced response networks using small molecule inhibitors and thus improving therapeutic efficacy

1.4.1 Targeting MDM2 signaling networks in GBM

GBM is a heterogenous tumor with numerous genetic instabilities requiring strategic targeting to achieve anti-tumor activity. MDM2 is one of the emerging targets in cancer [31] that serves as the platform for cell growth and DNA repair [32]. Inhibiting MDM2 has been the major strategy for p53 pathway reactivation. This leads to cell death and reduction in the tumor growth rate. MDM2 inhibitors bind to MDM2 and block its interaction with the protein p53/p73. This leads to the activation of p53/p73-mediated apoptosis [33, 34]. Blockade of MDM2-mediated signaling by an MDM2 inhibitor is one of the strategies for treating wild type p53 GBM cells [35]. PD studies demonstrated that inhibition of cell growth following TMZ/nutlin3a correlated with the activation of the p53 pathway, downregulation of the DNA repair proteins MGMT, persistence of DNA damage and increased apoptosis [36]. Dr. Pollok's lab conducted efficacy studies in an intracranial GBM xenograft model using GBM 10 cells derived from a recurrent wild type p53 GBM that is highly TMZ resistant. Three 5-day cycles of TMZ/nutlin3a resulted in a significant increase in survival of mice compared to single-agent therapy and was well tolerated [37] These data provided strong rationale to investigate additional combination regimens of TMZ with MDM2 inhibitor, with the end goal being to maximize therapeutic efficacy in GBM. Based on our extensive research, there is the strong rationale to explore targeting MDM2 in combination with a variety of signaling pathways in clinically relevant *in vivo* models of cancer [38-40].

1.4.2 Targeting AKT signaling networks in GBM

Activation of the PI3Kinase/AKT/mTOR pathway following DNA damage is a hallmark pro-survival mechanism for a variety of cancers, including GBM [41]. Some of the mechanisms that can lead to AKT activation are genetic alterations (loss of tumor suppressor PTEN) [42] and mutational PI3K activation [43]. Additionally, multiple growth factor receptors are coupled to the PI3Kinase/AKT/mTOR pathway and hyper activation of AKT occurs in ~70% of GBM tumors [44, 45]. AKT activation is related to resistance development with targeted and chemotherapeutic agents [46]. This makes AKT inhibitors a strategic target for GBM therapy. Dr. Pollok's lab [36] and others [47, 48] showed that TMZ and IR can increase AKT activity in wtp53 and mtp53 GBM cells. These data provide strong rationale to study additional combination regimens of TMZ and inhibitors of PI3K/AKT/mTOR.

1.5 Blood Brain Barrier, Blood Tumor Barrier and Rationale for SMIs selection

The blood brain barrier (BBB) is comprised of endothelial cells with distinct tight junctions and efflux transporters, and plays a critical role in controlling the exchange of molecules between the vasculature, neuroparenchyma and cerebrospinal fluid spaces [49]. Paracellular and transcellular routes, composed of tight junctions of endothelial cells, prevents passage of drug molecules from entering the brain [49]. The primary barrier site is comprised of cerebral capillary endothelial cells by tight junction formation [49]. Disruption of the BBB results in brain metastases and formation of the Blood Tumor Barrier (BTB). BTB is heterogeneously permeable; however, like the BBB, it prevents uptake and absorption of drugs into the neuroparenchyma [50]. Barrier function for both BBB and BTB results from the combination of physical tight junctions, transport mechanism mediating solute efflux and metabolic barrier, all hindering the permeability and uptake of drug molecule to the target site (tumors) in brain.

The SMIs investigated in this proposal have been studied as single agents in clinical trials. There is little known about the effects of drug combinations and the optimal dose combinations and sequencing of combinations, as well as the total doses of combinations needed to achieve optimal efficacy and safety *in vivo*. RG7112 is a 1st generation MDM2 inhibitor, RG7388 (Idasanutlin) is a 2nd generation, nutlin-class, selective MDM2 antagonist [51], GDC0068 (Ipatasertib) is a pan-AKT inhibitor with acceptable enzyme potency and a high degree of kinase selectivity [52], and ACB is a small molecule inhibitor of CDK4 and CDK6 notably showing greater selectivity for CDK4 compared with CDK6 [53]. These clinically relevant small molecule inhibitors (SMIs) have favorable physiochemical properties for BBB permeability [54], These agents, RG7388 (MDM2 inhibitor), GDC0068 (AKT inhibitor) and ACB, have been investigated as single agents in various types of cancer [53, 55, 56]. However, they have not been studied for optimal combinations and rational dosing regimens in association with TMZ for GBM treatment.

1.6 Investigated GBM patient derived xenografts models

The GBM human derived cell line GBM 10 is a recurrent GBM; it is wildtype with respect to p53, has a CDKN2A deletion, and possesses wildtype STAT3. The GBM human derived cell line GBM 43 is from a primary GBM; it is mutant with respect to p53, also has a CDKN2A deletion, and possesses wildtype STAT3 [57]. Unlike GBM 10 and GBM 43, U87 is a GBM, astrocytoma

cell line derived from human malignant gliomas. U87 cells are adherent epithelial cells. The karyotype is hypodiploid female with a modal chromosome number of 44 in 48% of cells and a 5.9% rate of higher ploidy [58]. MDM2 small molecule inhibitor RG7388 leads to potent tumor inhibition in p53 wild type tumors, and produces no inhibitory effect on p53 silenced xenografts [59]. GBM43 has mutant p53 and TMZ can induce the p53 family member p73. Both MDM2 inhibitors, RG7112 and RG7388, can block MDM2 from binding to wildtype p53 [60]. However, only RG7112 will block MDM2 from binding to p73. Therefore, in some cellular contexts RG7112 can promote p73-dependent apoptosis in cancer cells. In our study, RG7388 was used to treat mice bearing GBM 10 xenografts. RG7112 led to potent antitumor activity in mutant a p53 cell line [61] and was used to treat mice bearing GBM 43 xenografts.

1.7 Tumor Growth Inhibition models

Ordinary differential equations can be used to describe the net change in tumor volume and characterize the unperturbed tumor growth or tumor inhibition in the presence of treatment. Growth of the tumor in the absence of treatment can be described using various functions, such as linear, exponential, mixture of linear and exponential, Gompertz or logistic growth [62]. The linear model describes the zero-order growth rate, while the exponential model describes first order kinetic (cell-volume dependent) growth rate for the untreated tumor. Simeoni et. al used the mixture of both exponential and linear growth to describe the anti-tumor activity in-vivo.[63]. Logistic and Gompertz models become more biologically realistic when the tumor is allowed to grow for an unlimited time. The logistic growth model limits the growth of the tumor by carrying capacity reaching a plateau, while the Gompertz model assumes growth rates of the tumor decrease over time [64]. Having tried all these growth models, we selected the Simeoni growth model to capture the unperturbed tumor growth using the method of parsimony based on the Aikake Information Criterion (AIC) value [65]. AIC criteria penalize the log-likelihood by the number of model structure parameters so as to limit overfitting [66].

CHAPTER 2. APPROACH

We utilized a computational PKPD modeling approach to identify and optimize the target concentration/dose of SOC (TMZ) in combination with AKT (GDC0068) and/or MDM2 inhibitor (RG7388 or RG7112) to be aimed at clinically for targeting TMZ–induced resistance in GBM. **The central hypothesis is that application of a PKPD modeling approach that incorporates targeting of the TMZ triggered resistance signaling pathways, i.e., AKT, MDM2, CDK4/6 kinase, will identify strategic combinations of SMIs respective of these signaling pathways so as to improve our ability to develop combination regimes and thereby improve therapeutic outcome in GBM.**

2.1 Study rationale:

Our rationale is that predictive PKPD modeling of tumor growth kinetics via tumor volume data in xenograft models will improve combination treatment therapy design, and readily support translation to human therapy. The objective of tumor growth inhibition modeling in combination therapy is evaluation and comparison of different dose combinations with respect to efficacy and identification of synergistic effects. Oncology clinical trials differ from other diseases because Phase 1 trials are never conducted and comparison for the new drug is never made to placebo. Instead, outcome for a new treatment is always compared to a SOC [67]. In GBM, the presence of complex intra-tumoral heterogeneity leads to resistance development to standard of care TMZ monotherapy. When developed as monotherapy agents, novel drug candidates are expected to inhibit tumor growth. Alternatively, these novel agents can be combined with already approved and older cytotoxic drugs, the latter which kill the dividing cells non-specifically [67]. Currently, many combination therapies are being evaluated in clinical trials that focus on exploiting the underlying mechanism of oncogenesis and also focus on developing better treatment regimens [6]. Treatments that combine two or more drugs are being tested in ongoing clinical trials for various GBM subtypes [6]. Based on understanding of therapeutic targets and signaling networks in GBM, an approach to alter these multiple pathways with specific small molecule inhibitors is critically important for developing rational drug combinations. Published data indicate sustained activation of the TMZ induced p53/p73 pathway by MDM2 inhibition [25-27]. In addition, existence of a

growth promoting link between MDM2 and AKT networks provides rationale for dual targeting of MDM2 and AKT pathways activated by SOC [4, 9, 28]. Due to tumor heterogeneity, some drug combinations produce synergistic effects and some combinations produce antagonistic effects [68, 69]. This latter unresponsiveness to the targeted therapy may be due to the functional and phenotypic heterogeneity arising among the cancer cells that presents as a sub-population of resistant cells. Quantitative approaches based on mathematical modeling identify possible synergism or antagonism; thus, this approach is important in visualizing drug combinations in the dose-response matrix.

2.2 Study Aims and Objectives

In this study, we present mathematical cell growth/cell kill models involving single agent and two or more agents. We extend this basic model to a combination therapy in which two drugs will act synergistically, additively, or antagonistically. We then used TSC curves derived from mathematical models to demonstrate how combination of two drugs is more effective than either drug would have been individually. The objective of our study was to perform predictive PKPD modeling of tumor growth kinetics via tumor volume data in various GBM xenograft models (U87 gliomas, GBM 10, and GBM 43) to demonstrate the potential for combination treatment therapy, and better describe the emergence of resistance to TMZ treatment in primary and recurrent GBM. The objective of tumor growth inhibition modeling in combination therapy is to evaluate and compare different dose combinations with respect to efficacy. To aid visualizing drug combinations in the dose-response matrix, Tumor Static Concentration (TSC) curves were constructed to demonstrate how combinations of two or more drugs could be more effective than either drug alone [70] . Towards this objective, the following specific aims were pursued.

Aim 1: Develop population pharmacokinetic models for TMZ, and MDM2/AKT inhibitors, that target TMZ induced MDM2/p53/p73 and PI3K/AKT/mTOR signaling pathways in GBM

Hypothesis: Population PK models describe the plasma concentration profile of TMZ and Small Molecule Inhibitors

Aim 2: Perform population pharmacokinetic-pharmacodynamic (PKPD) modeling of tumor growth kinetics in xenograft mouse models in various cell lines (U87, GBM 10, GBM 43) following administration of TMZ with MDM2, CDK4/6 kinase and AKT inhibitors in combination treatment

Hypothesis: Population PKPD models describe the anti-tumor activity of TMZ monotherapy and TMZ plus SMIs combination therapy

Aim 3: Perform simulations and derive Tumor Static Concentration curves that identify single concentration values or pairs of drug concentration combinations that would achieve tumor shrinkage

Hypothesis: Developed TGI PKPD models can be applied to conduct simulations that would aid visualization and rationalizing drug combinations in a dose response matrix

CHAPTER 3. METHODS

3.1 Preparation of reagents to support original studies

TMZ and AKT inhibitor, GDC0068, were purchased from MedChem Express. The MDM2 inhibitors, RG7112 and RG7388, were purchased from ShangHai Biochempartner Co.,Ltd and Chemitek, respectively.

TMZ was dispersed in 100mM citric acid buffer (0.11 g Citric acid and 0.13 g of Sodium Citrate dihydrate dissolved in 10 mL of distilled water by sonication, adjusted to pH 3 using 1M HCl), prepared using Hydroxypropyl methylcellulose (0.5% w/v) and polysorbate 80 (0.5%). Small molecule inhibitors, RG7388 and GDC0068, were formulated in 0.5% methylcellulose (Sigma-Aldrich) and 0.05% Tween 80 (Fisher Scientific) for in-vivo studies.

3.2 Published Data Sources

To facilitate development of a robust PKPD model, data from published studies derived from various doses, formulations, and routes of administration under either fasted or fed conditions were used along with the data from our original experimental studies. PK data from published sources for mice were included in the study and rats were excluded from the study. Published anti-tumor activity data in GBM cell lines for the investigated molecules were included in the study. Details of these published studies, including Tables 3.1 and 3.2, are described in the following two sub-sections.

3.2.1 Pharmacokinetic Data

The live phase and sample analysis from original studies of male NSG immunocompromised mice plasma pharmacokinetics for TMZ were conducted following administration of 5 mg/kg or 66 mg/kg as single oral (p.o.) doses. Additional TMZ doses: 20 mg/kg p.o. [71, 72], 50 mg/kg p.o. [73], 66 mg/kg intraperitoneal (i.p.) [7, 74] and 10 mg/kg [75] intravenous (i.v.) used to support TMZ pharmacokinetic model development were obtained by digitization of data for mean plasma TMZ concentration time profile from the published literature [7, 71-75] using Enguage Digitizer (https://github.com/markummitchell/engauge-digitizer). Mouse plasma pharmacokinetic study parameter estimates of RG7112 (also an MDM2 inhibitor)

were obtained from a published study [76]. Mean plasma ACB concentration time profile data following 30 mg/kg oral ACB were obtained by digitization from a published study [2]. Original mouse plasma pharmacokinetic studies for RG7388 and GDC0068 were conducted following administration of a single oral dose of 50 mg/kg and 25 mg/kg, respectively. Table 3.1 provides a summary of the above-mentioned published studies and their respective conditions.

Table 3.1: Summary of Digitized Data Used to Support PK Model Development

Drugs	Study reference	Route	Dose (mg/kg)	Formulation	Sample Matrix	Animal Used
Temozolomide	Ballesta, et al., CPT Pharmacometrics Syst Pharmacol, 2014. **3**: p. e112.	Oral	20	Dissolved in 0.9% NaCL containing 25% DMSO	Plasma	NIH-Swiss nude mice (nu/nu)
	J.M. Gallo, et al., Clinical Cancer Research, 2008. **14**(5): p. 1540-1549.	Oral	20	Dissolved in 0.1 mol/L citrate buffer (pH 4.7)	Plasma	Male NIH-swiss nude mice (nu/nu)
	Liu, H.-L., et al., PLoS One, 2014. **9**(12): p. e114311.	Oral	50	Pellet for Feeding	Plasma	Pathogen free male NU/NU mice
	Goldwirt, L., et al., Cancer chemotherapy and pharmacology, 2014. **74**(1): p. 185-193.	Intra-peritoneal	66	Dissolved in 0.9% NaCl	Plasma	Female CF1 *mdrla* (-/-) mice
	Goldwirt, L., et al., Biomedical Chromatography, 2013. **27**(7): p. 889-893.	Intra-peritoneal	66	Dissolved in 0.9% NaCl	Plasma	Female Swiss mice
	Kumari, S., et al., Scientific reports, 2017. **7**(1): p. 6602.	Intra-venous	10	TMZ loaded lactoferrin Nanoparticles	Plasma	Healthy C57BL/6 mice

Table 3.1: Continued						
RG7112 (MDM2 inhibitor)	Vu, B., et al., ACS medicinal chemistry letters, 2013. **4**(5): p. 466-469.	Oral	50	-	Plasma	Not specified in literature
Abemaciclib (CDK4/6 kinase inhibitor)	Raub, T.J., et al., Drug Metabolism and Disposition, 2015. **43**(9): p. 1360-1371.	Oral	30	Suspension; TMZ in 1% (w/v) hydroxyethylcellulose, 0.25% (v/v) polysorbate 80, 0.05% (v/v) antifoam in purified water	Plasma	Female CD-1 mice

3.2.2 Pharmacodynamic Data

Tumor volume data from male NSG mice bearing GBM 10 subcutaneous xenografts treated with TMZ alone or in combination with one or two SMIs (RG7388, GDC0068) were from an original study, in which 66 mg/kg TMZ, 50 mg/kg RG7388 and 25 mg/kg GDC0068 was given orally (once daily 5 days/week (Monday through Friday) for three cycles, starting on day 49 after tumor implantation).

Mice bearing GBM 43 subcutaneous xenografts were also from an original study, and included animals treated with TMZ alone or in combination with one or two SMIs (RG7112, GDC0068), in which 10 mg/kg TMZ, 100 mg/kg RG7112 and 100 mg/kg GDC0068 were given orally (3 days/week (Monday, Wednesday, Friday) for two/three cycles, starting on day 13 after tumor implantation). Several TMZ monotherapy studies were conducted in mice bearing GBM 43 flank tumors to assess the TMZ dose response effects on tumor volume. TMZ was dosed orally (once daily 5 days/week for two/three cycles) at 0.3 mg/kg, 1 mg/kg, 5 mg/kg, 10 mg/kg, 33 mg/kg, and 66 mg/kg for three separately carried out original monotherapy studies in mice bearing the GBM 43 cell line. Also, an original study of mice bearing GBM 43 xenografts was conducted with several treatment groups: TMZ alone dosed at 33 mg/kg and 66 mg/kg alternatively (33 mg/kg for the first two weeks and 66 mg/kg for the last two weeks or vice-versa in a four weeks dosing regimen), TMZ alone dosed at 33 mg/kg and 66 mg/kg with a holiday week in-between (66 mg/kg

for the first two weeks, vehicle on the third week, and 33 mg/kg or 66 mg/kg for the last two weeks) in a five week dosing regimen, TMZ dosed at 66 mg/kg in combination with 50 mg/kg GDC0068 (AKT inhibitor) and a holiday week in-between (66 mg/kg TMZ for the first two weeks, vehicle on the third week and 50 mg/kg GDC0068 or 33 mg/kg TMZ + 50 mg/kg GDC0068 for the last two weeks) in a five week dosing regimen.

In addition, to support PD model development across different GBM cell lines, tumor volume data from mice receiving subcutaneous implants of U87 gliomas treated with TMZ alone or in combination with ACB were obtained by digitization from published sources [2, 28]. These were the data from a study reported by Wang, et.al. [28] on GBM combination therapy, in which 5 mg/kg TMZ was given orally once daily 5 days/week for two cycles, or from a Raub, et. al. study [2], in which 3 mg/kg TMZ was administered IP twice (7 days starting on day 11 after tumor implantation), and 50 mg/kg ACB dosed orally once daily for 21 days. These additional studies are summarized in Table 3.2.

Table 3.2: Summary of Digitized Data Used to Support PD Model Development

Drugs	Study reference	Route	Dose (mg/kg)	Formulation	U87 Tumor Implants	Animal Used
Abemaciclib (CDK4/6 kinase inhibitor)	Raub, T.J., et al., Drug Metabolism and Disposition, 2015. **43**(9): p. 1360-1371.	Oral	50	ACB in 1% hydroxy ethyl cellulose and 0.1% antifoam in 25 mM phosphate buffer, pH 2	Subcutaneous/Flank	CD-1 Nu/Nu female mice
Temozolomide	Wang, H., et al., Journal of neurosurgery, 2017. **126**(2): p. 446-459.	Oral	5	Dissolved in phosphate buffer saline (PBS) or cell culture media	Subcutaneous/Flank	Male NSG mice
Temozolomide	Raub, T.J., et al., Drug Metabolism and Disposition, 2015. **43**(9): p. 1360-1371.	Intra-peritoneal	3	TMZ in distilled water containing 1% carboxymethyl cellulose and 0.25% tween 80	Subcutaneous/Flank	CD-1 Nu/Nu female mice

3.3 Original In-vivo Experiments

A breeding colony of NOD.Cg-*Prkdc*^{scid} *Il2rg*^{tm1Wjl}/SzJ (NSG) mice was established at the Indiana University School of Medicine (IUSM) Laboratory Animal Research Center (LARC) and all experiments were conducted in accordance with the In-vivo Therapeutics Core at the Indiana University Simon Comprehensive Cancer Center (IUSCCC)/IUSM. IUSM-LARC holds an accreditation from American Association for the Accreditation of Laboratory Animal Care and all procedures were approved by the Institutional Animal Care and Use Committee (IACUC) under IACUC study #20139.

3.3.1 Pharmacokinetic Studies

Single dose pharmacokinetics of TMZ, RG7388 and GDC0068 were investigated in separate groups of immunocompromised male NSG mice. Three mice per time point for a total of 8 time points were used for the assessment. Stable drug suspensions were formulated in citric acid buffer, pH 3. Blood samples (~10% of circulating blood volume) were collected as per IUCAC protocol by one terminal bleed (tail vein draw) for each mouse at 0hr, 30 min, 1hr, 1.5hr, 2hr, 4hr, 6hr, 8hr (for TMZ and GDC0068) and 0hr, 1hr, 2hr, 3hr, 4hr, 6hr, 8hr, 24hr (for RG7388). The blood samples were collected in heparinized tubes, centrifuged at 3000 rpm for 10 mins and stored at -80°C until time of analysis. The plasma concentrations of the drug were determined using LC-MS/MS in the Clinical Pharmacology Analytical Core. The lower limit of quantification (LOQ) was 1 ng/mL for all three drugs.

3.3.2 Pharmacodynamic Studies

Immunocompromised male NSG mice were obtained from IUSM-LARC. Animals were subjected to acclimation for seven days on TD06596 Irradiated Global 2018 feed (Uniprim, Harlan Laboratories). Uniprim food was in continuous use during this study. For flank studies, cells were injected subcutaneously into the right flank. The GBM 10 and GBM 43 PDX xenolines were a kind gift from Dr. Jann Sarkaria (Mayo Clinic, Rochester, MN). Confirmation of cell line identity was done by DNA fingerprint analysis (IDEXX BioResearch) and short-tandem repeat base-line analysis testing. Both GBM 10 and GBM 43 cell lines were 100% human, and a nine-marker short-tandem repeat analysis is maintained. GBM 10 and GBM 43 xenolines were established from

PDX flank tumors and they were maintained in FBS 2.5% for four days on matrigel-coated plates (BD Biosciences) to remove murine-fibroblasts. Cells were then expanded in DMEM/F12 (Dulbecco's Modified Eagle Medium; 4.5g/L D-glucose and L-Glutamine) with FBS 10% for less than two weeks prior to implantation. All cells were negative for mycoplasma. [37]

For the GBM 10 and GBM 43 flank studies, mice were injected in the right flank with 5 x 10^6 cells that were suspended in a 1:1 mixture of Matrigel/PBS (BD Biosciences, San Jose, CA). Once tumor volumes reached 150-200 mm^3, mice were treated as per the study protocol. Tumor volumes and body weights were measured by caliper every 2-3 days. Tumor volume was determined by electronic caliper that was interfaced with StudyLog software (San Francisco, CA) and using formula $(\alpha^2 \times \beta)/2$, where α is the shorter and β is the longer of the two dimensions). Finally, mice were euthanized, and tumor tissue and organs were harvested for further analysis. The endpoint of the flank studies was when the tumor reached ~2000 mm^3 for ethical reasons. These studies were all conducted by Dr. Pollok's laboratory with technical support from the In Vivo Therapeutics Core in the Melvin and Bren Simon Comprehensive Cancer Center at the Indiana University School of Medicine.

THEORETICAL

3.4 Development of Integrated PKPD Models

3.4.1 Pharmacokinetic Model

Disposition of TMZ following p.o. or i.p. administration was described by a first order absorption one-compartment population PK model with non-linear bioavailability. A one-compartment model also described TMZ pharmacokinetics by the i.v. bolus route. A one-compartment pharmacokinetic model with first order absorption was also developed for the small molecule inhibitors (SMIs) i.e. ACB, RG7388 and GDC0068, based on data from a published study for ACB [2], and an original study conducted for RG7388 and GDC0068. PK data were simultaneously fitted to characterize the PK profile of TMZ after administration by either the oral, intraperitoneal, or intravenous route and small molecule inhibitors after administration by oral route. PK models were described using the following equations.

$$C_{TMZ,oral\ or\ i.p.} = \frac{FDK_a}{V_d(K_a - K_e)} . (e^{-K_e.t} - e^{-K_a.t}) \text{ , compute } Cl = \frac{D.F}{AUC} \quad (1)$$

$$C_{TMZ,i.v.bolus} = \frac{D}{V_d} . e^{-K_e.t} \quad (2)$$

$$C_{ACB\ or\ RG7388\ or\ GDC0068} = \frac{FDK_a}{V_d(K_a - K_e)} . (e^{-K_e.t} - e^{-K_a.t}) \quad , \quad \text{compute } \frac{Cl}{F} = \frac{D}{AUC} \quad (3)$$

where K_a is the absorption rate constant, K_e the elimination rate constant, F the bioavailability, C the drug concentration, D the dose, V the volume of distribution, and Cl the clearance. The schematic illustration is presented in Figure 3.1.

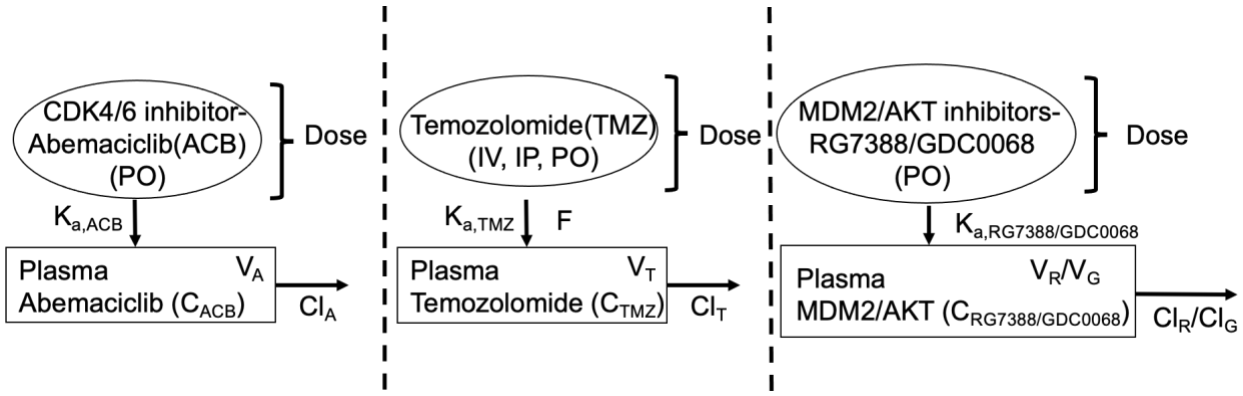

Figure 3.1: Schematic representation of pharmacokinetic model for TMZ and small molecule inhibitors (ACB, RG7388, GDC0068)

For TMZ pharmacokinetics, based on data from the original studies and various published sources, saturable drug absorption was identified. The Ka parameter was categorized and separately estimated based on the administration route and formulation type (solution, suspension, and fed). Bioavailability (F) estimates were stratified by dose level.

3.4.2 Pharmacodynamic Model

Tumor Growth Inhibition (TGI) Model

Base TGI model

A pharmacodynamic tumor growth model was developed to best describe the time course of tumor growth and inhibition of growth in the presence of drug treatments. Growth rate of U87 /GBM 10/GBM 43 xenograft tumors in vehicle treated (control) mice was described using the model developed by Simeoni, et al [63]. For mice bearing U87 glioma cells treated with TMZ and/or ACB, the model describing the inhibitory effect of ACB is driven by inhibition of cell proliferation [77] , while TMZ elicits a cytotoxic effect [18]. These mechanisms of drug action were incorporated into the TGI model. Modeling of each compound as cytostatic and cytotoxic were examined using both linear and E-max functions. Using parsimonious approach, final model selection was based on AIC. Based on preliminary in vitro experiments (results not shown), in vitro IC50 >> in vivo drug concentration, which reduces the Hill equation to E_{max}/EC_{50} that we define as term 'b' (linear function of drug action) in our models. Transit compartments were also incorporated into the model to account for the delay between drug administration to eventual cell death [1, 63]. Shown below are the differential equations that describe the system, with initial conditions V1 (0) = V_0, V2 (0) = 0, V3 (0) = 0, V4 (0) = 0.

$$\frac{dV1}{dt} = \frac{k_{g,exp} * V1}{\left(1 + \left(\frac{k_{g,exp}}{k_{g,lin}} * TV\right)^{\psi}\right)^{\frac{1}{\psi}}} * (1 - b_{ACB} * C_{ACB}) - b_{TMZ} * C_{TMZ} * V1 \quad (4)$$

$$\frac{dV2}{dt} = b_{TMZ} * C_{TMZ} * V1 - k_k * V2 \quad (5)$$

$$\frac{dV3}{dt} = k_k * (V2 - V3) \quad (6)$$

$$\frac{dV4}{dt} = k_k * (V3 - V4) \quad (7)$$

(8)

$$TV = V1 + V2 + V3 + V4$$

V1 is the main compartment of proliferating cancer cells, V2, V3 and V4 are damage (transit) compartments that cells exposed to TMZ go through before dying, $k_{g,exp}$ and $k_{g,lin}$ are the exponential and linear tumor growth rate constants, respectively. The parameter ψ is a constant value fixed to 20 to allow the system to pass through first order to zero order growth sharply [78], k_k is the cell death rate, and b_{ACB} and b_{TMZ} are the drug potency parameters for ACB and TMZ, respectively. Total tumor volume (TV) comprises both the proliferating cell compartment, V1, and the compartments V2 to V4 representing dying cells.

The base TGI model was also developed for mice bearing GBM 10 xenografts treated with TMZ monotherapy or TMZ combination therapy with MDM2 inhibitor (RG7388) and/or AKT inhibitor (GDC0068). Modeling of each compound as cytostatic and cytotoxic was examined using both linear and E-max functions. Using a parsimonious approach, final model selection was based on AIC. Similarly, mice bearing GBM 43 subcutaneous xenografts treated with TMZ monotherapy and/or combination therapy with one or two SMIs (RG7112, GDC0068) were subjected to fit the base TGI model structure. However, treatment arms in GBM 43 xenolines were best described by a resistance integrated tumor growth inhibition model (discussed later) and the model fit was superior to the base TGI model structure. The schematic of the base TGI model structure is shown in Figure 3.2.

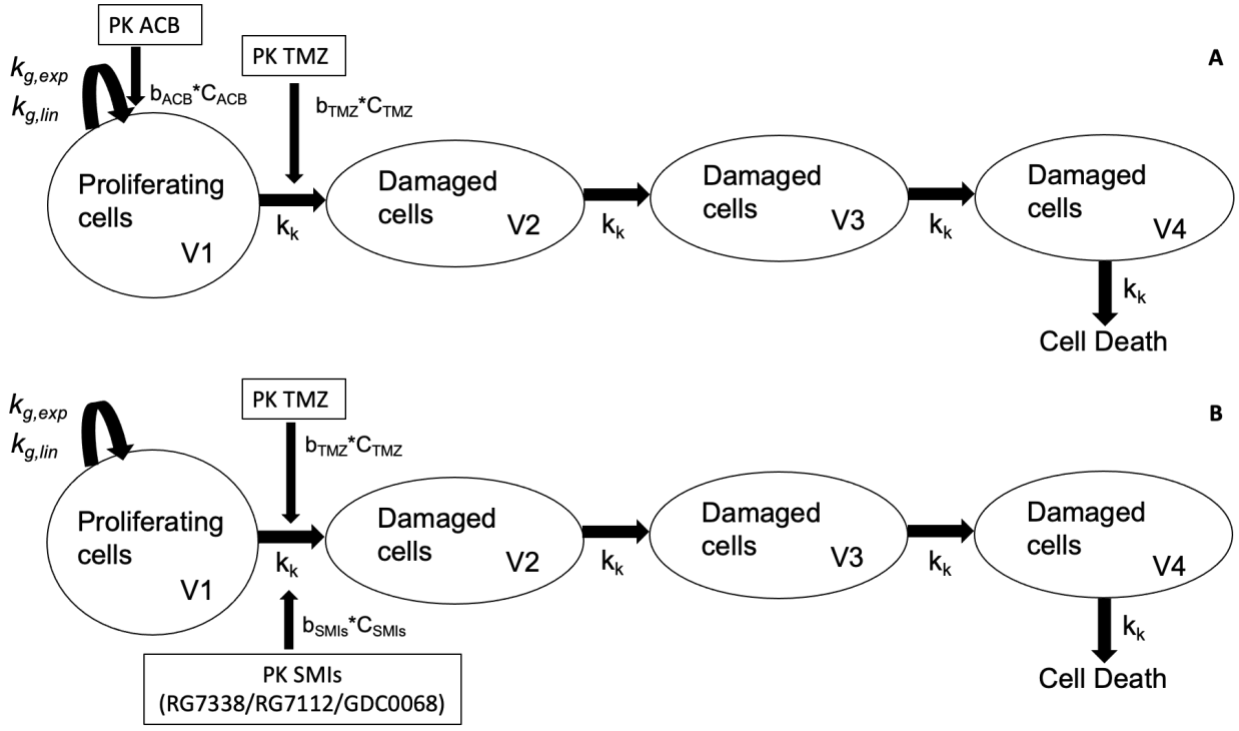

Figure 3.2: Schematic representation of a final base tumor growth inhibition (TGI) PKPD model for combination therapy various GBM xenografts. The model of drug action inhibiting cell growth (abemaciclib, ACB) and drug action responsible for cell killing (temozolomide (TMZ) and small molecule inhibitors (SMIs)). **A:** PD of mice bearing U87 xenografts was linked with TMZ and ACB concentrations predicted from their corresponding PK models. **B:** PD of mice bearing GBM 10 / GBM 43 xenografts was linked TMZ and MDM2/AKT SMI concentrations predicted from their corresponding PK models. Pharmacodynamic parameters are defined in the text.

Drug resistance integrated TGI model

The base TGI model was expanded to incorporate resistance development due to standard of care therapy (TMZ monotherapy) in mice bearing GBM 43 xenografts that received monotherapy with TMZ or SMIs (RG7112, GDC0068) or, with these agents in dual or triple combination. A resistance development component to model structure was accomplished by introducing a resistance cell compartment, R, where the population of resistant tumor cells start to appear during TMZ treatment. When the treatment with anti-cancer drug is initiated, tumor cells that are sensitive to drug treatment stop proliferating and pass through the different progressive stages of damage and eventually die [1, 63], as in the base model. However, a fraction of cells that escape death are converted to cells that are resistant to initial therapy, and the conversion process is described using a first order rate constant [79]. The growth rate of the resistant cell population was described using the same structural model as the model describing the TMZ sensitive cell

population, except that it was substituted with distinct zero order (linear) and first order (exponential) growth rate constants representative of resistant cell growth only. Conversion of TMZ sensitive cells into TMZ resistant cells was integrated into the TGI model as a delayed process consistent with the delayed drug effect. In the TMZ resistance integrated TGI model, total tumor volume is the sum of sensitive (V1), resistant (R) and damaged cells (V2, V3), as shown in Equation (13). A schematic representation of the model structure is presented in Figure 3.3 and is described by the system of differential equations shown in Equations (9) – (13) below:

$$\frac{dV1}{dt} = \frac{k_{g,exp} * V1}{\left(1 + \left(\frac{k_{g,exp}}{k_{g,lin}} * TV\right)^{\psi}\right)^{\frac{1}{\psi}}} - b_{TMZ} * C_{TMZ} * V1 \quad (9)$$

$$\frac{dV2}{dt} = b_{TMZ} * C_{TMZ} * V1 - k_k * V2 \quad (10)$$

$$\frac{dV3}{dt} = k_k * (V2 - V3) - k_{S-to-R} * V3 \quad (11)$$

$$\frac{dR}{dt} = \frac{k_{gR,exp} * R}{\left(1 + \left(\frac{k_{gR,exp}}{k_{gR,lin}} * TV\right)^{\psi}\right)^{\frac{1}{\psi}}} + k_{S-to-R} * V3 - b_{SMIs} * C_{SMIs} * R \quad (12)$$

$$TV = V1 + V2 + V3 + R \quad (13)$$

with initial conditions V1 (0) = V_0, V2 (0) = 0, V3 (0) = 0, R (0) = 0, and where $k_{gR,exp}$ and $k_{gR,lin}$ are the rate constants for exponential growth and linear growth of the resistant cell population, respectively. The parameter $k_{S\text{-}to\text{-}R}$ is the first order transformation rate constant for sensitive cells to convert to resistant cells following initial treatment with TMZ, and b_{SMIs} are the drug potency parameters for small molecule inhibitors (RG7122, GDC0068).

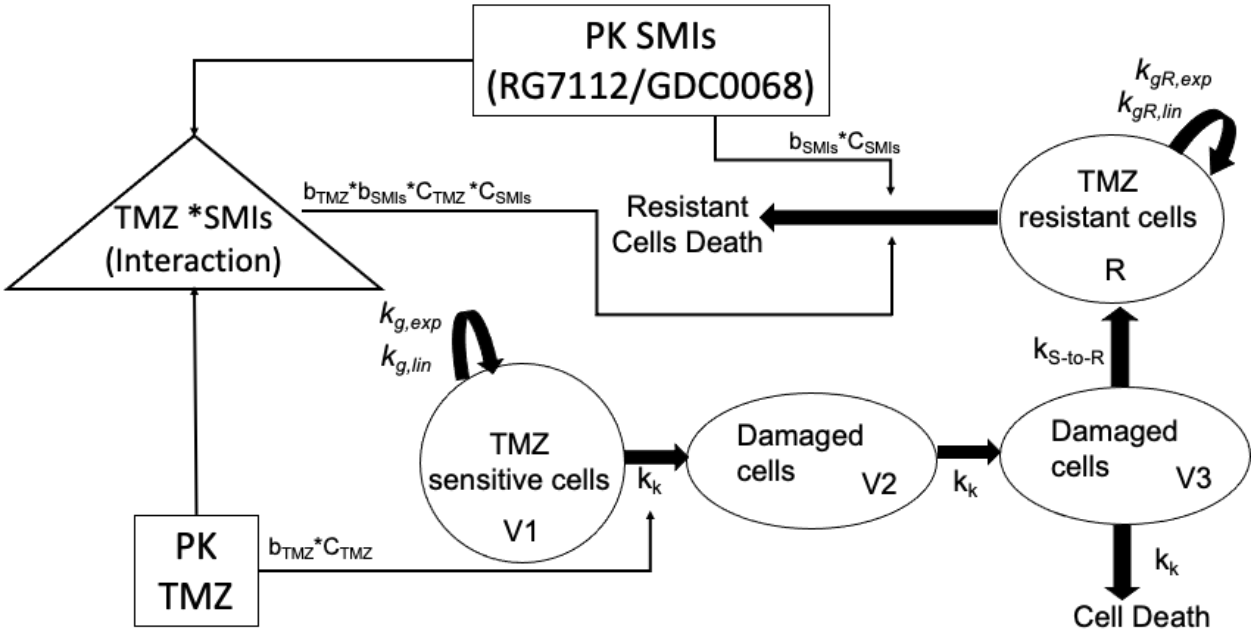

Figure 3.3: Schematic representation of the final resistance integrated tumor growth inhibition (TGI) PKPD model for combination therapy in mice bearing GBM 43 xenografts. Change in tumor volume was linked with PK models of temozolomide (TMZ) and small molecule inhibitors (SMIs). Tumor cells sensitive to TMZ treatment (V1) go through stages of progressive damage (V2-V3) before they die or convert into drug resistant cells (R) over time as function of TMZ treatment. Resistant cells are eliminated via the action of SMIs alone and a PD interaction of TMZ and SMIs. Pharmacodynamic parameters are defined in the text.

Secondary model parameters, such as ratio for growth rates of resistant to sensitive cells (φ) and average time (τ) for sensitive cells to eradicate or convert into the resistant cell phenotype, can be computed from the acquired resistance TGI model [79]. These parameters were derived from the drug resistance integrated TGI model using equations (14) and (15).

$$\varphi = \frac{k_{gR,exp}}{k_{g,exp}} = \frac{k_{gR,lin}}{k_{g,lin}} \quad (14), \quad \tau = \frac{\#\ of\ damage\ compartments}{k_k} \quad if\ k_{S-to-R} \ll k_k \quad (15)$$

3.5 Model implementation and validation

Population pharmacokinetic analyses of drug concentrations and pharmacodynamic analysis of tumor volume growth were conducted with Phoenix NMLE version 8.1 (Pharsight Corporation, Certara, L.P., Princeton, NJ). PKPD parameters were estimated first using a population approach with Naïve Pooled estimation (single function fit to the combination of all individuals) followed

by nonlinear mixed effects (NLME) modeling with first order conditional estimation – extended least square analyses (FOCE). NLME-FOCE allowed for estimation of model parameters (fixed effects) and inter-subject and/or inter-occasion variability around model parameters (random effects). While NLME FOCE is widely accepted for estimating random effects for individuals, when determining the best fixed effects, the trade-off of this approach is its tendency to perform poorly if the data is not rich [80]. Poor estimation of random effects causes individual parameter estimates to shrink back towards the population mean, evidenced by a high amount of shrinkage in random effects [81]. The amount of shrinkage is dependent on the data quality, sample informativeness, and number of observation points [81]. High shrinkage could mislead the assessment of estimated inter-individual variability parameters. In building the population PKPD models, when the shrinkage observed for random effects was found to be higher than 40%, models were executed using the Naïve Pooled approach only. The population modeling approach [82] was of importance to develop robust PKPD models by enabling incorporation of data collected from original studies as well as several published sources [2, 7, 28, 71-76]. For both PK and PKPD models, a proportional residual error model was selected to describe residual error that may arise from model structure misspecification, inaccurate dosing and sampling times, and errors in concentration analyses.

During PD model structure optimization, PK parameters were frozen. However, following the identification of the best PD model structure, the PK parameters were unfrozen in the final PD model. Since there was no significant change in the PK parameters in the final PD model they were not reported. For nested models, model structure evaluation and selection were based on the likelihood ratio test with p value < 0.05 for statistical significance. For non-nested models, the AIC value was used, with the difference of more than 10 units considered favorable for the model with lower AIC [83]. Model selection and performance (goodness-of-fit) were also accomplished based on precision of parameter estimates, and diagnostic plots: conditional weighted residual (CWRES) vs time, CWRES vs population predicted concentrations or tumor volume measurements, observed concentrations or tumor volume measurements vs individual/population predicted concentrations or tumor volume measurements. Internal validation of the models was performed by graphical visual predictive checks that compared experimental data used to develop the model with the 5^{th}, 50^{th} and 95^{th} percentiles of model-derived simulated drug concentration or tumor volume datasets ($N = 500$).

3.6 Simulation Studies

3.6.1 Tumor Static Concentration Curves

Derivation of equations to estimate tumor static concentrations for a single agent

The treatment goal is reduction of tumor volume. Therefore, the objective is to determine the plasma concentrations that result in tumor shrinkage. To accomplish this, it is first necessary to determine the drug concentration at which growing and dead cell compartments are in balance. Accordingly, plasma concentrations above this level will result in tumor shrinkage [67]. For TMZ monotherapy, this suggests that the right-hand side of equations (4)-through-(7) should be zero. However, because V2 through V4 compartments only act to delay cell death, only the main proliferating compartment (V1) needs to be considered. For TMZ monotherapy treatment, it should hold that,

$$0 = \frac{k_{g,exp} * V1}{\left(1 + \left(\frac{k_{g,exp}}{k_{g,lin}} * TV\right)^{\psi}\right)^{\frac{1}{\psi}}} - b_{TMZ} * C_{TMZ} * V1$$

which implies,

$$0 = \left(\frac{k_{g,exp}}{\left(1+\left(\frac{k_{g,exp}}{k_{g,lin}} * TV\right)^{\psi}\right)^{\frac{1}{\psi}}} - b_{TMZ} * C_{TMZ} \right) * \mathrm{V1}$$

$$0 = \left(\frac{k_{g,exp}}{\left(1 + \left(\frac{k_{g,exp}}{k_{g,lin}} * TV\right)^{\psi}\right)^{\frac{1}{\psi}}} - b_{TMZ} * C_{TMZ} \right) \tag{16}$$

In order for shrinkage to occur, drug effect ($b_{TMZ} * C_{TMZ}$) needs to be larger than cell growth. When total tumor volume (TV) is below the exponential to linear growth switch threshold for the initial treatment cycle, the term in the denominator $\left(\frac{k_{g,exp}}{k_{g,lin}} * TV\right)^{\psi}$ is negligible compared with 1,

thus the tumor growth rate can be defined by $k_{g,exp} * V1$ (exponential growth). Subsequently, equation (16) can be solved for C_{TMZ}, as shown in Equation (17).

$$C_{TMZ} = k_{g,exp} \left(\frac{1}{b_{TMZ}}\right) \tag{17}$$

Equation (17) describes the tumor static concentration (TSC) value of TMZ monotherapy. At any given time, the TSC value holds for the tumor volume. Thus, plasma exposures above the TSC curve should be maintained to ensure tumor shrinkage over time.

TSC values for SMIs monotherapy can be derived similarly. For cytostatic ACB, when $C_{ACB} = 0$, the condition for stasis is described as

$$0 = \frac{k_{g,exp} * V1}{\left(1 + \left(\frac{k_{g,exp}}{k_{g,lin}} * TV\right)^{\psi}\right)^{\frac{1}{\psi}}} * (1 - b_{ACB} * C_{ACB}) \tag{18}$$

Solving equation (18) for TSC value of ACB monotherapy

$$C_{ACB} = \frac{1}{b_{ACB}} \tag{19}$$

For cytotoxic SMIs (RG7112/RG7338/GDC0068), when $C_{SMIs} = 0$ condition for stasis is described as

$$0 = \left(\frac{k_{g,exp}}{\left(1 + \left(\frac{k_{g,exp}}{k_{g,lin}} * TV\right)^{\psi}\right)^{\frac{1}{\psi}}} - b_{SMIs} * C_{SMIs} \right) \tag{20}$$

Solving equation (20) for C_{SMIs} to obtain

$$C_{SMIs} = k_{g,exp}\left(\frac{1}{b_{SMIs}}\right) \quad (21)$$

Equation (21) describes the tumor static concentration (TSC) value of RG7112/RG7338/GDC0068 monotherapy.

Deriving tumor static concentration curves for multiple agents in combination

Assuming similar conditions to that of single agent treatment for groups receiving multiple agents, the proliferating cell compartment (V1) can be factored out

$$0 = \frac{k_{g,exp} * V1}{\left(1 + \left(\frac{k_{g,exp}}{k_{g,lin}} * TV\right)^{\psi}\right)^{\frac{1}{\psi}}} * (1 - b_{ACB} * C_{ACB}) - b_{TMZ} * C_{TMZ} * V1$$

such that,

$$0 = \left(\frac{k_{g,exp}}{\left(1 + \left(\frac{k_{g,exp}}{k_{g,lin}} * TV\right)^{\psi}\right)^{\frac{1}{\psi}}} * (1 - b_{ACB} * C_{ACB}) - b_{TMZ} * C_{TMZ} \right) \quad (22)$$

The denominator $\left(\frac{k_{g,exp}}{k_{g,lin}} * TV\right)^{\psi}$ in equation (22) is negligible compared with 1 during initial treatment cycles and the tumor growth rate is defined by exponential growth. Equation (22) describes the curvature (TSC curve) in the concentration plane when concentration pairs, C_{TMZ} (cytotoxic effect) and C_{ACB} (cytostatic effect), are plotted against the X-axis (C_{TMZ}) and Y-axis (C_{ACB}). Solving Equation (22) for C_{ACB} yields Equation (23).

$$C_{ACB} = \frac{1}{b_{ACB}} - \frac{b_{TMZ} * C_{TMZ}}{k_{g,exp} * b_{ACB}} \quad (23)$$

Equation (23) plots the curve of concentration pairs, C_{ACB} and C_{TMZ}. Any pairs of concentration above the curve will produce shrinkage and any concentration pairs below this curve will result in tumor growth. The intercepts on the X and Y coordinate axes are the TSC values for a single agent, also expressed in the form of equation (17) for TMZ and equation (19) for ACB. To achieve tumor

shrinkage, dosing of the two agents should be such that concentration pairs, C_{TMZ} and C_{ACB}, are above the TSC curve all the time.

Equation (23) introduces the TSC curve for TMZ and ACB combination therapy in U87 glioma cells. Similar TSC curves can be derived for TMZ in combination with RG7388 or GDC0068 in GBM 10 and TMZ in combination with RG7112 or GDC0068 in GBM 43 xenolines. Assuming similar derivation conditions, TSC curves can be computed for TMZ and SMI combinations (both cytotoxic drug action) in GBM 10/ GBM 43 cell lines. Specifically, the following equation is obtained for the TSC,

$$0 = \frac{k_{g,exp} * V1}{\left(1 + \left(\frac{k_{g,exp}}{k_{g,lin}} * TV\right)^{\psi}\right)^{\frac{1}{\psi}}} - (b_{TMZ} * C_{TMZ} + b_{SMIs} * C_{SMis}) * V1$$

which can be simplified,

$$0 = \left(\frac{k_{g,exp}}{\left(1 + \left(\frac{k_{g,exp}}{k_{g,lin}} * TV\right)^{\psi}\right)^{\frac{1}{\psi}}} - b_{TMZ} * C_{TMZ} - b_{SMIs} * C_{SMis} \right) \qquad (24)$$

During the initial treatment cycle, the denominator $\left(\frac{k_{g,exp}}{k_{g,lin}} * TV\right)^{\psi}$ is negligible compared with 1 and the growth rate is exponential. Simplifying and solving for C_{SMIs} in equation (24) we get,

$$C_{SMIs} = \frac{k_{g,exp}}{b_{SMIs}} - \frac{b_{TMZ} * C_{TMZ}}{b_{SMIs}} \qquad (25)$$

Equation (25) introduces the TSC curve for GBM 10 and GBM 43 xenografts where the drug action of both C_{TMZ} and C_{SMIs} are cytotoxic. TSC values for individual agents can be expressed in the form of equation (21).

Tumor static exposure for TMZ and SMIs

Among the different combination treatment arms, i.e., TMZ combined with SMIs, the combination treatment arm that showed the highest efficacy in-vivo in each of the tested GBM cell

lines was considered for the simulation studies. Based on the system of differential equations (4-through-13) describing tumor volume over time, conditions for tumor stasis in combination therapy were investigated (equations 16-through-25).

In monotherapy, analyses resulted in an estimate of the tumor static concentration (TSC) value; whereas, for combinations of two compounds, analyses resulted in an estimate of TSC pair values producing a TSC curve [67, 70]. An expression of a TSC curve is based on the following reasoning. In Figure 3.2, the main compartment, V1, is the only compartment where cells proliferate. If V1 is eradicated entirely, the tumor will eventually be eradicated as well, i.e., if $\frac{dV1}{dt} < 0$, the tumor will eventually be eradicated. The TSC curve, which separates tumor growth from tumor shrinkage, consists of concentration pairs (C_{TMZ}, C_{SMIs}) such that the left-hand side in the equation equals zero (equation (22) and equation (24)). In combination therapy, solving for concentration in equations (23) and (25) gives the TSC curves for the U87 cell line (combination of cytostatic and cytotoxic agent) and the GBM 10 / GBM 43 cell lines (combination of cytotoxic agents), respectively. Inserting the PD parameter estimates from the base TGI model for U87 and GBM 10 into equation (23) and equation (25), respectively, produced a TSC curve. Monte Carlo simulations were performed to construct the TSC curves relevant to the combination treatment arm that showed highest efficacy in each cell line (U87, GBM 10, GBM 43), for 500 hypothetical individuals (N=500) consistent with the coefficient of variation (%CV) reported for the potency (b) PD parameter terms.

3.6.2 Translational potential

Mouse xenograft flank tumors derived from human GBM tumors were used for translation to clinical doses of combination drug regimens to achieve effective human plasma target concentrations of TMZ. Simulation studies were also performed to translate the PKPD tumor models to a clinical environment. Parameters were assumed to be species independent [84]. For illustration, the PD model describing tumor growth in U87 GBM subcutaneous xenografts was linked to the reported human TMZ plasma pharmacokinetics in [85, 86] to predict the tumor volume at clinically relevant exposures based on a standard dose of 200 mg/m2 given once daily

for five days in a single 28 day treatment cycle. Initial size of the tumor for simulations was considered approximately to be 3 cm* 3 cm, which is based on the clinical observation [11].

3.7 Statistical Analysis

Statistical analysis of the pharmacodynamic efficacy data were performed using 1-way ANOVA or 2-way ANOVA with repeated measures across the varying time points using Excel. The difference in the mean among the individual pairs was determined by Holm-Šídák post hoc test. Comparisons were performed and data were considered significant at $p < 0.05$.

CHAPTER 4. RESULTS

Aim 1: *Develop population pharmacokinetic models for TMZ, and MDM2/AKT inhibitors that target TMZ induced MDM2/p53/p73 and PI3K/AKT/mTOR signaling pathways in GBM*

4.1 Population pharmacokinetic modeling

4.1.1 Pharmacokinetic modeling of temozolomide

Dose-nonlinear bioavailability was observed for TMZ in mouse plasma over a dose range of 5-66 mg/kg. Among the several PK studies used to develop the TMZ PK model, incorporation of TMZ into food, and solution or suspension formulations were used. Thus, bioavailability (F) and absorption rate constant (k_a) parameters were estimated separately by dose and formulation type. Model PK parameters for TMZ were estimated with reasonable precision (coefficient of variation < 40%). Results are summarized in Table 4.1.

Table 4.1. Final parameter estimates for the population PK model: Temozolomide (TMZ).

Parameter[a]			**Temozolomide (TMZ)**		
			Estimate	**%CV[b]**	**%IOV (%shrinkage)**
V (mL)			3.70	16.5	1.06 (43.9)
CL (mL/hr)			3.94	13.9	16.53 (4.9)
Kapo (hr^{-1})	Formulation Type	Solution	27.81	13.8	-
		Suspension	0.33	25.6	34.48 (59.9)
		Incorporation into food	1.86	37.6	-
Kaip (hr^{-1})			7.59	15.4	-
Fp.o.		5 mg/kg	0.177	24.9	-
		20 mg/kg	0.107	9.4	
		50 mg/kg	0.247	10.8	-
		66 mg/kg	0.074	23.4	-
Fi.p.	66 mg/kg mpkmg/	CF1 mdrla (+/+) mice	0.074	17.1	-
		CF1 mdrla (-/-) mice	0.036	18.9	-
Proportional residual error (%CV)			0.24 (14.1)		-

CV, coefficient of variation; IOV, Inter-occasion variability.
CF1 mdrla (-/-): p-glycoprotein knock-out mice
[a]V, Volume of distribution; CL, Clearance; kapo, oral absorption rate constant; kaip, intraperitoneal absorption rate constant; Fp.o. Oral bioavailability; Fi.p. Intraperitoneal bioavailability. [b]The CVs related to the PK model were computed based on Phoenix NLME variance covariance matrix (sandwich method).

In addition, rate and extent of TMZ absorption following intraperitoneal administration [7, 74] in mice with or without efflux transporter, ABCB1, were also estimated, as shown in Table 4.1. Post-absorption disposition of TMZ was best described by a one-compartment PK model. The developed PK Model for TMZ reproduced the mean plasma concentration-time course data, as shown in Figure 4.1.

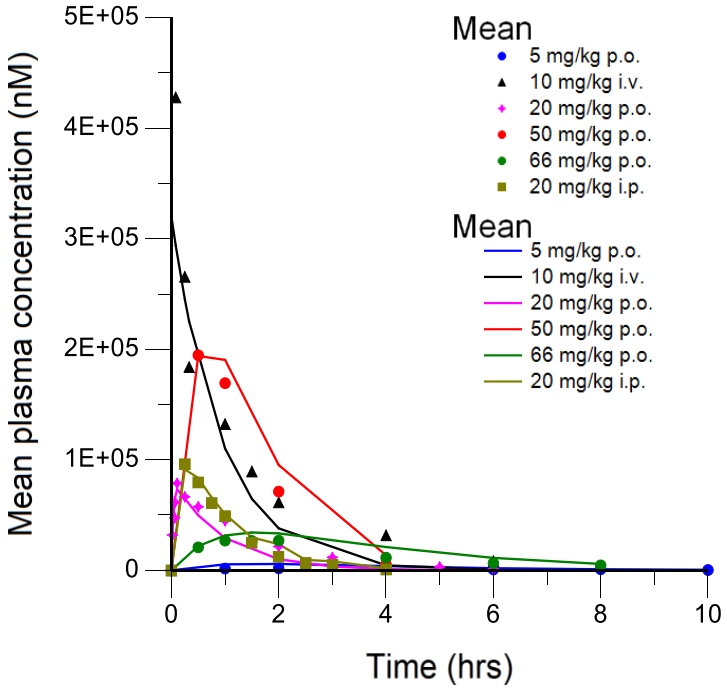

Figure 4.1: Temozolomide (TMZ) pharmacokinetic profiles in mice. Exposure profiles of observed (colored dotted symbols) mean plasma concentrations for TMZ at various doses and routes (top). TMZ plasma concentration data include an original study at 66 mg/kg p.o. and several studies from published sources. The solid lines represent the plasma concentrations fitted by the PK model structure described in Figure 3.1.

Model diagnostic plots: TMZ

Visual predictive checks (VPCs) for TMZ also supported good model performance. VPCs across the range of 5-66 mg/kg TMZ dose for the data obtained from original study and published sources are shown in Figure 4.2. Model predicted vs. observed concentrations, the conditional weighted residuals vs. time and population predicted concentrations for TMZ are summarized in Figure 4.3.

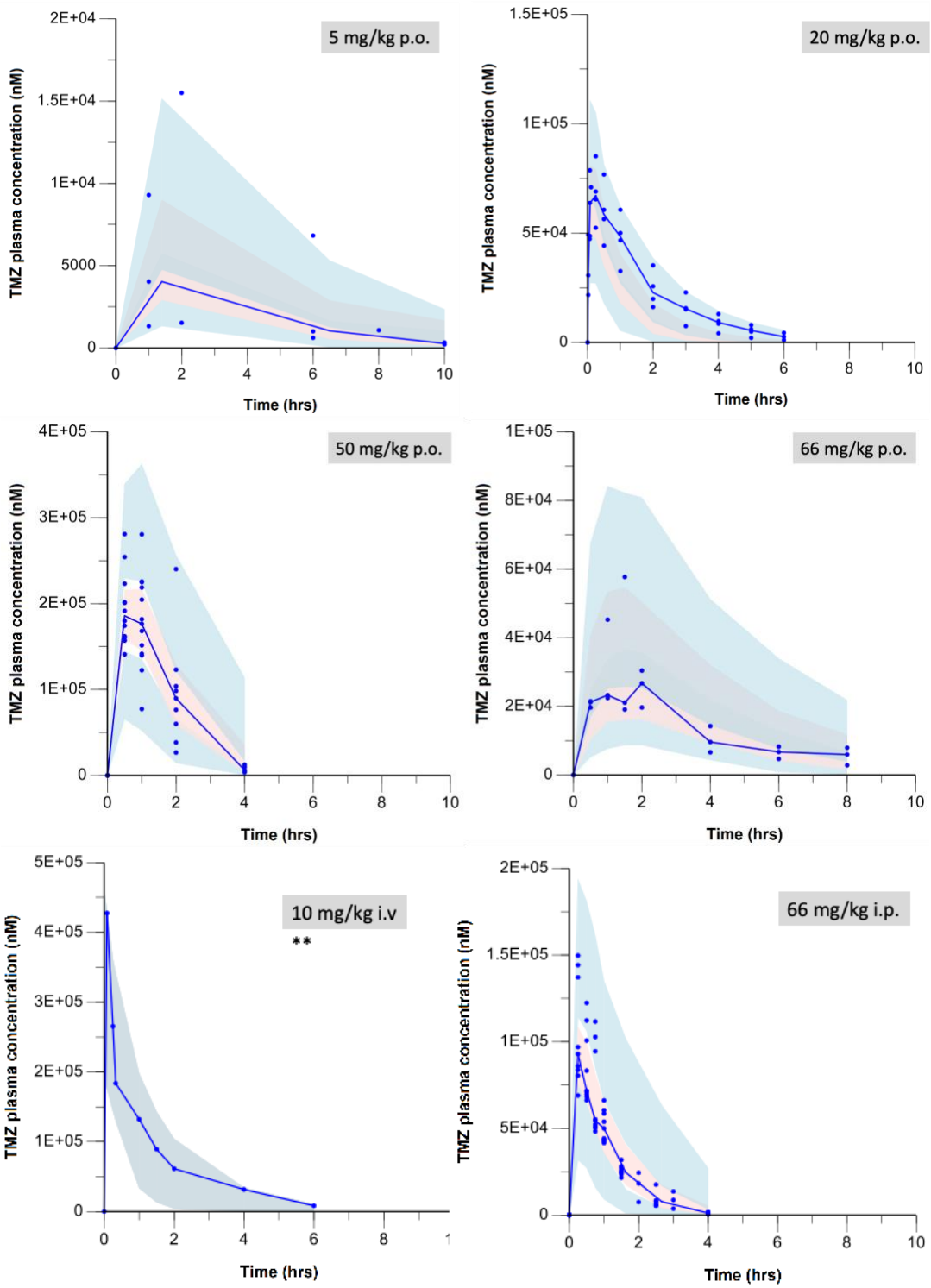

Figure 4.2: Prediction corrected visual predictive checks (pcVPCs) of plasma concentration time courses for TMZ at various doses and routes. The solid blue line represents median (observed) values. Shaded areas are the 95% confidence intervals of the predicted 5th ,50th (pink) ,95th percentiles computed from the simulated datasets (N = 500). The blue dots are the individual data from an original study (5mg/kg p.o., 66 mg/kg p.o.) and published sources (20 mg/kg p.o., 50 mg/kg p.o., 10 mg/kg i.v., 66 mg/kg i.p.). **Mean data at each time point for 10 mg/kg i.v. were extracted from a published source. The shaded area is the 95% confidence interval of the predicted median percentile computed from the simulated datasets (N = 500).

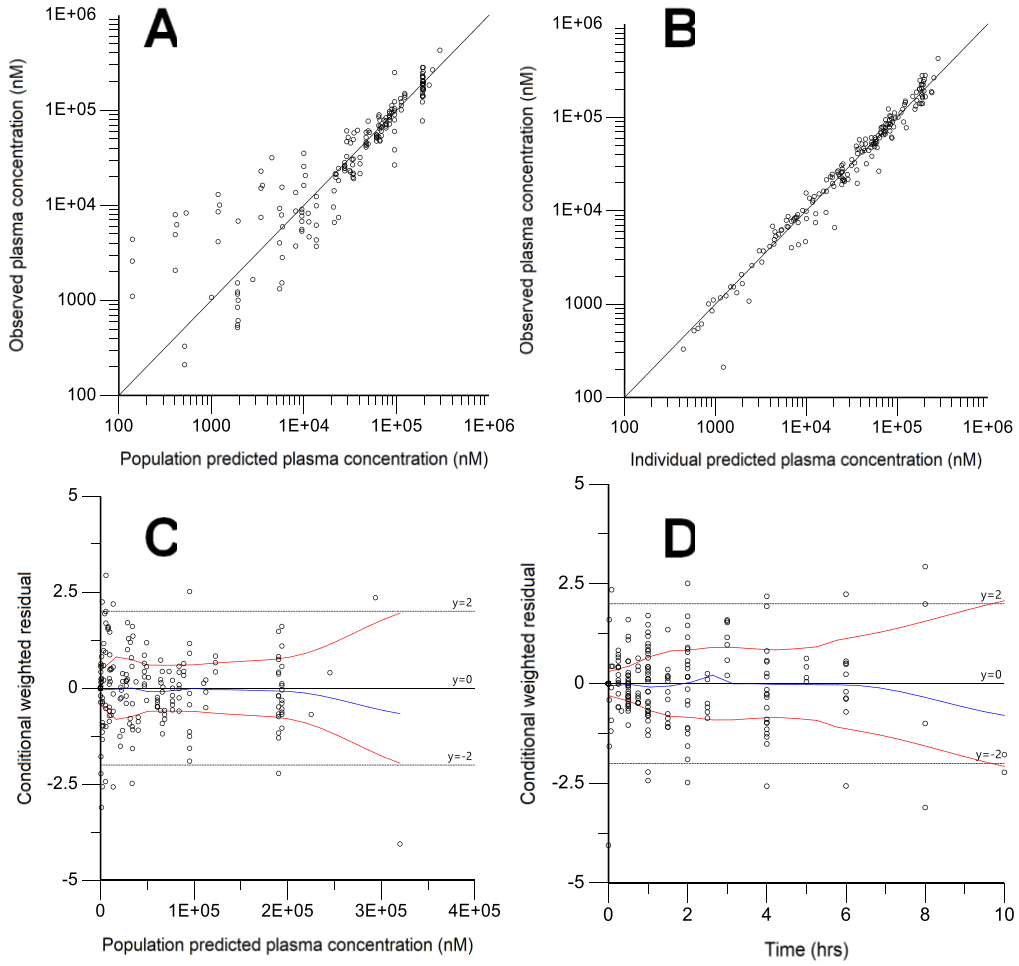

Figure 4.3: Model diagnostic plots for TMZ monotherapy. Observed and model predicted temozolomide plasma concentrations in mice in relation to population predicted plasma concentrations (**A**), and in relation to individual predicted plasma concentrations (**B**). Conditional weighted residual observed in mice in relation to population predicted values (**C**), and in relation to time (**D**).

4.1.2 Pharmacokinetic modeling of small molecules inhibitors

The pharmacokinetics of SMIs (RG7388, GDC0068, and ACB) were described by a one-compartment model with dose-linear kinetics. For ACB, PK data were limited, as these were collected from one published study [2]. The PK parameter (CL/F) was calculated using the descriptive PK parameter estimates information available in that published study [2], and the derived CL/F value was frozen during model development for estimation of the other PK parameters (V/F and ka). PK models for the three SMIs, ACB, RG7388 and GDC0068, reproduced the mean plasma concentration-time course data, as depicted in Figure 4.4.

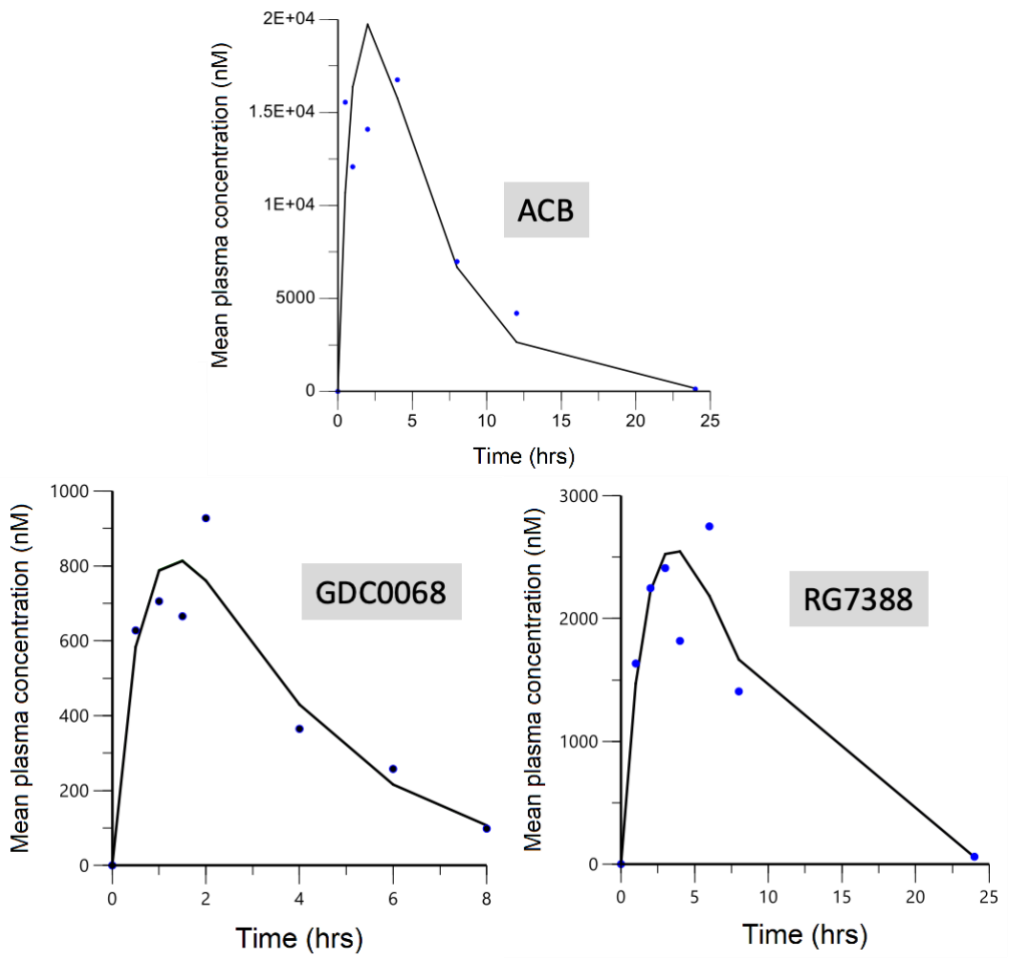

Figure 4.4: Small molecule inhibitor (SMI) pharmacokinetic profiles in mice. Mean observed (blue dotted symbols) plasma concentration profiles for SMIs: abemaciclib (ACB) dosed at 30 mg/kg (top), GDC0068 at 25 mg/kg (bottom left), and RG7388 at 50 mg/kg (bottom right). Solid lines represent plasma concentration profiles fitted by the pharmacokinetic model structure illustrated in Figure 3.1.

PK parameters for small molecule inhibitors (RG7388, GDC0068, and ACB) were estimated with reasonable precision (coefficient of variation < 40%), except the absorption rate constant (kapo) for ACB, which is attributed to scarcity of plasma concentration data for ACB. Parameter estimates for the pharmacokinetic model of RG7112 were taken from the literature [76]. Results are summarized in Table 4.2.

Table 4.2: Final parameter estimates for the population PK model: SMIs.

Parameter[a]	Small Molecule Inhibitors (SMIs)							
	Abemaciclib (ACB)		RG7388			GDC0068		
	Estimate	%CV[b]	Estimate	%CV[b]	% BSV (% shrinkage)	Estimate	%CV[b]	% BSV (% shrinkage)
V* (mL)	42.80	19.1	305.12	6.3	-	1094.1	17.1	-
CL* (mL/hr)	9.96 (fixed)	-	88.28	2.7	-	386.6	6.23	-
kapo (hr^{-1})	0.88	50.9	0.27	4.5	-	1.33	33.76	3.6 (42.4)
Proportional residual error (%CV)	0.3 (3.1)		0.24 (14.3)			0.28 (15.8)		

CV, coefficient of variation; BSV, Between-subject variability.
[a]V*, apparent Volume of distribution (V/F); CL, apparent clearance, (CL/F); kapo, oral absorption rate constant; [b]The CVs related to the PK model were computed based on Phoenix NLME variance covariance matrix (sandwich method).

Model diagnostic plots: SMIs

Visual predictive checks (VPCs) for each SMI also supported good model performance. VPCs are summarized in Figure 4.5. Model predicted vs. observed concentrations, and the conditional weighted residuals vs. time and population predicted concentrations of all SMIs are shown in Figure 4.6 (A-C), confirming that the PK model structure adequately described the data.

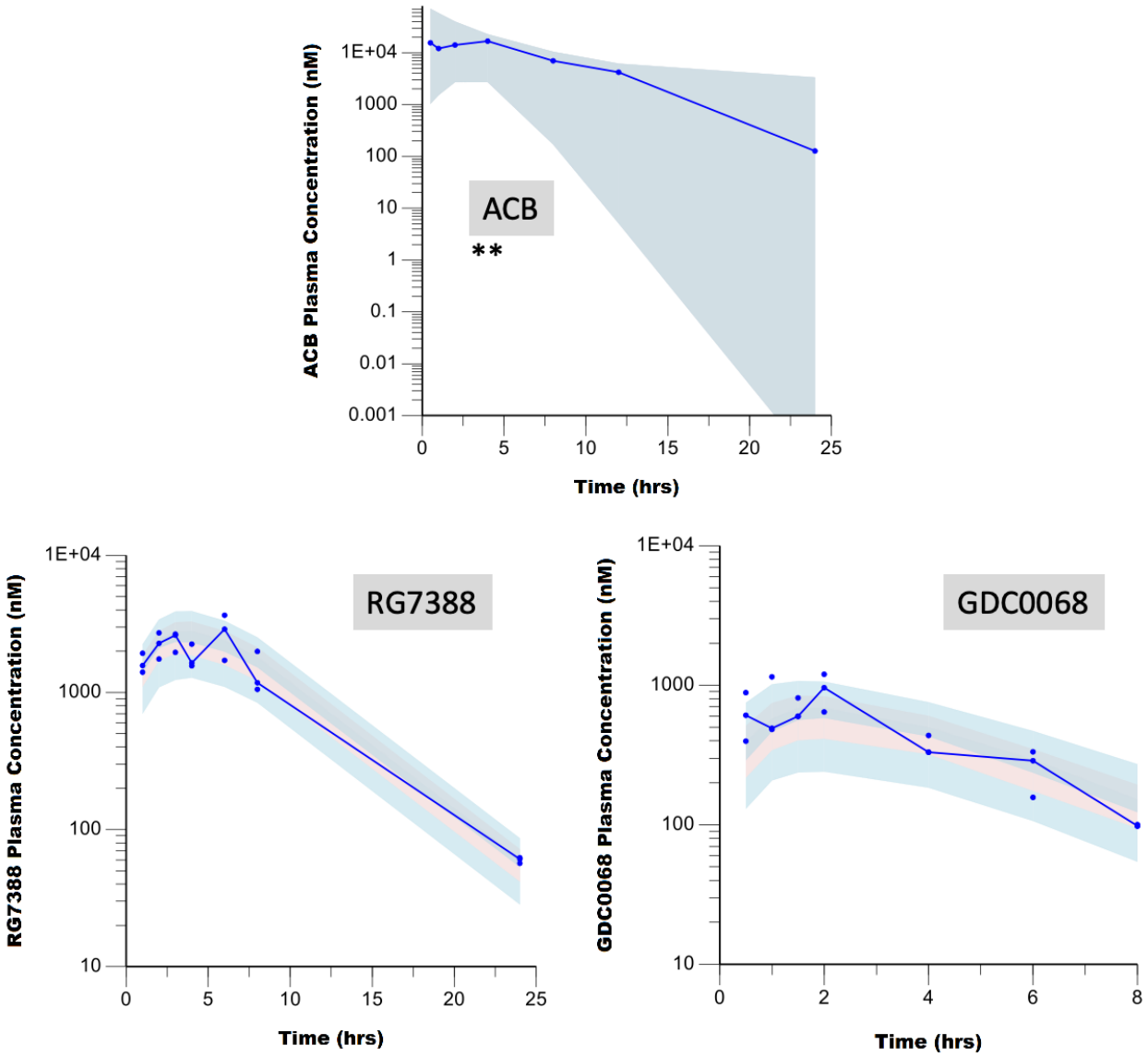

Figure 4.5: Prediction corrected visual predictive checks (pcVPCs) of model predicted drug plasma concentrations over time. Concentrations of abemaciclib (ACB) (top), RG7388 (bottom left) and GDC0068 (bottom right) following, respectively, a 30 mg/kg p.o., 50 mg/kg p.o. or 25 mg/kg p.o. dose. The solid blue line represents median (observed) values. The shaded areas are the 95% confidence intervals of the predicted 5th, 50th (pink), 95th percentiles computed from the simulated datasets (N = 500). The blue dots are the observed data from an original study (RG7388, GDC0068) and published sources (ACB). ACB was extracted from Raub, et al. (2002). **Mean data at each time point for 30 mg/kg p.o. The shaded area is the 95% confidence intervals of the predicted median percentile computed from the simulated datasets (N = 500).

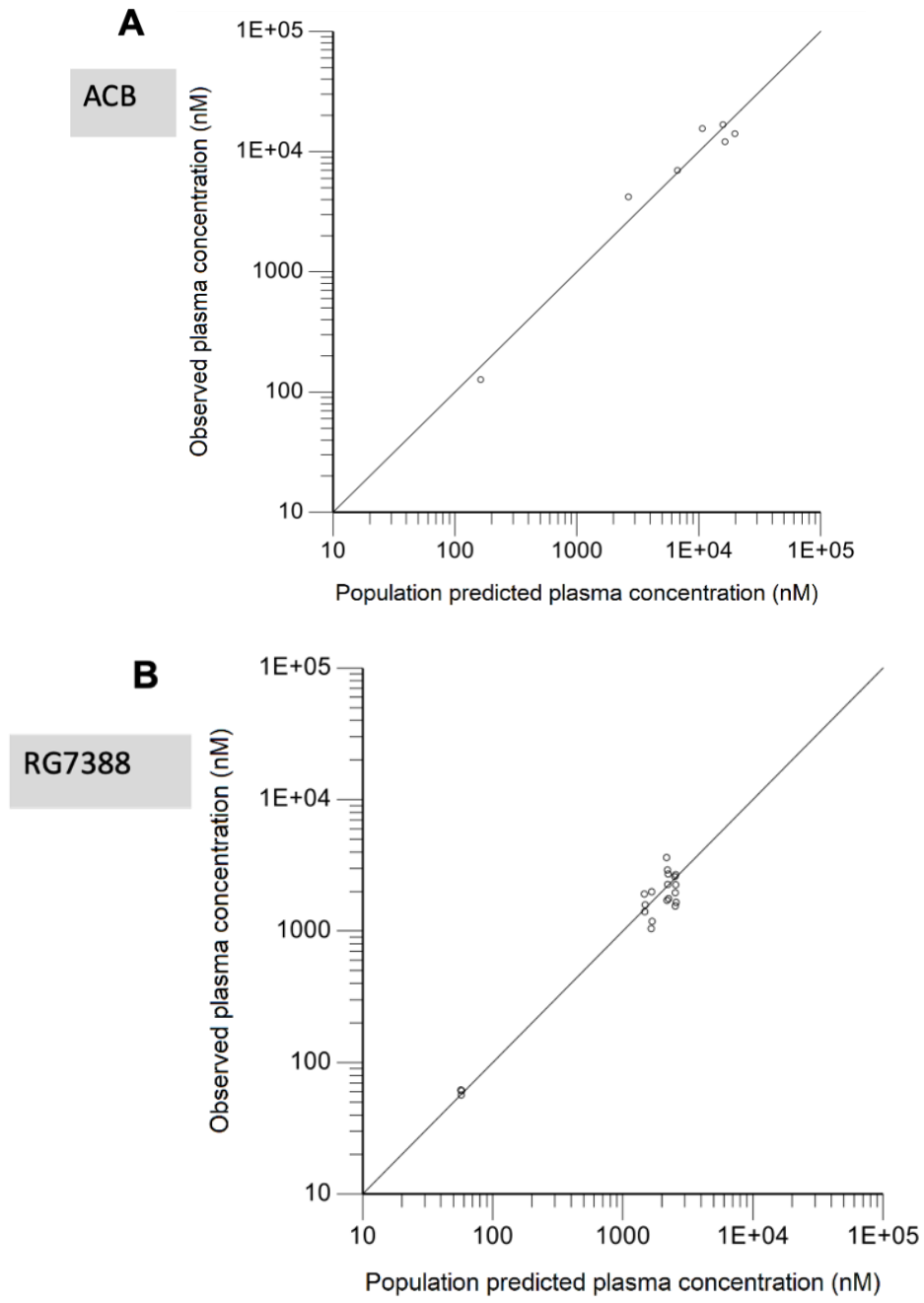

Figure 4.6: Model diagnostic plots of the TMZ and SMIs pharmacokinetic model. (**A**) Observed and model predicted abemaciclib (ACB) plasma concentrations in mouse in relation to population predicted plasma concentrations. Method of Estimation: Naïve pooled approach. (**B**) Observed and model predicted RG7388 plasma concentrations in mice in relation to population predicted plasma concentrations. Method of Estimation: Naïve pooled approach. (**C**) Observed and model predicted GDC0068 plasma concentrations in mice in relation to population predicted plasma concentrations (**I**), and in relation to individual predicted plasma concentrations (**II**). Conditional weighted residual observed in mice in relation to population predicted values (**III**), and in relation to time (**IV**).

Figure 4.6 continued

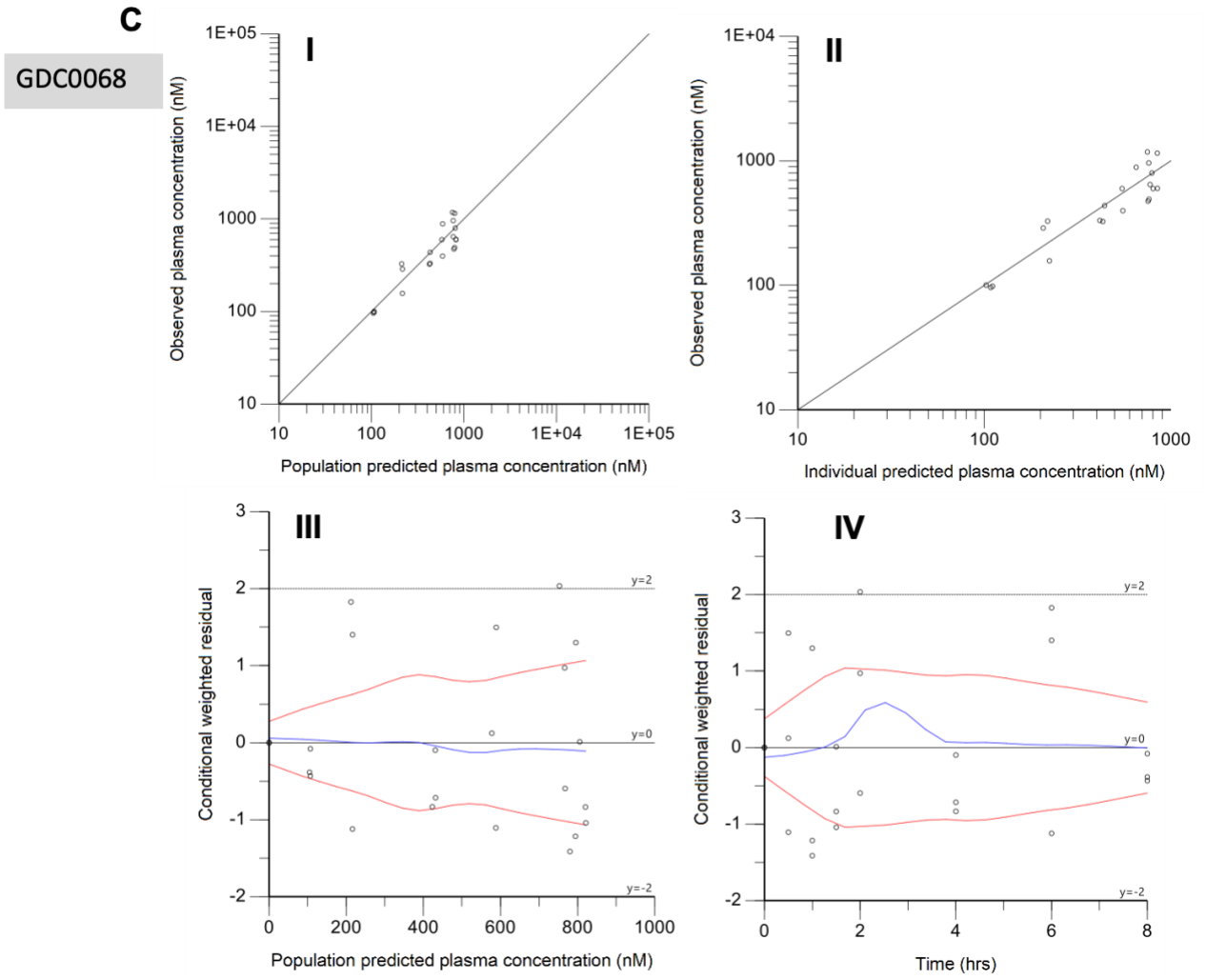

Aim 2: *Perform population pharmacokinetic-pharmacodynamic (PKPD) modeling of tumor growth kinetics in xenograft mouse models in various cell lines (U87, GBM 10, GBM 43) following administration of TMZ with MDM2, CDK4/6 kinase and AKT inhibitors in combination treatment*

4.2 Pharmacodynamic efficacy in various GBM tumor models

TMZ, an alkylating agent previously shown to have activity against human GBM xenografts of diverse histological origin, demonstrated an excellent antitumor activity following oral administration to mice when given alone or in combination with other antitumor agents [2, 37, 87, 88]. In this study, the efficacy of TMZ, when administered alone and/or in combination with

various small molecule inhibitors: CDK46 kinase inhibitor, MDM2 inhibitor, AKT inhibitor across multiple GBM cell models (U87, GBM 10 and GBM 43), was assessed. Small molecule inhibitors used in this experiment: RG7388, GDC0068, and ACB, either given alone or in combination with TMZ, have been studied extensively for potentiating effects in suppressing GBM tumor growth [89-91]. Original efficacy experiments were conducted in Dr. Karen Pollok's laboratory (our collaborator), in the Department of Pharmacology, Indiana University School of medicine.

4.2.1 Temozolomide and CDK4/6 kinase inhibitor (ACB) efficacy in U87 cells

In PKPD modeling, time dependent data of pharmacological events are extremely important. Published data of relevant interest as such can provide additional leverage and aid the model development process. Thus, efficacy data for TMZ and ACB in U87 cells was digitized from the literature.

The study by Wang et. al [37] assessed the efficacy of TMZ 5 mg/kg oral administration in U87 ectopic flank tumors. In ectopic cancer models, the cancer cells are transplanted to the site different from tumor origin site. The data of TMZ efficacy in U87 xenografts were incorporated into the PKPD model. In the published experiment, mice bearing U87 xenografts received TMZ for 5 days/week (Monday through Friday) for two weeks. This was consistent with the TMZ dosing regimen that is used clinically [10]. After the two-treatment cycles, TMZ monotherapy produced significant reduction of tumor volume compared to the vehicle. Tumor growth was inhibited for the duration of the TMZ administration cycle; however, tumor volume began to rebound after stopping the treatment. Body weights were unaffected indicating no treatment related toxicities. This data indicated that TMZ could inhibit U87 growth for around 4 weeks after the dosing stopped. The efficacy of TMZ 5 mg/kg in U87 glioma cells from Wang et al [37] is shown in Figure 4.7(A).

The study by Raub et. al [2], mice bearing U87 subcutaneous xenografts were used to evaluate the effect of ACB antitumor activity when given alone or in combination with TMZ. In this experiment, ACB dosed at 50 mg/kg p.o. or TMZ dosed at 3 mg/kg i.p., suppressed tumor growth, both as monotherapy and in combination. Simultaneous treatment with both compounds produced greater tumor growth inhibition than monotherapy. Treatments showed little effect on changes to body weight, indicating no treatment related toxicities. The published data were

incorporated in building the PKPD model. Efficacy data from Raub et al. [2] are summarized in Figure 4.7 (B).

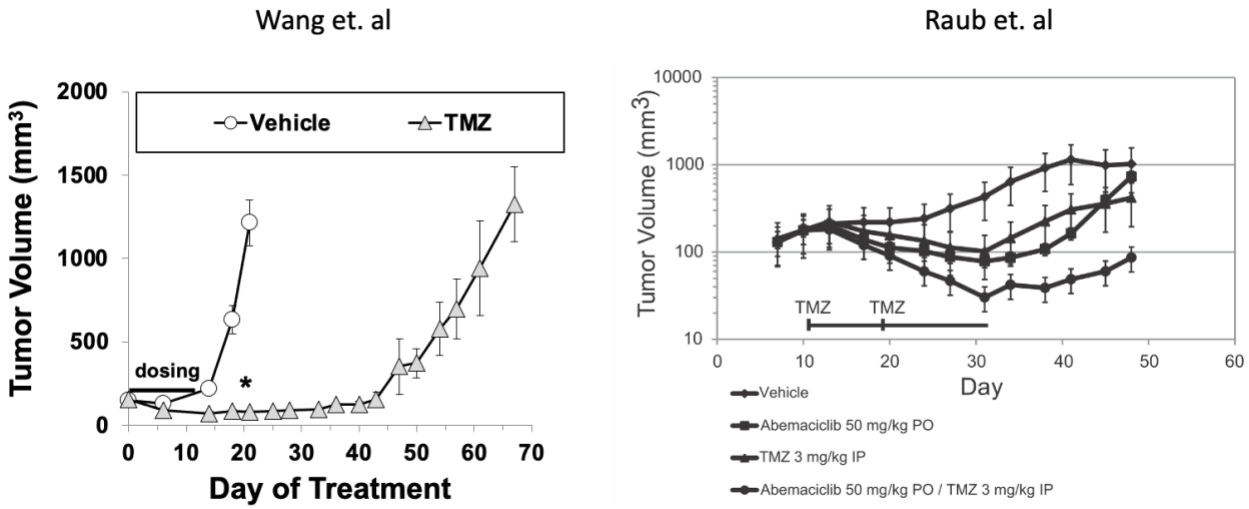

Figure 4.7: Effect of temozolomide (TMZ) and abemaciclib (ACB) on U87 xenograft tumor volume. (**A**) Tumor volume effects on U87 glioma cells after treatment with TMZ. * = $p < 0.05$ compared to vehicle (left graph). The horizontal line indicates the treatment period. (**B**) Tumor volume effects of ACB in combination with TMZ (right graph). ACB was administered orally daily for 21 days and TMZ was administered intraperitoneally one day per week for two weeks, or both drugs together.

The horizontal line indicates the treatment period. IP, intraperitoneal; PO, Oral.

4.2.2 Temozolomide and MDM2 (RG7388) /AKT (GDC0068) inhibitor combinations effects on GBM 10 xenograft tumor volume

Efficacy of TMZ monotherapy and TMZ plus small molecule inhibitors (MDM2/AKT) combination therapy was evaluated in mice bearing subcutaneous GBM 10 xenografts. In this study, TMZ was dosed at 66 mg/kg alone or in combination with RG7388 and/or GDC0068 given at 50 mg/kg and 25 mg/kg, respectively. The study implemented a 5 consecutive days/week dosing regimen, followed by two days holiday, for a total dosing duration of three weeks which mimics the clinical scenario [13]. TMZ produced significant reduction in tumor volume as compared to vehicle for the duration of treatment ($p < 0.05$). After the end of the dosing cycle, tumor slowly started to grow back, indicating that tumors were not completely eradicated. TMZ plus RG7388 and TMZ plus GDC0068 also showed significant inhibition of tumor volume expansion compared with vehicle ($p < 0.05$). TMZ dosed with both the small molecule inhibitors (TMZ plus RG7388 plus GDC0068) showed statistically significantly higher efficacy compared to vehicle ($p < 0.001$), as well as TMZ combined with one of the SMIs ($p < 0.05$). Comparison of body weights to vehicle

control showed little effect of treatment, suggesting that the treatments were well tolerated. Tumor volume effects and body weight measurements are shown in Figure 4.8 (A-B).

Figure 4.8 (C) summarizes the effects of the various treatments on survival. The treatment group that received the combination therapy treatment of TMZ plus both small molecule inhibitors, RG7388 and GDC0068, significantly increased survival by 58 days ($p < 0.001$) compared to vehicle treated animals. TMZ monotherapy increased survival by 39 days compared to vehicle ($p < 0.05$); whereas TMZ combined with either RG7388 or GDC0068 increased survival by 49 days and 35 days, respectively, compared to the vehicle group ($p < 0.05$). Also, TMZ combined simultaneously with both SMIs (TMZ plus GDC0068 plus RG7388) significantly increased survival of GBM 10 bearing mice by 23 days ($p < 0.05$) compared to TMZ plus RG7388/GDC0068 combination. This suggests that combination of two small molecule inhibitors was better able to inhibit the tumor growth and keep the mice alive compared to TMZ plus one SMI.

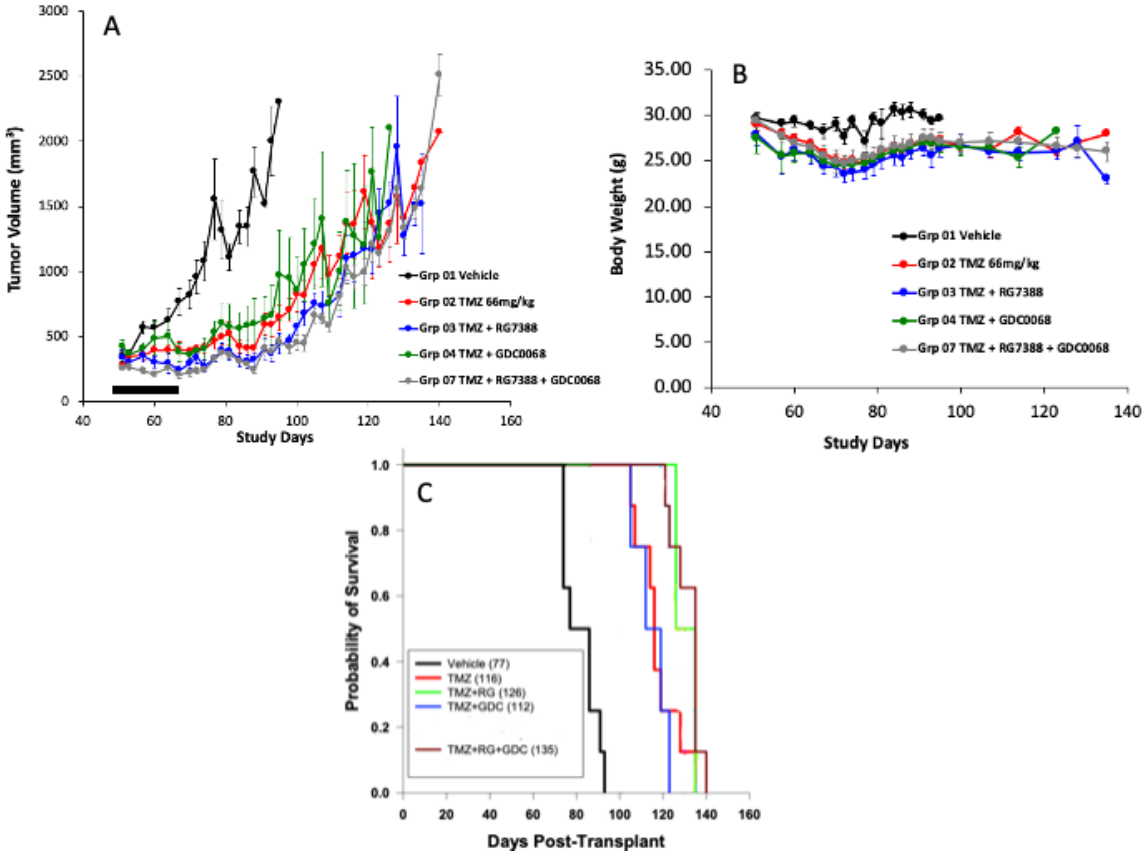

Figure 4.8: Effect of TMZ and small molecule inhibitors on GBM 10 xenograft growth, body weight and survival. **(A)** Effects of TMZ monotherapy and TMZ plus SMIs combination therapy on tumor volume (top left); **(B)** comparison of body weight; the horizontal line indicates the treatment period; **(C)** Kaplan Meier Survival Plots for the various treatment groups. Mean survival time is shown in parentheses in the figure legend. Mice were euthanized when tumor volume reached 2000 – 2500 mm^3. This was considered as the pre-death endpoint.

4.2.3 Temozolomide and MDM2 /AKT inhibitors (RG7112/GDC0068) efficacy in GBM 43

Original experiments were conducted to assess the efficacy of TMZ and MDM2/AKT small molecule inhibitors in GBM 43 cell line flank tumor xenograft bearing mice. In this study, the effect of TMZ monotherapy on tumor volume and survival was evaluated over a wider dose range (0.3 mg/kg to 66 mg/kg) compared to the studies conducted in GBM 10 bearing mice (3.2.2). For TMZ monotherapy, an initial study was conducted at the following doses: 0.3 mg/kg, 1 mg/kg, 5 mg/kg, 10 mg/kg. In two subsequent studies, 10 mg/kg (one study only), 33 mg/kg, and 66 mg/kg doses were evaluated. Efficacy data for the TMZ dose below 10 mg/kg was comparable to vehicle and was not statistically different ($p > 0.05$). TMZ dosed at 33 mg/kg inhibited growth for the first treatment cycle, however, tumor started to grow back by the second week even with continued treatment. This was suggestive of the onset of resistance development to TMZ treatment in mice bearing GBM 43 glioma cells. A higher dose of TMZ (66 mg/kg), though, was able to keep the tumor growth suppressed up to one week after the end of dosing. Tumor volume effects of TMZ monotherapy at various doses across three different studies are shown in Figure 4.9.

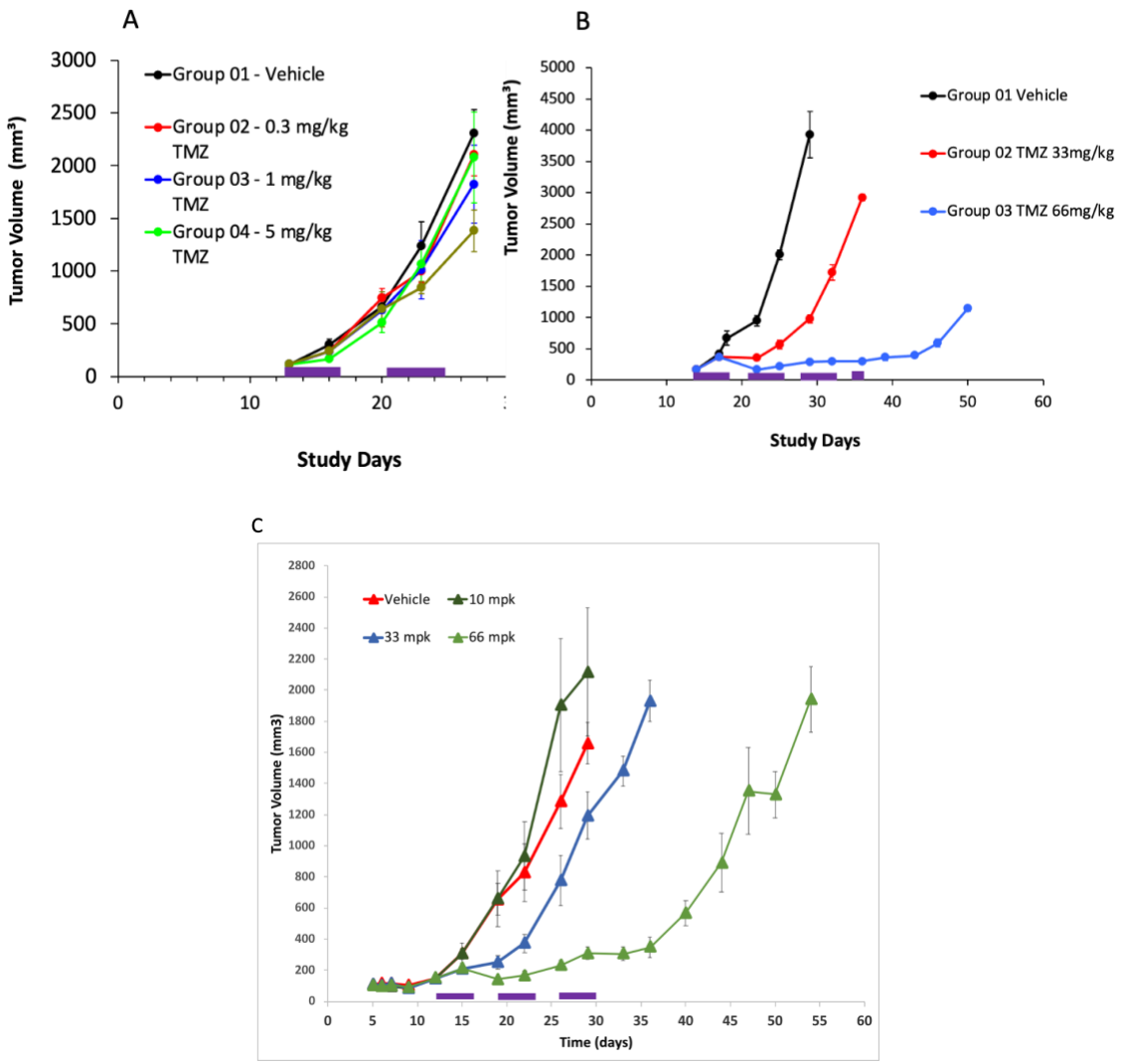

Figure 4.9: TMZ dose response effects on GBM 43 tumor volume in NSG mice. Results are shown as average mean ± standard error of mean for 4 animals per treatment group (**A** & **C**) and 15 animals per treatment group (**B**). The horizontal bar represents the treatment period, dose administered through Monday to Friday with weekend dose holidays.

For TMZ plus small molecule inhibitors (SMI) combination therapy, GBM 43 cells were implanted under the right flank of NSG mice treated by oral gavage with combination of TMZ (10 mg/kg), RG7112 (100 mg/kg) and GDC0068 (100 mg/kg). Figure 4.10 (A-B) demonstrates the statistically significant ($p < 0.05$) delay in tumor growth of two and three drug combinations of SMIs of MDM2 (RG7112) and AKT (GDC0068) variably combined with TMZ in GBM 43 flank tumors relative to TMZ alone. Figure 4.10 (C) demonstrates preservation of body weight for the various combinations, indicating that they were reasonably well tolerated. Safety of these

combinations is also supported by H&E staining of all major organs, which did not show signs of tissue toxicity.

Another pilot study was conducted in mice with GBM 43 flank tumors, wherein animals were treated with 2 cycles of vehicle, TMZ alone or in combination with RG7112 and GDC0068. NSG mice with GBM 43 flank tumors were treated with vehicle, TMZ (10 mg/kg) alone or in combination with 100 mg/kg RG7112, and 100 mg/kg GDC0068. All compounds were delivered by oral gavage QOD for 2 cycles of treatment. As observed in the GBM 43 flank xenograft study summarized in the preceding paragraph, TMG+RG7112+GDC0068 produced a significant decrease in tumor growth compared to vehicle or TMZ monotherapy. Results from this study are summarized in Figure 4.10 (D).

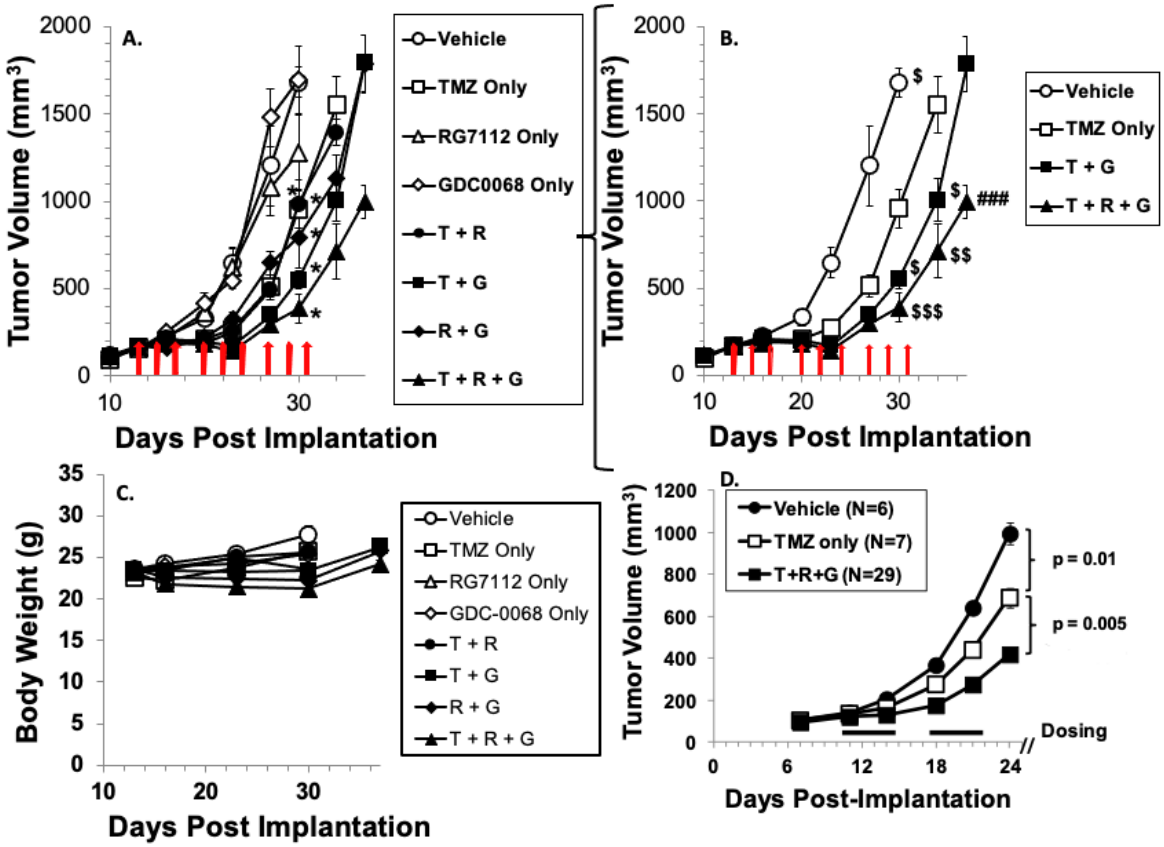

Figure 4.10: Tumor volume effects over time after treatment with TMZ monotherapy and TMZ plus small molecule inhibitors (SMIs) combination therapy on mice bearing GBM 43 subcutaneous xenografts. (**A-B**) Combination of TMZ/GDC0068/RG7112 decreases tumor cell growth significantly using an intermittent dosing regimen with minimal toxicity. Left Upper Panel, Day 30: *p < 0.001 vs Vehicle, Holm-Sidak post-hoc test. Right Upper Panel: $^{\$}$p<0.05, $^{\$\$}$p<0.01, $^{\$\$\$}$p<0.001 vs TMZ Only, Holm-Sidak post-hoc test; $^{\#\#\#}$p<0.001, TMZ+GDC vs TMZ+RG7112+GDC, *t*-test. Arrows represent the dosing duration. **(C)** Body weight measurements over time from the same study depicted in Figures A-B. **(D)** Tumor volume effects over time of TMZ monotherapy and TMZ+RG7112+GDC combination from a separate study. Combination significantly decreases the tumor growth compared with monotherapy p=0.005, TMZ vs TMZ+RG7112+GDC, *t*-test. Horizontal bars show the dosing duration.

Interestingly, among the three GBM PDX models, GBM 43 flank tumors were the only xenografts that evidenced tumor regrowth during TMZ treatment. It was inferred that this rebound in tumor growth while under treatment was due to the onset of resistance to TMZ. To validate this hypothesis and confirm the reproducible resistance development to TMZ monotherapy while under treatment, an efficacy study wherein TMZ was given at 33 mg/kg and 66 mg/kg doses was conducted. A sequential dosing profile for administering TMZ was designed. Administration of antitumor drugs in sequential fashion rather than simultaneously may increase efficacy and provides a promising solution in tumor treatment [92, 93]. TMZ was dosed alternatively at 33 mg/kg and 66 mg/kg and a week dosing holiday was introduced in the third week of a five-week dosing regimen. Sequential dosing paradigms with optimized gaps between treatments have been tried in tumors of other histological origins [94]. Effect of TMZ+GDC combination in tumors already primed with TMZ treatment was also studied. We selected TMZ plus GDC combination based on our efficacy results in GBM 43 xenografts (Figure 4.10). Results of several sequential dosing regimens on tumor volume demonstrated reproducible resistance development to TMZ monotherapy in GBM 43 flank tumors. Results from these studies are summarized in Figure 4.11.

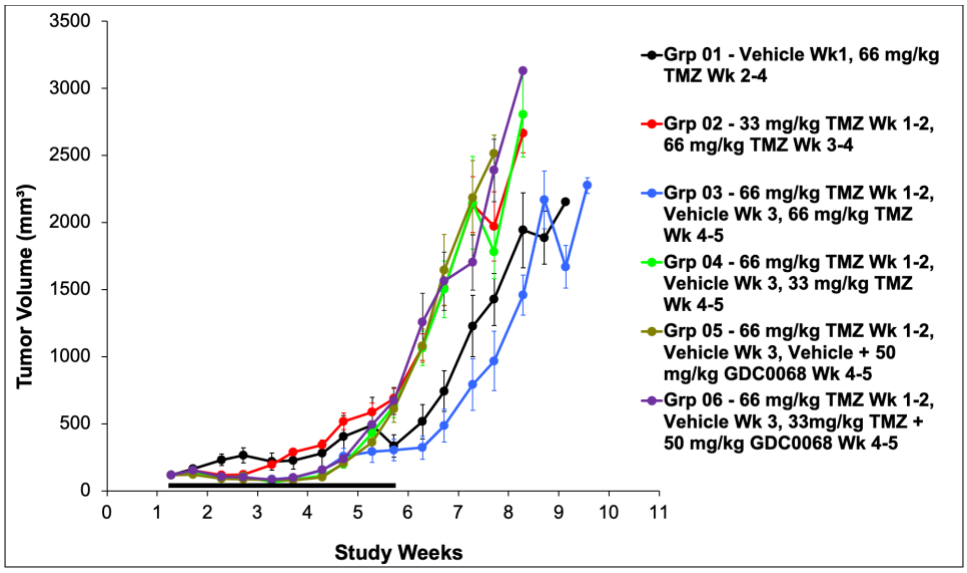

Figure 4.11: Tumor volume effects over time after treatment with sequential schedules of TMZ and TMZ plus small molecule AKT inhibitor GDC0068 in mice bearing GBM 43 subcutaneous xenografts. Results are shown as average mean ± standard error of mean for 10 animals per treatment group. The horizontal bar represents the treatment period, doses administered Monday through Friday for four weeks (Groups 1-2), or with a holiday during the third week in a five-week dosing regimen (Groups 3-6).

4.3 Population pharmacodynamic modeling

The time course of vehicle treated mice in U87, GBM 10 and GBM 43 subcutaneous xenografts was described using the Simeoni et. al. [63] unperturbed growth model (mixed exponential and linear growth). This model of tumor growth gave a superior fit compared to the Gompertz [95] and Jumbe et. al [67, 96] growth models that employ only exponential growth based on the AIC and goodness of fit plots (Observed vs. population predicted, CWRES vs population predicted/time).

4.3.1 PKPD model for mice bearing U87 patient derived xenografts

The previously discussed PK model for TMZ was linked to the tumor volume data from U87 subcutaneous xenografts obtained by digitization of data from Wang et al [28], and Raub, et al [2]. For the latter study, the PK portion was based on 66 mg/kg i.p. plasma concentration data, while the PD treatment arm was from 3 mpk i.p. data. This extent of extrapolation for the dose-bioavailability relationship was not reasonable, because of lack of evidence to identify gaps for effects at very low and very high TMZ doses, the PK parameter for bioavailability ($F_{i.p.}$) was predicted using the developed PKPD model for 3 mpk i.p. and was found to be 0.27 with 6% RSE. Tumor size dynamics were best described using a cytostatic drug action of ACB and cytotoxic drug action of TMZ. The fully integrated population PKPD model (base tumor growth inhibition model) as illustrated in Figure 3.2 successfully described tumor volume change for the vehicle arm, the TMZ treatment arm in relation to the Wang et al study [28], and a vehicle arm and various treatment arms (TMZ treatment arm, ACB treatment arm and TMZ/ACB combination treatment arm) in relation to the Raub, et al study [2]. The PK parameters value did not change and were same as presented in Table 4.1 and Table 4.2 for TMZ and SMIs, respectively. The model results are shown in Figure 4.12, and model PD parameter estimates summarized in Table 4.3. The developed resistance integrated TGI model did not apply to the U87 efficacy data because the dosing was stopped early, prior to tumor regrowth.

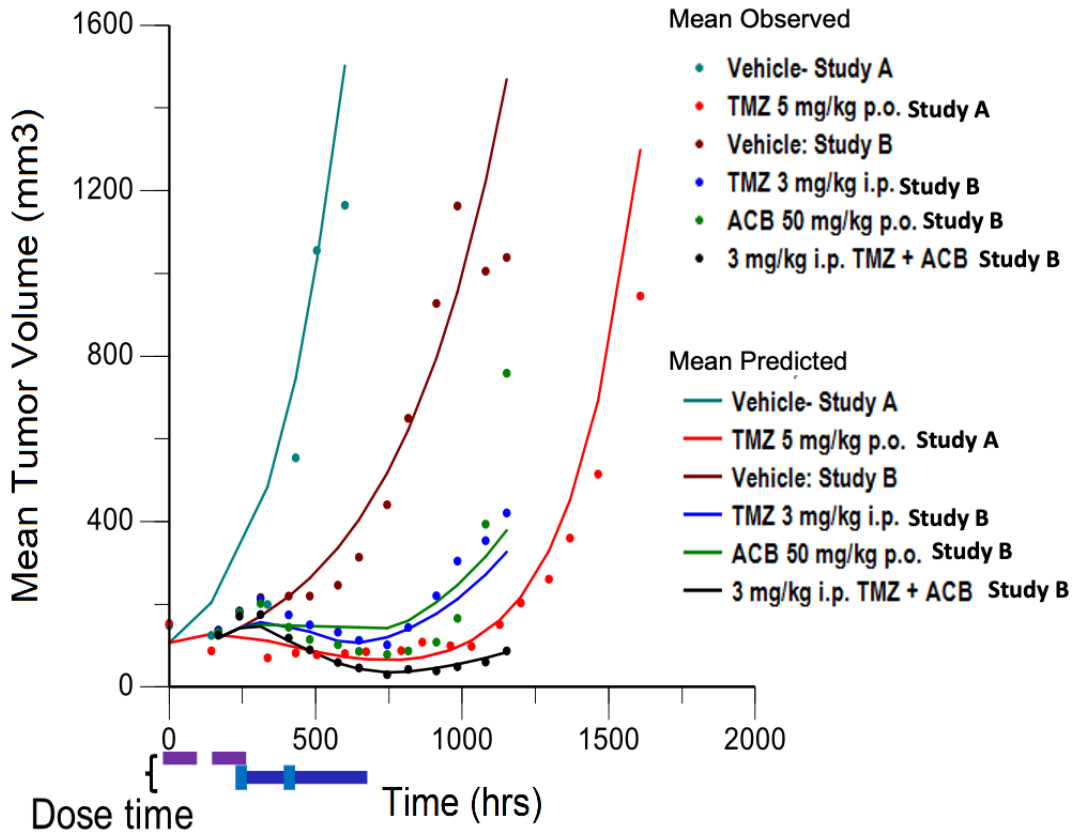

Figure 4.12: PKPD model of U87 xenograft tumor volume growth in NSG mice. Reported mean volumes for tumors are shown as symbols, and predicted volumes are shown as corresponding lines. Dose schedules for the different treatments are shown as the solid color-coded bars labeled as 'Dose time' and are further specified in the text. The purple bars refer to Wang Haiyan et al., and the blue bars refer to Raub, et al, with dark blue referring to ACB and light blue to TMZ. In the legend, study A refers to reported mean volumes from Wang et.al., and study B refers to reported mean volumes from Raub et. al.

Table 4.3: Final parameter estimates for the population PD model for U87 xenografts,

Parameter[a]	Model parameter estimates for efficacy data from Wang Haiyan et. al. [28]			Model parameter estimates for efficacy data from from Raub et. al. [2]	
	Estimate	%CV[b]	%BSV (%shrinkage)	Estimate	%CV[b]
V0 (mm3)	106.64	4.1	-	76.99	10.1
b_{TMZ} (ml/pmol*hr)	1.1E-05	29.5	-	3.0E-05	6.6
b_{ACB} (ml/pmol)	-	-	-	0.00011	5.5
k_g0 (hr-1)	0.0045	6.3	4.3 (51.8)	0.0025	11.3
k_g1 (hr-1)	4.98	11.6	-	9.82	3.9
k_k (hr-1)	0.0055	18.0	-	0.018	7.6
Ψ (psi)	20 (fixed)	-	-	20 (fixed)	-
Proportional residual error (%CV)	0.32 (7.0)				
Time interval for cells to eradicate (τ) (hr)	543.5	-	-	165.17	-

CV: Coefficient of Variation BSV: Between-Subject Variability.
[a]V0; Initial tumor volume, b_{TMZ}; TMZ potency, b_{ACB}; abemaciclib potency, k_g0; exponential growth rate, k_g1; linear growth rate, k_k; transit rate, Ψ; fixed term
[b]The CVs related to the PK model were computed based on Phoenix NLME variance covariance matrix (sandwich method).
Wang Haiyan, et al. [28], 5 mg/kg TMZ was given orally once daily 5 days/week for two cycles. Raub, et al. [2], 3 mg/kg TMZ was administered intraperitoneally once a week for a total of two doses and 50 mg/kg ACB was administered orally once daily for 21 days. [b]The CVs related to the PD model were computed based on Phoenix NLME variance covariance matrix (sandwich method). A Naïve pooled approach was used for parameter estimation.

For the Raub, et al. study, the TMZ/ACB combination treatment arm showed enhanced efficacy compared to the TMZ monotherapy treatment arm. The time for tumor cell eradication following treatment was calculated to be approximately 22 days (543.5 hrs) for TMZ alone. In the case when TMZ was given in combination with ACB, the time for tumor eradication was approximately 7 days (165.17 hrs) (Table 4.3).

Model diagnostic plots: Population PD model for U87 xenografts

Visual predictive checks (VPCs) to validate the PKPD model of U87 efficacy are summarized in Figure 4.13. VPCs supported good model performance. VPCs for the Raub, et al study were not constructed because of scarcity of data, as only mean data were digitized. Model predicted concentrations for U87 gliomas relative to those observed, as well as conditional

weighted residuals, both confirming that the developed PKPD model adequately fits the data, are summarized in Figure 4.14.

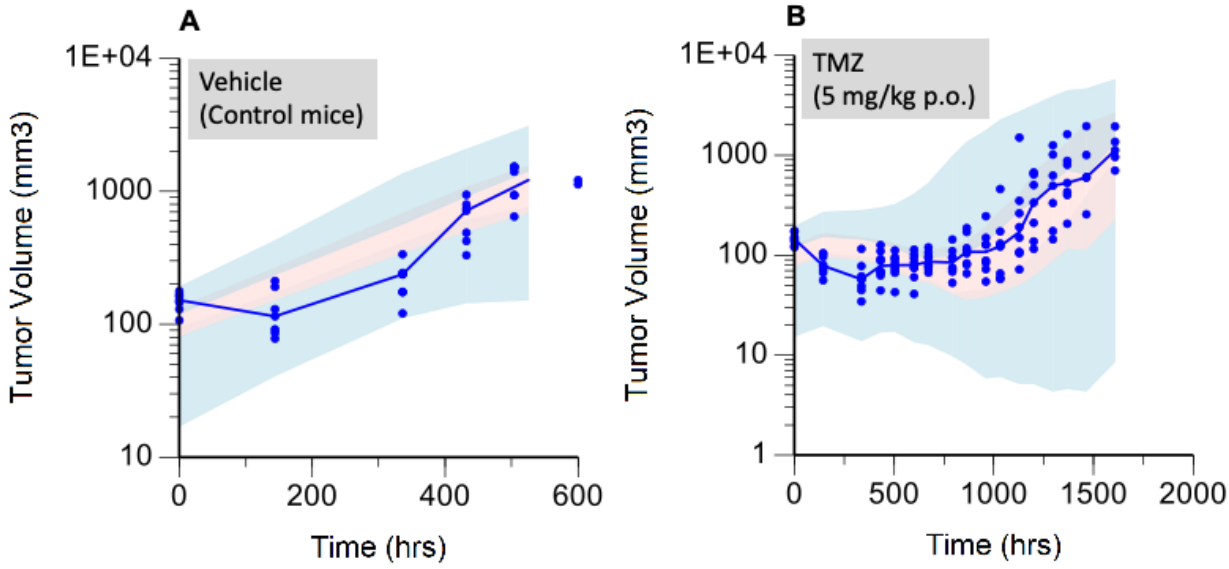

Figure 4.13: Prediction corrected visual predictive checks (pcVPCs) derived from the developed PKPD model of U87 flank tumors in NSG mice from the Wang Haiyan, et al. study. Vehicle **(A)** and TMZ at 5mg/kg p.o. **(B)** tumor volume time courses. The solid blue line represents median of the observed values. The shaded areas are the 95% confidence intervals of the predicted 5th, 50th (pink), 95th percentiles computed from the simulated datasets (N = 500). The blue dots are the observed experimental data.

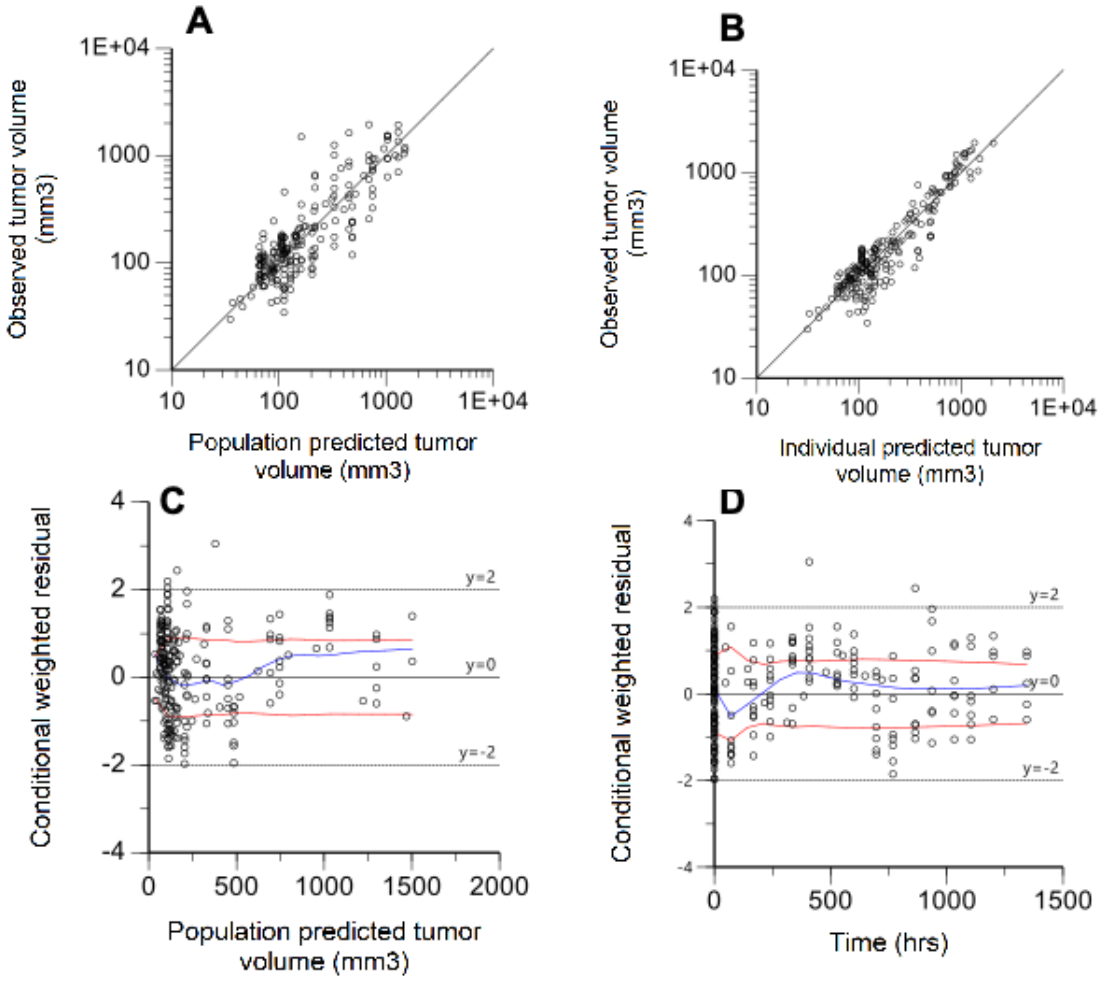

Figure 4.14: Graphical diagnostic plots from the developed PKPD model of predicted tumor volumes in NSG mice bearing U87 flank tumors. Observed tumor volume in relation to population predicted tumor volume (**A**), and in relation to individual predicted tumor volume (**B**). Model conditional weighted residuals observed in relation to population predicted values (**C**), and in relation to time (**D**).

4.3.2 PKPD model for mice bearing GBM 10 patient derived xenografts

For mice bearing GBM 10 subcutaneous xenografts, the efficacy data were best described by the integrated PKPD base model structure depicted in Figure 3.2. Incorporation of resistance into the TGI model was not applicable to the GBM 10 efficacy data because dosing was stopped before the tumor started to grow back. GBM 10 subcutaneous xenografts experienced slow tumor growth after the first treatment dose at day 49 following tumor implantation when tumor size reached approximately 150 mm^3. Interestingly, monotherapy with TMZ demonstrated efficacy equivalent to combination treatment arms in GBM 10 subcutaneous xenografts as shown in Figure 4.15. This is attributed to the high dose of TMZ (66 mg/kg) administered orally in GBM 10 tumor

bearing mice as opposed to mice bearing U87 gliomas (5 mg/kg p.o.) or GBM 43 xenografts (10 mg/kg p.o.). However, the final PKPD model successfully captured all the treatment arms including vehicle (Figure 4.15).

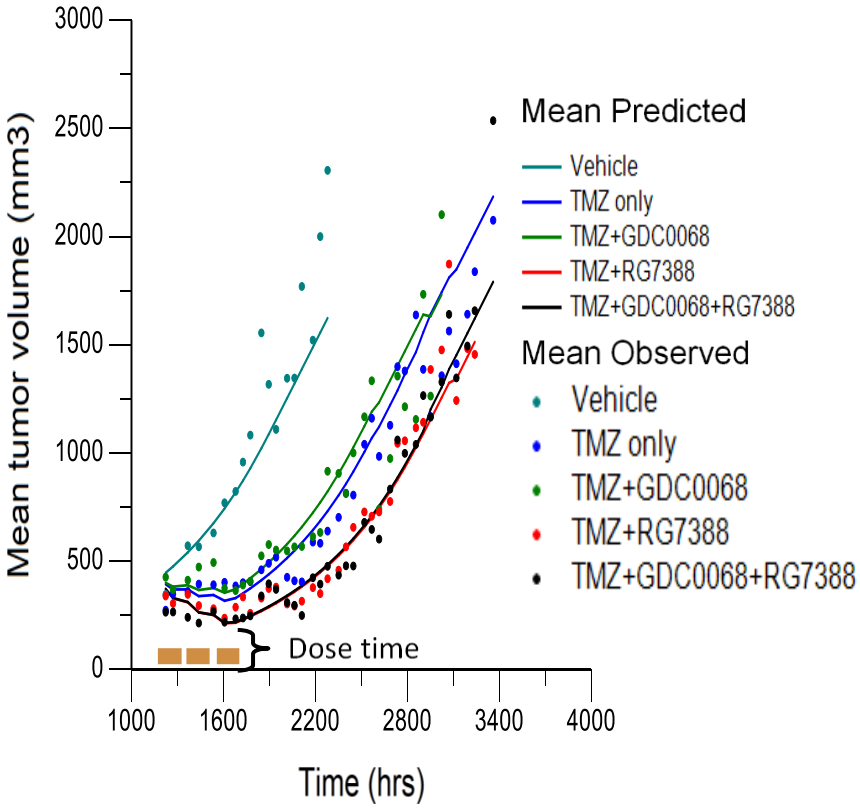

Figure 4.15: PKPD model of tumor volume in NSG mice bearing flank GBM 10 tumors. Observed mean tumor volumes are shown as symbols, and predicted volumes are shown as corresponding lines. Dose schedule is shown as the solid color-coded bars labeled as 'dose time' and consists for 5days/week dosing for consecutive 3 weeks.

The PK parameters value did not change and were same as presented in Table 4.1 and Table 4.2 for TMZ and SMIs, respectively. Model PD parameters were estimated with reasonable precision (coefficient of variation < 40%) (Table 4.4). The exception was the drug potency parameter for GDC0068 ($b_{GDC0068}$), which was estimated to be -1.39E-06 ml/pmol*hr and could not be precisely estimated. This is attributed to the high efficacy of TMZ alone treatment (Figure 4.15); the negative sign indicates an antagonistic effect.

Table 4.4: Final parameter estimates for the population PKPD model for GBM 10 xenografts.

Parameter[a]	**Estimate**	**%CV[b]**
V0 (mm3)	87.47	9.6
b_{TMZ} (ml/pmol*hr)	3.4E-07	13.9
b_{RG7388}(ml/pmol*hr)	1.24E-06	25.4
$b_{GDC0068}$(ml/pmol*hr)	-1.39E-06	-141.1
k_g0 (hr-1)	0.0013	4.4
k_g1 (hr-1)	1.4	11.3
k_k (hr-1)	0.79	20
Ψ (psi)	20 (fixed)	-
Proportional residual error (%CV)	0.36 (5.8)	

BSV: Between-Subject Variability
[a]V0; Initial tumor volume, b_{TMZ}; TMZ potency, b_{RG7338}; MDM2 potency, $b_{GDC0068}$; AKT potency, k_g0; exponential growth rate, k_g1; linear growth rate, k_k; transit rate, Ψ; fixed term
[b]The CVs related to the PD model were computed based on Phoenix NLME variance covariance matrix (sandwich method). A Naïve-pooled estimation approach was used.

Model diagnostic plots: Population PKPD model for GBM 10 xenografts

The TGI model adequately described the data as assessed by visual predictive checks stratified by various treatment arms, where TMZ was given alone or in combination with one or two SMIs (RG7388, GDC0068), as shown in Figure 4.16. Model predictions of GBM 10 tumor volume relative to those observed, as well as conditional weighted residuals are summarized in Figure 4.17. These diagnostic plots supported good model performance.

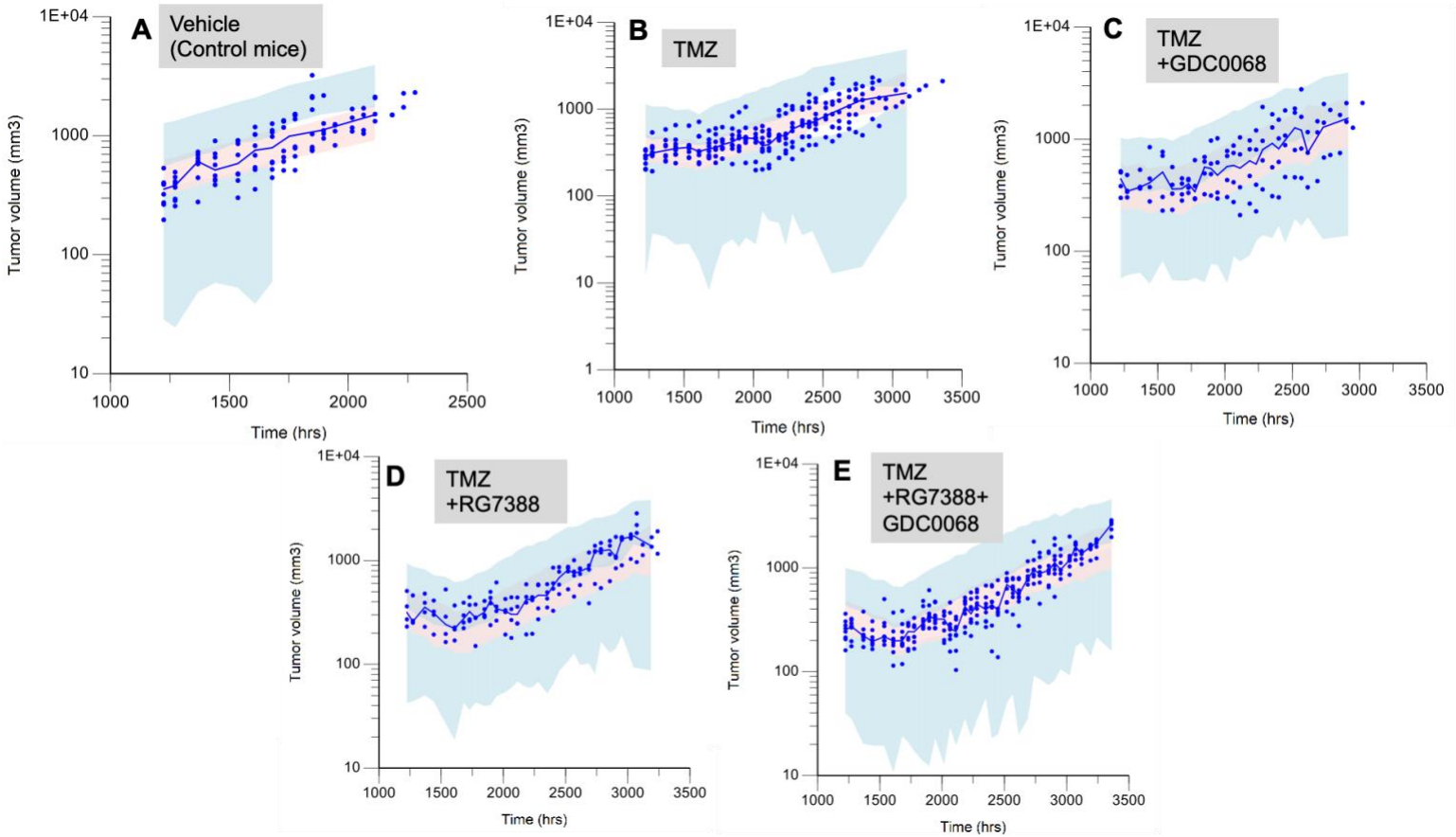

Figure 4.16: Prediction corrected visual predictive checks (pcVPCs) of GBM 10 xenograft tumor growth inhibition model. Tumor volume time course for vehicle **(A)**, TMZ **(B)**, TMZ+GDC0068 **(C)**, TMZ+RG7388 **(D)**, and TMZ + GDC0068+RG7388 **(E)**. The solid blue line represents median observed values. The shaded areas are the 95% confidence intervals of the predicted 5^{th}, 50^{th} (pink), 95^{th} percentiles computed from the simulated datasets (N = 500). The blue dots are the observed experimental data.

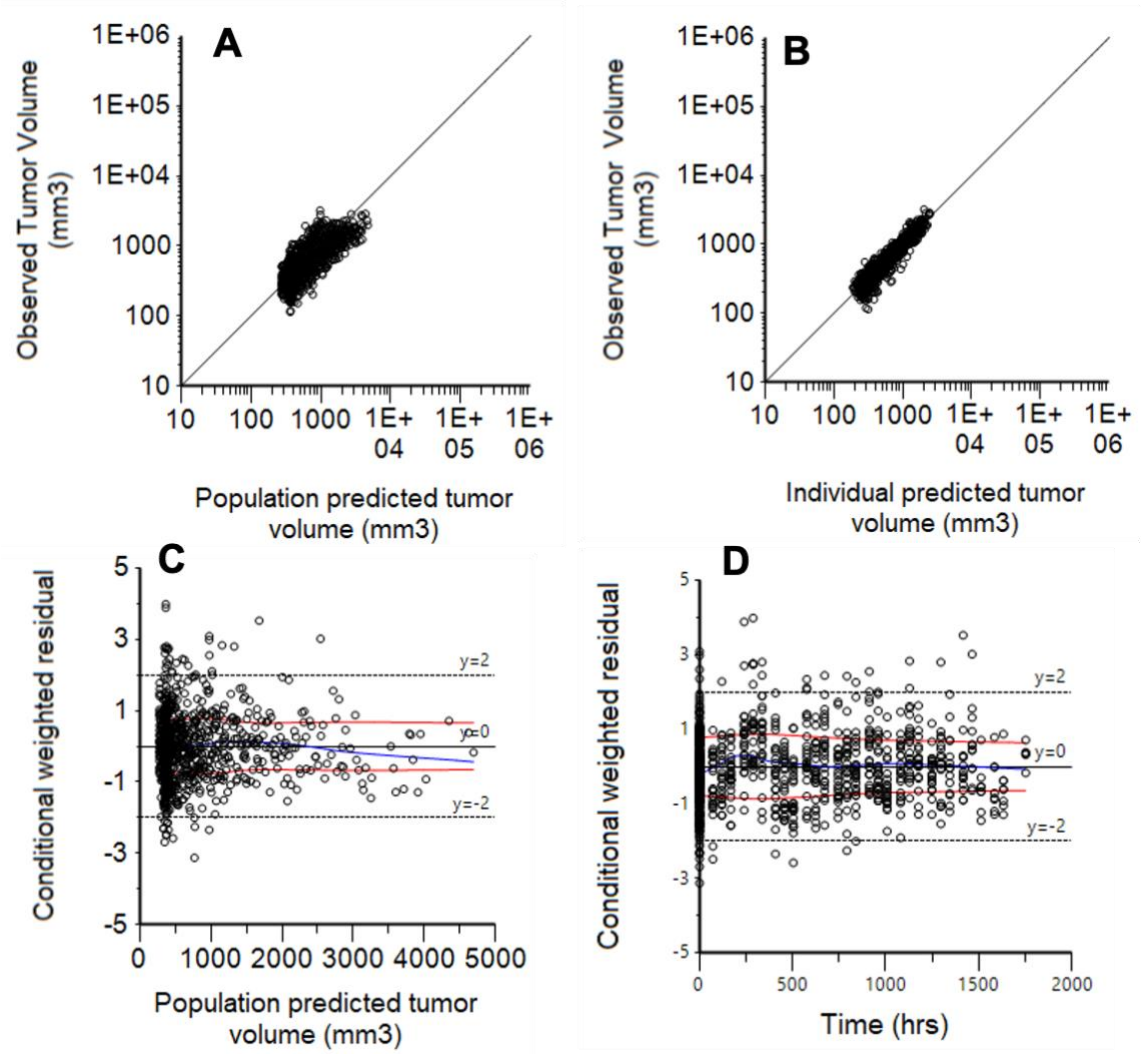

Figure 4.17: Graphical diagnostic plots of PKPD model developed for NSG mice bearing GBM 10 flank tumors. Observed and model predicted tumor volume data in relation to population predicted tumor volume (**A**), and in relation to individual predicted tumor volume (**B**). Model conditional weighted residuals in relation to population predicted values (**C**), and in relation to time (**D**). A Naïve-pooled estimation approach was used.

4.3.3 PKPD model for mice bearing GBM 43 flank xenografts

Exploration of the GBM 43 tumor volume data showed that response to treatment declined toward the end of the second cycle of treatment. Tumor suppression response following the third treatment cycle became negligible (Figure 4.10A-B). This non-responsiveness to the later cycle of drug treatment followed by emergence and continued re-growth of tumor is attributed to the development of resistance. In response to this observation, a resistance component to the base PKPD model (no resistant tumor component) was developed in response to monotherapy only. Because of this evidence of development of resistance in the GBM 43 model, a resistance

component was added to the previously defined model structure (Figure 3.2). This resistance integrated tumor growth inhibition model (Figure 3.3) was used to describe the GBM 43 tumor growth observations. For TMZ monotherapy across the multiple studies and doses ranging from 0.3mg/kg to 66mg/kg, the resistance integrated TGI model was developed and compared with the TGI model without resistance i.e., base tumor growth inhibition model. Both models were evaluated for model performance using AIC. PKPD model fit improved significantly upon incorporation of resistance development (Table 4.5). The results are shown in Figure 4.18.

Table 4.5: Model performance metrics comparison: base TGI model versus resistance integrated TGI model for TMZ monotherapy in GBM 43,

TGI Model TMZ monotherapy	**GBM 43 subcutaneous xenografts**	
	Base TGI model	**Resistance integrated TGI Model**
No. of parameters	8	11
AIC Value	23136.6	23016.6 ($p < 0.001$)
Proportional residual error	0.54	0.52

In contrast to GBM 43 tumors, U87 and GBM 10 tumor growth models incorporating development of resistance did not improve model performance compared to the base model (Table 4.6). In the case of U87 and GBM 10 tumors, lack of resistance development is ascribed to termination of the drug treatment cycle prior to resistance development (see dose legends, Figure 4.12, and Figure 4.15).

Table 4.6: Model performance metrics comparison: base and resistance integrated TGI model in U87 and GBM 10 tumors

TGI Model	**U87 gliomas**		**GBM 10 subcutaneous xenografts**	
	Base TGI model	**Resistance integrated TGI Model**	**Base TGI model**	**Resistance integrated TGI Model**
No. of parameters	15	21	11	14
AIC Value	7586.8	7654.3	16970.6	16994.1
Proportional residual error	0.46	0.52	0.36	0.37

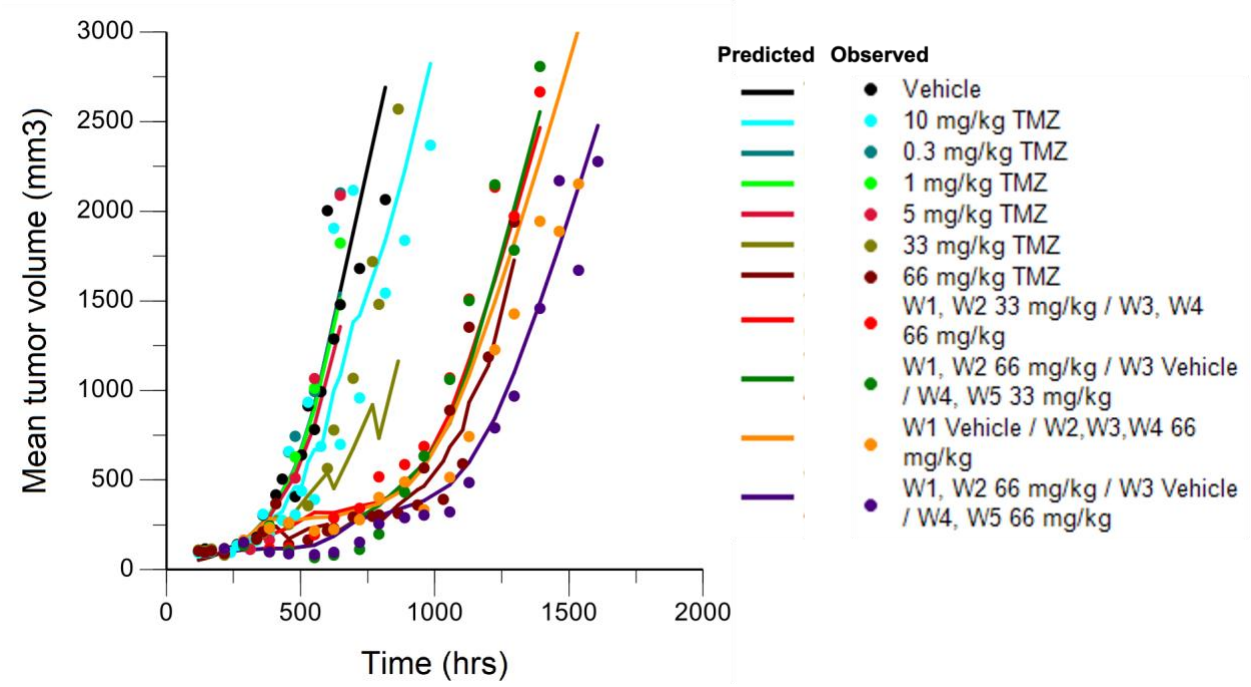

Figure 4.18: PKPD model of tumor volume growth in NSG mice bearing GBM 43 flank tumors and treated with TMZ monotherapy at various doses (0.3-66 mg/kg) across five different studies. Observed mean volumes are shown as symbols, and model predicted volumes are shown as corresponding lines. Dose schedules for the different treatments are shown as the horizontal line and are further specified in the text. Figure legends describe the dosing and sequence regimens. W (1-5) refers week one through five.

TMZ exposure at 33 mg/kg showed an initial response to the treatment, but started to grow back, regrowth evident from the second treatment cycle. TMZ dose at 10 mg/kg and below did not show any significant effect compared to vehicle. TMZ exposure with 66 mg/kg dose was able to keep the tumor growth inhibited for the duration of the treatment, however, tumor growth resumed approximately one week after the dosing ended. Interestingly, for sequential dosing administration of TMZ dosed at 33mg/kg for two weeks, followed by 66 mg/kg for two weeks, TMZ did not suppress tumor growth and it rebounded during the second week of the dosing cycle (Figure 4.18).

For TMZ monotherapy efficacy data across multiple studies and various doses (0.3-66 mg/kg), final model parameters for the PD portion of the resistance integrated TGI model in GBM 43 are summarized in Table 4.7. The PK parameters value did not change in the final PKPD model and were same as presented in Table 4.1 and Table 4.2 for TMZ and SMIs, respectively.

Table 4.7: Final parameter estimates of the population PD resistance integrated TGI model for TMZ monotherapy in GBM 43 xenografts.

Estimate	PD system parameters[a]							
	V0 (mm3)	**Drug potency parameters** (ml/pmol*hr)	**TMZ sensitive cells**			**TMZ resistant cells**		
		b_{TMZ}	**$k_{g,exp}$** (hr^{-1})	**$k_{g,lin}$** (hr^{-1})	**k_k** (hr^{-1})	**$k_{gR,exp}$** (hr^{-1})	**$k_{gR,lin}$** (hr^{-1})	**$k_{S\text{-}to\text{-}R}$** (hr^{-1})
Population value	24.5	1.7 E-06	0.006	6.75	0.035	0.0025	2.18	0.012
% CV[b]	6.5	8	2.6	8.2	20	28.8	17.6	59.4
Proportional residual error (%CV)	0.052 (4.9)							

[a]V0; Initial tumor volume, b_{TMZ}; TMZ potency, $k_{g,exp}$; exponential growth rate, $k_{g,lin}$; linear growth rate, k_k; transit rate, $k_{gR,exp}$; exponential growth rate (resistant cells), $k_{gR,lin}$; linear growth (resistant cells), $k_{S\text{-}to\text{-}R}$; sensitive to resistant conversion rate Ψ; fixed term

[b]The CVs related to the PD portion of the model were computed based on Phoenix NLME variance covariance matrix (sandwich method).

For TMZ-SMIs combination therapy efficacy data, final model parameters for the PD portion of the integrated TGI model are summarized in Table 4.8. The PK parameters value did not change in the final PKPD model and were same as presented in Table 4.1 and Table 4.2 for TMZ and SMIs, respectively. Pharmacodynamic system parameters (TMZ sensitive tumor and resistant tumor parameters) were common for all treatment arms, whereas drug potency parameters were estimated for each drug alone (TMZ, RG7112 and GDC0068) or in combination. Secondary parameters were calculated for growth rates as a ratio for resistant to sensitive cells (equation 14). Ratios for exponential and linear growth rates of resistant to sensitive cells were found to be 2.5 and 1.2, respectively, indicating faster growth of resistant cells. Estimates for average time to tumor cell eradication or resistance emergence (equation 15) is shown in Table 4.8. SMIs administered as monotherapy in mice with GBM 43 subcutaneous xenografts demonstrated comparable growth to the vehicle (control mice). Administration of TMZ in combination with one or both SMIs (RG7112 + GDC0068) showed enhanced efficacy compared to TMZ monotherapy.

Table 4.8: Final parameter estimates of population PD model for GBM 43 xenografts from combination therapy regimens.

Estimate	PD system parameters[a]									
	V0 (mm3)	Drug potency parameters (ml/pmol*hr)			TMZ sensitive cells			TMZ resistant cells		
		b_{TMZ}	$b_{GDC0068}$	b_{RG7112}	$k_{g,exp}$ (hr^{-1})	$k_{g,lin}$ (hr^{-1})	k_k (hr^{-1})	$k_{gR,exp}$ (hr^{-1})	$k_{gR,lin}$ (hr^{-1})	$k_{S\text{-}to\text{-}R}$ (hr^{-1})
Population value	25.21	2.2E-05	1.6E-05	1.3E-09	0.0059	5.76	0.0167	0.0154	6.97	0.0020
%CV[b]	5.8	19.2	23.6	43.7	2.7	9.5	31.5	12.1	6.5	47.9
Proportional residual error (%CV)					0.34 (4.5)					
Average time for resistance cell emergence from sensitive cells (τ)					179.6 hrs					

[a]V0; Initial tumor volume, b_{TMZ}; TMZ potency, b_{RG7338}; MDM2 potency, $b_{GDC0068}$; AKT potency $k_{g,exp}$; exponential growth rate, $k_{g,lin}$; linear growth rate, k_k; transit rate, $k_{gR,exp}$; exponential growth rate (resistant cells), $k_{gR,lin}$; linear growth (resistant cells), $k_{S\text{-}to\text{-}R}$; sensitive to resistant conversion rate Ψ; fixed term.
[b]The CVs related to the PD portion of the model were computed based on Phoenix NLME variance covariance matrix (sandwich method). A naïve-pooled approach was used.

Model diagnostic plots: Population PD model for GBM 43 xenografts.

Model predicted vs. observed tumor volume data for TMZ monotherapy and TMZ-SMIs combination therapy in GBM 43 subcutaneous xenografts are depicted in Figure 4.19 (A-B). The resistance integrated TGI model for TMZ monotherapy and TMZ-SMIs combination therapy in GBM 43 accurately captured the tumor volume data as illustrated by VPCs stratified by treatment arm in Figure 4.20 and Figure 4.21, respectively.

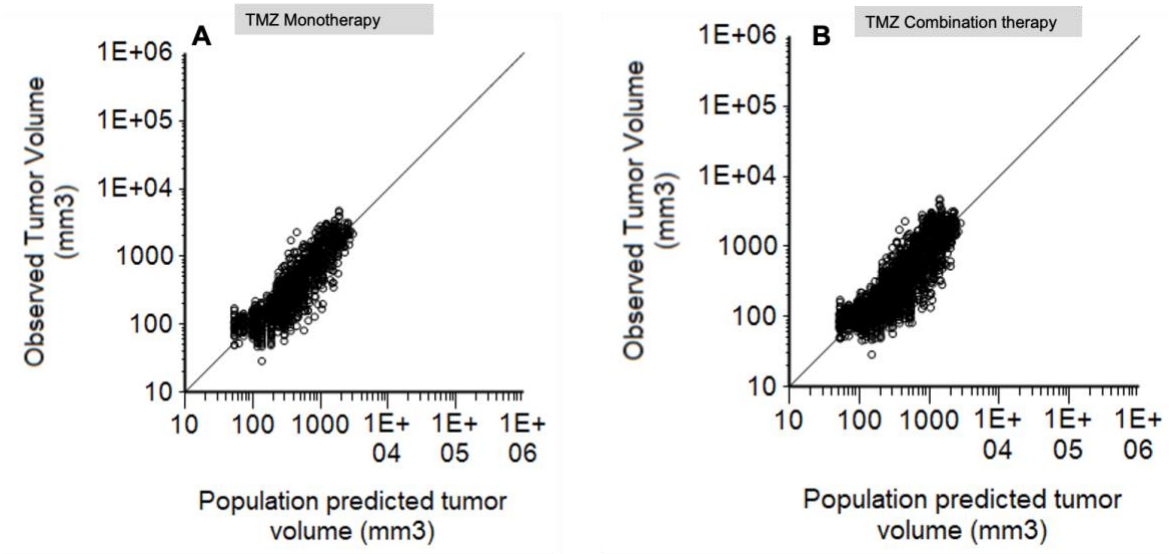

Figure 4.19: Model diagnostic plots of the developed PKPD model from NSG mice bearing flank GBM 43 tumors. Observed and model predicted tumor volume data for TMZ monotherapy (**A**), and for TMZ-SMIs combination therapy (**B**).

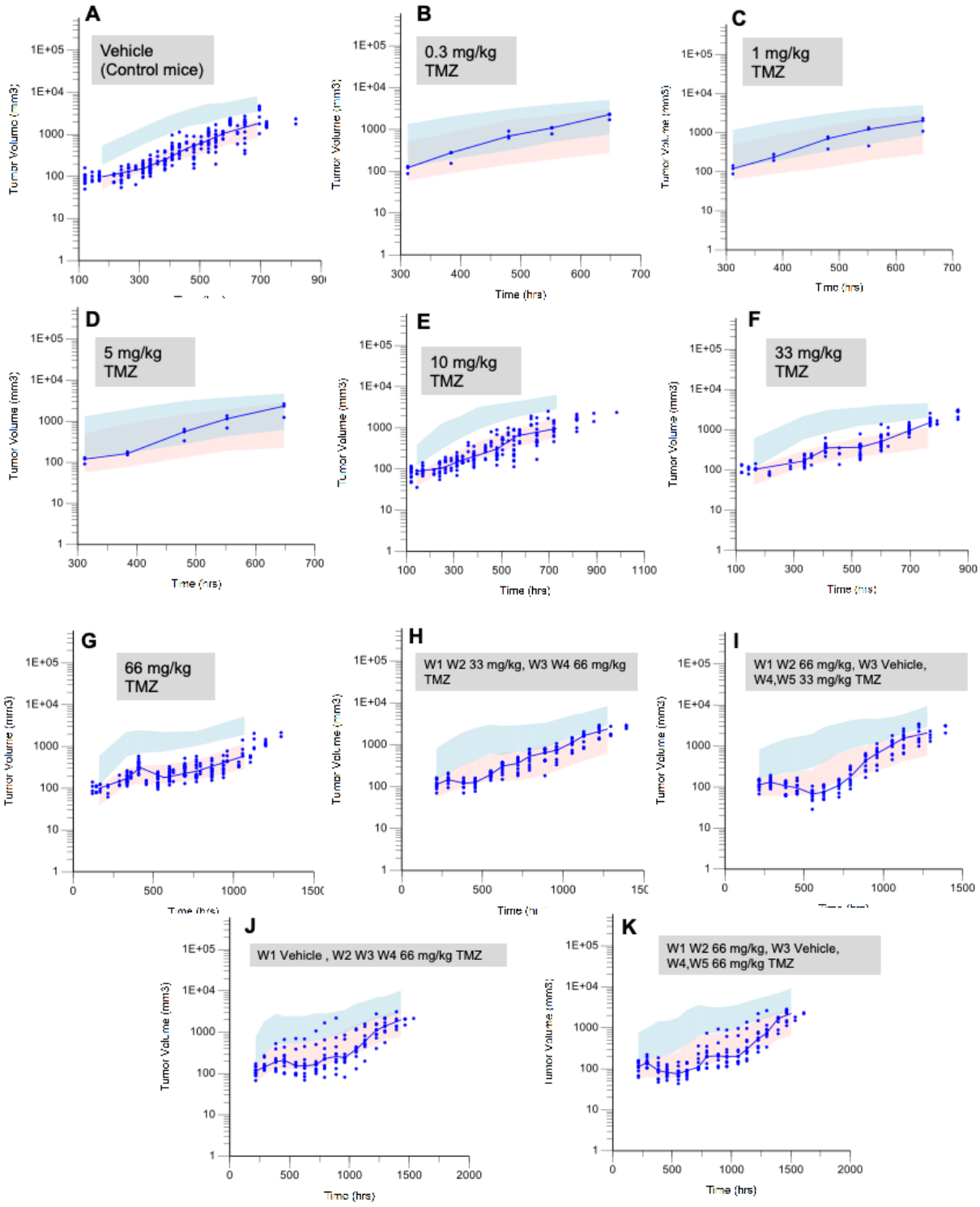

Figure 4.20: Prediction corrected visual predictive checks (pcVPCs) from simulations of the final PKPD model developed from NSG mice bearing GBM 43 flank tumors and treated with TMZ monotherapy. Tumor volume time course for various doses of TMZ monotherapy **(A-G)**, and sequential dosing of various doses of TMZ (**H-K).** The solid blue line represents median observed values. The shaded areas are the 95% confidence intervals of the predicted 50^{th} (pink) ,95^{th} percentiles computed from the simulated datasets (N = 500). Predicted 5^{th} percentile could not be shown in log scale because of the predicted negative values. The blue dots are the observed individual data.

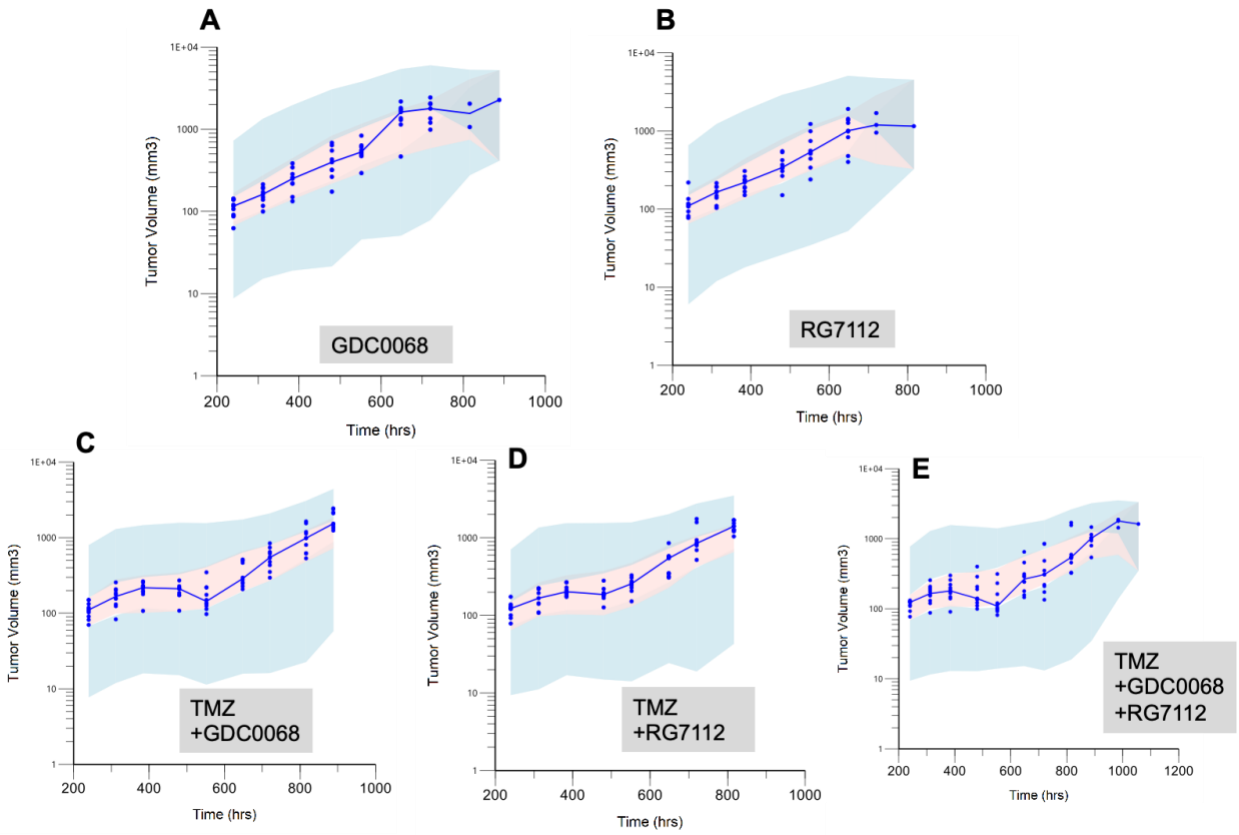

Figure 4.21: Prediction corrected visual predictive checks (pcVPCs) from simulations of the final PKPD model developed from NSG mice bearing GBM 43 flank tumors and treated with TMZ plus small molecule inhibitors. GDC0068 monotherapy **(A)**, RG7112 monotherapy **(B)**, TMZ+GDC0068 **(C)**, TMZ+RG7112 **(D)**, TMZ + GDC0068+ RG7112 **(E)**. The solid blue line represents median observed values. The shaded areas are the 95% confidence intervals of the predicted 5th, 50th (pink), 95th percentiles computed from the simulated datasets (N = 500). The blue dots are the observed individual data.

Aim 3: *Perform simulations and derive Tumor Static Concentration curves that identify single concentration values or the pair of drug concentration combinations that would achieve tumor shrinkage*

4.4 Simulating tumor static concentration curves (TSCs) in combination therapy

The system of differential equations (16-through-25) were applied to predict drug concentrations needed to achieve stasis of tumor growth for either single agent treatments or combination treatments. An expression of a TSC curve is based on the following reasoning: In the TGI model structure (Figure 3.2 and Figure 3.3), the main compartment, V1, is only the compartment in which cells proliferate. If V1 is eradicated entirely, the tumor will eventually be

eradicated as well, i.e., if dV1/dt <0, the tumor will eventually be eradicated. In monotherapy, this analysis results in an estimate of the tumor static concentration value (TSC value); whereas, for combinations of two or more compounds, this analysis results in a TSC curve [70].

4.4.1 TSC curve of ACB-TMZ combinations in U87 xenografts

The developed TGI PKPD model was used to calculate plasma concentrations of TMZ and ACB that would inhibit tumor growth. These concentrations, termed tumor static concentrations (TSCs), are shown in Figure 4.22.

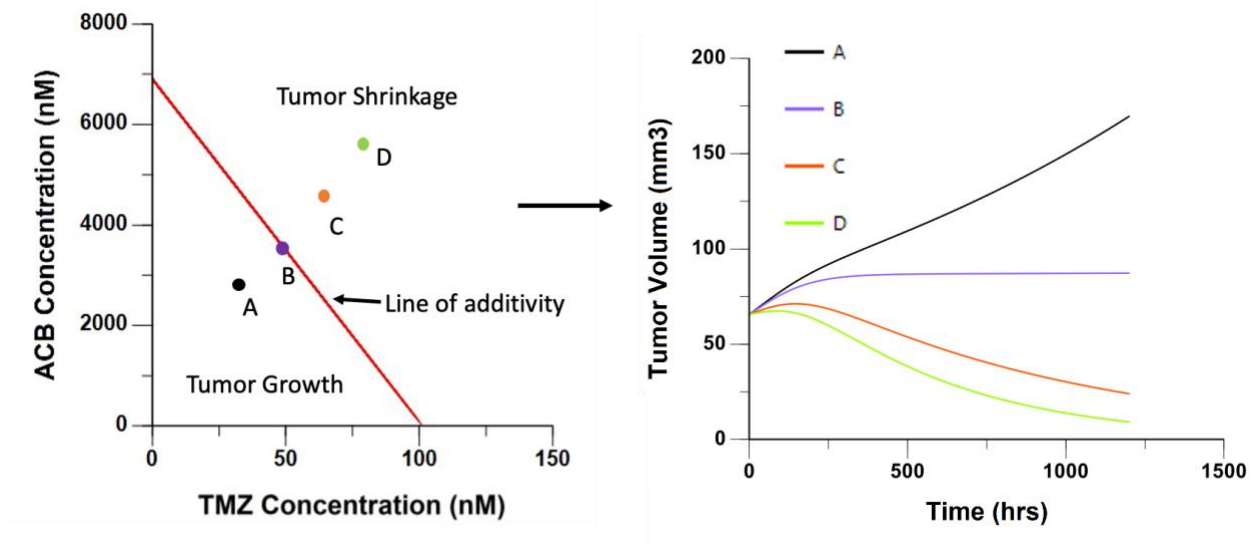

Figure 4.22: Simulation of TMZ/ACB concentrations exerting influence on tumor volume. Tumor static concentration curve for TMZ and ACB combinations and predicted effects of various hypothetical dose regimens (A-D) on tumor growth (left)**.** Predicted tumor volume effect on hypothetical dose regimens (A-D) (right).

In monotherapy, predicted TSCs for TMZ and ACB are the x-axis and y-axis intercepts, respectively. Thus, a dose regimen of TMZ alone that provides an average concentration of 101 nM, or a regimen of ACB alone that provides an average plasma concentration of 6900 nM, would be predicted to arrest tumor growth. (Figure 4.22). The red line connecting the two axes is referred to as the TSC curve. It represents average plasma concentrations of each of the two drugs that would also arrest tumor growth if the drugs were administered as a combination regimen. As an example, a combination regimen resulting in an average TMZ plasma concentration of 50 nM and an ACB concentration of 3500 nM (Point B on TSC line), would inhibit tumor growth, and the tumor would remain in stasis, as shown in graph 3.22 (right). In contrast, a combination regimen

resulting in average concentrations of the two agents below the TSC line, point A (35 nM TMZ and 3000 nM ACB), would be insufficient to arrest, let alone inhibit tumor growth. For combinations of average concentrations of each agent above the TSC line (points C and D), tumor shrinkage would be predicted, as illustrated in graph 3.22 (right). Relevant to the Raub et al. study [97], predicted average ACB concentration over the daily dose interval was 8093 nM, higher than its TSC and, thus, consistent with observed tumor shrinkage (Fig. 3.22). Predicted average TMZ concentration was 40.2 nM over the 24-hour dosing interval, smaller than its TSC of 101 nM. However, simulations (not shown) demonstrated that TMZ concentrations following each of the two doses were > TSC for approximately 4 hours, which apparently was of sufficient duration to kill cells and eventually result in tumor shrinkage.

4.4.2 TSC Curve of RG7388-TMZ combinations in GBM 10

The developed PKPD model of tumor volume growth in GBM 10 adequately described the efficacy data for TMZ-SMIs combination therapy (Figure 4.15). In GBM 10, TMZ plus two SMIs (RG7388 and GDC0068) combination treatment arm showed higher efficacy, however our equations to simulate TSC curves were limited to two drug combinations. Thus, we predicted the TSC curve for the TMZ-MDM2 inhibitor combination treatment arm for demonstrating its qualitative and quantitative application (Figure 4.23).

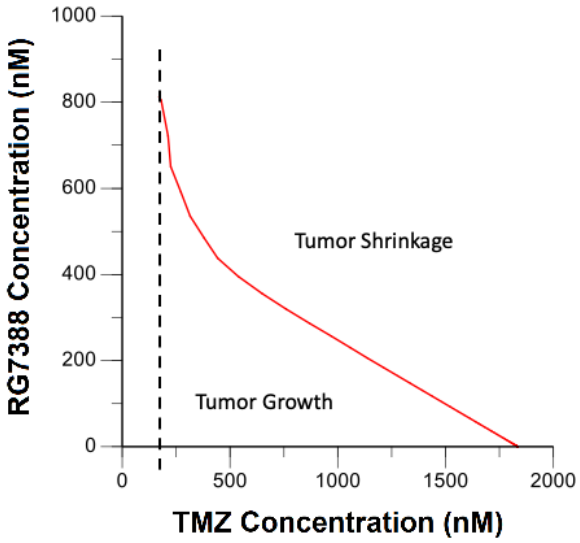

Figure 4.23: Tumor static concentration curve for TMZ and MDM2 inhibitor (RG7388) combination from PKPD model predicted tumor volumes in GBM 10 flank tumor bearing NSG mice. The X-axis intercept shows that the TMZ alone can have the desired effect; whereas absence of a Y-axis intercept for RG7388 shows that it cannot tumor stasis or shrinkage on its own.

Dose regimen of TMZ alone that provides an average concentration of 1600 nM would bring the tumor to stasis. However, when treated with MDM2 inhibitor alone, the compound has no effect on reduction of tumor volume (Figure 4.23). This prediction agrees with the results obtained from experimental studies (Figure 4.10A). It is also consistent with the mechanism of action of MDM2 inhibitor, which triggers the TMZ-induced MDM2/p53 pathway. In fact, TMZ-induced p53/p73 pathway by an MDM2 protein-protein interaction inhibitor improves efficacy in xenografts of recurrent GBM [98]. TSC curves also provide qualitative information. In this regard, the shape of the line indicates if the effect of combination therapy between two or more agents is additive (straight line), synergistic (concave line) or antagonistic (convex line) [70]. Figure 4.23 shows a slight curvature at higher MDM2 concentrations and lower TMZ concentrations, indicating that certain TMZ-RG7388 combination regimens can produce slightly synergistic effects on tumor growth inhibition. The predicted average TMZ concentration from monotherapy (X-axis intercept, 1600 nM) was found to be higher than that predicted for U87 derived xenografts (Figure 4.22). However, it is to be noted that the vehicle growth profile is completely different for these two PDX tumors and the dose of TMZ was very high for GBM 10 xenografts relative to U87 gliomas.

4.5 Translation of a TGI model to predict human exposure

The PKPD model developed to describe tumor growth in NSG mice implanted with U87 cells to generate flank tumors and their response to TMZ and ACB treatment was translated to a clinical environment. To accomplish this, the mouse TMZ PD model was linked to published human TMZ plasma PK parameters [85, 86]. Simulations were performed at clinically relevant exposures following a dose of 200 mg/m2 given once daily for five days in a single 28-day treatment cycle. Subsequently, these exposures were linked with PD parameters describing tumor volume derived from the U87 GBM subcutaneous xenograft model. Initial size of the tumor for simulations was 3cm* 3cm, which is based on clinical observation [4]. This analysis predicted that the tumor would not be eradicated fully, as evidenced by its regrowth (Figure 4.24). Prediction from this translational simulation aligns with the study performed by Wong et. al. [99]. These investigators observed a better correlation between simulated xenograft human TGI linked with human PK at clinically effective doses as compared to TGI based on a maximum tolerated dose (MTD) approach. This approach to translate non-clinical TSC predictions to humans shows how the PD system

parameters from the mouse studies (kg, V0, kk) can be used to identify doses that achieve tumor shrinkage in humans.

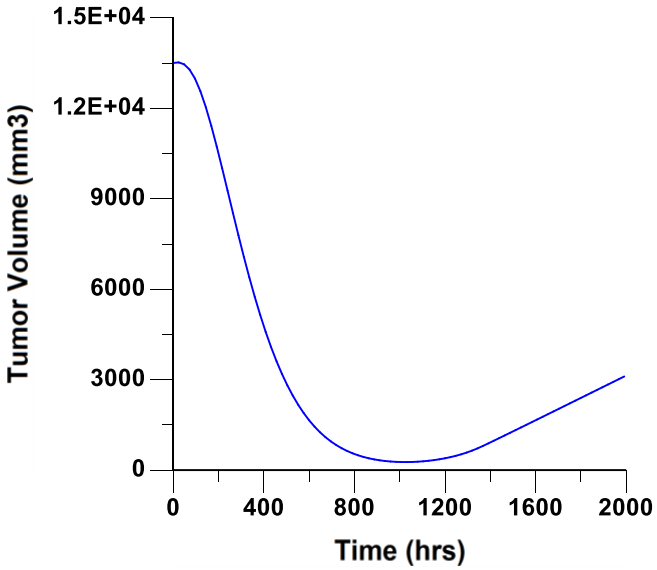

Figure 4.24: Predicted tumor volume time course in humans

CHAPTER 5. DISCUSSION

Molecular characterization of patient derived GBM xenografts has identified several TMZ triggered DNA damage response signaling networks [100, 101]. Preliminary studies in Dr. Pollok's laboratory (our collaborator) have established that TMZ in combination with an MDM2 inhibitor and/or an AKT inhibitor is well tolerated and significantly delays tumor growth in PDX xenografts as compared to TMZ alone. We have extended these findings by developing a PKPD tumor growth inhibition modeling and simulation approach in control animals, and animals receiving TMZ alone or in combinations of TMZ with SMIs. These tumor growth inhibition PKPD models have demonstrated application in identifying combinations predicted to inhibit tumor growth.

Currently, several clinical trials aim to use combination drug regimens to exploit the underlying mechanism of oncogenesis and resistance development [6]. Based on current understanding of therapeutic targets and signaling networks in GBM, we approached inhibiting TMZ-induced signaling pathways with brain penetrant small molecule inhibitors as a means to prolong survival time in GBM. Published data indicate sustained activation of the TMZ induced p53/p73 pathway by MDM2 inhibition [25-27]. In addition, existence of a growth promoting link between MDM2 and AKT networks provided good rationale for dual targeting of Mdm2 and AKT pathways activated by TMZ [4, 9, 28]. The specific contribution of the present work was development of models that predicted tumor growth in response to TMZ administered alone and in combination with targeted small molecule inhibitors (SMIs) of the pro-survival PI3K/AKT/mTOR DDR network, and the anti-apoptotic MDM2/p53/p73 response in patient derived xenograft GBM mouse flank tumors. The value of the developed PKPD models relating chemotherapeutic exposure to pharmacodynamic response, i.e., reduction in tumor size, is that they can be used to explore via simulations the vast arena of possible combinations predicted to be superior to TMZ monotherapy. In this way, they reduce experimentation to identify combination regimens with the highest possible efficacy.

In this modeling analysis, an integrated PKPD tumor growth inhibition model was developed to describe the anti-tumor activity of various small molecule inhibitors: CDK4/6 kinase inhibitor, MDM2 inhibitor and AKT inhibitor when administered in combination with TMZ. Several growth model constructs were evaluated[102], such as the Gompertz model [103], the Jumbe model, and

the logistic regression model; however, the modified Simeoni tumor growth model, which incorporates both exponential and linear growth phases, best described the data. Efficacy data from TMZ-SMIs combinations or TMZ alone were successfully modeled across multiple cell lines of GBM: U87, GBM 10 and GBM 43. The resulting TGI PKPD models (a so-called base model that was applicable to absence of resistance development) and a resistance model (to describe development of resistance to TMZ in GBM 43 xenografts), integrated the pharmacokinetics of TMZ and SMIs to the TMZ elicited induction of DNA damage response, and subsequent change to the tumor cell proliferation cycle and subsequent SMI inhibition of tumor growth. Developing these PKPD models against data across multiple cell lines increases model robustness regarding its application via simulations to identify optimal combination regimens.

Aim 1: *Develop population pharmacokinetic models for TMZ, and MDM2/AKT inhibitors, that target TMZ induced MDM2/p53/p73 and PI3K/AKT/mTOR signaling pathways in GBM*

5.1 Pharmacokinetic Modeling

The integrated PKPD model was developed in a sequential manner. Firstly, a one compartment PK model with first order rate absorption was used to describe the exposure of TMZ and SMIs used in combination. We included all the possible exposure data available; this included data from original studies and data from the literature. This gave a robust PK model for TMZ exposure. However, one of the disadvantages of digitizing mean data is that individual animals are expected to have the same exposure profile and there is no possible way to estimate the between subject variability. This could lead to inaccuracies regarding estimation of pharmacokinetic parameters. In addition, TMZ data obtained from three different routes were used: oral (including a formulation in which TMZ was incorporated into food, as well as solution and suspension formulations), intravenous and intraperitoneal. The model predicted a very high absorption rate for 20 mg/kg TMZ exposure data (Table 4.1). This was attributed to the presence of a high percentage of DMSO in this solution formulation. Also, a one compartment model with first order rate absorption was used to describe the pharmacokinetic profile of small molecule inhibitors. Secondly, plasma concentrations of TMZ and SMIs were related to the in-vivo efficacy data from mouse flank xenografts derived from GBMs obtained from patients.

We observed nonlinear pharmacokinetics over the dose range of 5-66 mg/kg for TMZ in mouse plasma. Non-linear kinetics may be attributed to various pharmacokinetic mechanisms; binding, metabolism and elimination [104]. In our study, we identified dose non-linear bioavailability of TMZ in mouse plasma. This is attributed to either or both the absorption rate constant and bioavailability decrease with increasing doses. A one compartment model with first order absorption generated a poor fit for TMZ pharmacokinetics data. One of the main reasons for this disagreement is the variability in the PK data that we obtained from the various literature sources to develop the TMZ PK model. Pharmacokinetic data for TMZ from multiple sources incorporated TMZ into various formulation: solution, suspension, and food. This variability in formulation type may have contributed to saturation of the dissolution process, resulting in less TMZ available for absorption even with the increasing dose. The modeling approach that we adopted in this scenario was to stratify absorption rate constants and bioavailability parameter estimates by dose and formulation type. Thus, bioavailability (F) and absorption rate constant (k_a) parameters were estimated separately for each formulation type and dose.

Aim 2: *Perform population pharmacokinetic-pharmacodynamic (PKPD) modeling of tumor growth kinetics in xenograft mouse models in various cell lines (U87, GBM 10, GBM 43) following administration of TMZ with MDM2, CDK4/6 kinase and AKT inhibitors in combination treatment*

5.2 Pharmacodynamic Modeling

For U87 tumors, a TGI model with TMZ as cytotoxic agent and ACB as cytostatic compound was used to describe efficacy data in the final PD model. Similarly, TGI model with TMZ and RG7388 as cytotoxic agent was used to describe the efficacy data for GBM 10 xenografts. The PD modeling of each compound, whether it is cytostatic or cytotoxic, was evaluated using either a linear drug effect function or a nonlinear function. The linear drug action was ultimately selected and was based on the AIC criterion. Based on preliminary in vitro experiments (results not shown), in-vitro IC50s (double-digit to triple-digit µM) were much larger than in vivo drug concentrations (nM), which reduced the Hill equation to E_{max}/EC_{50} that we define as term 'b' (linear function of drug action) in our models. The cell death rate (k_k) was 3-fold faster for efficacy data from Raub et. al study as compared Wang et.al study (Table 4.3). This is due to the additive effects of TMZ

and ACB combination therapy. Other PD parameter estimates, such as tumor growth rates and TMZ potency were similar between these two studies in U87 xenografts.

For the base PD model structure (Figure 3.2), it was assumed that there was no PK interaction. This assumption is based on the metabolism of TMZ that, once in circulation, prodrug TMZ spontaneously hydrolyzes to give active metabolite MTIC. MTIC further liberates methyl diazonium ion that alkylates the DNA. The half-life of TMZ is 1.8 hrs. and cleared rapidly from the circulation [14]. Since, ACB is considered cytostatic and TMZ cytotoxic [18], the PD model was structured such that TMZ describes drug action on the loss term (kill rate) of the proliferating cell compartment and ACB inhibits further tumor growth of the proliferating cell compartment. Independence of drug action was also assumed for the MDM2 and AKT SMIs relative to each other and TMZ.

Tumor volumes were distributed to the main proliferating compartment only at the beginning of the treatment. In effect this approach reasonably assumes that the tumor was already existent prior to treatment initiation. For GBM 43 xenografts, an additional resistance compartment was used to describe tumor growth and even regrowth during ongoing TMZ treatment. In the development of this resistance model, a series of models were executed (data not shown) to determine structure with respect to independence of drug action versus pharmacodynamic interaction when two drugs were given in combination. The model structure (Figure 3.3) that incorporated pharmacodynamic interaction showed superior model performance compared to independent drug action as based on the AIC value.

The capability of tumor growth inhibition models to predict the effects of combination regimens is highly resource sparing and reduces the time to identify efficacious regimens. Some of these TGI models now predict tumor growth in response to drug pharmacokinetics [71, 105, 106]. These kinetic descriptions of drug exposure connected to tumor growth facilitate simulations of the multitude of different dosing scenarios possible when combining chemotherapeutic agents that target multiple cancer survival mechanisms. In GBM, there have been a couple of studies from models incorporating unperturbed and perturbed tumor growth model structures that point to unique administration schedules of TMZ with a targeted agent to prolong survival relative to the simultaneous dosing paradigm [107, 108]. The presently developed model descriptions of GBM growth in mouse xenografts in response to combining TMZ with agents targeting TMZ-induced

responsive networks may also be utilized to predict alternative TMZ plus targeted agent dose schedules that would achieve reduction in tumor volume.

In data specific to GBM 43 xenografts, we observed the emergence of resistance to TMZ treatment. We then investigated the acquired resistance to treatment with TMZ and TMZ-SMI combination in patient-derived xenografts for GBM 43. A model structure that incorporated development of resistance supported these observations. The proposed resistance integrated TGI model is the refinement to the base model to accurately capture the TMZ efficacy data in GBM 43 xenografts. It describes the rebound of the tumor after initial treatment while the mice are still undergoing treatment. The model assumes that the drug treatment will affect the tumor cells in the proliferating compartment. In response to the treatment, sensitive cells undergo several stages of damage and are either killed or converted to the resistant cells. In our model we incorporate this conversion as a delayed process, which is consistent with the delayed drug effect [109]. The resistance integrated TGI model adds three more parameters to the model: $k_{g,exp}$, $k_{g,lin}$ (exponential and linear growth of resistant cells) and the first order conversion rate, $k_{s\text{-}to\text{-}r}$ (k sensitive-to-resistant) for sensitive cells that don't die and convert to resistant cells. The time required for emergence of the resistant cells was calculated to be 180 hours. This is the time calculated between the starting of the treatment and when cells reach the resistance compartment. This time can be of value on defining dosing strategy targeting the onset of resistance.

Both the base and resistance integrated TGI models were fitted to the TMZ monotherapy and TMZ in combination with ACB, MDM2 (RG7112/RG7388) and AKT (GDC0068) small molecule inhibitors. With respect to GBM 43 xenografts, based on the principle of parsimony, the resistance integrated tumor growth inhibition model showed a superior fit compared to the base model (based on AIC values, goodness of fit plots and lower residual errors of model parameter estimates). Drug potency specific parameters were estimated separately for TMZ and SMIs in combination with TMZ. Pharmacodynamic system parameters (growth parameters, sensitive cells parameter, resistance cells parameters) were estimated for TMZ monotherapy and TMZ-SMIs combination therapy. On addition of combination treatment arms to TMZ monotherapy, parameter estimates retained their value except for addition of potency parameters for RG7112 and GDC0068 (Table 4.7 and Table 4.8). The assumption that there is a delay between treatment and pharmacodynamic effect is captured by transit rate (k_k), also known as kill rate. Importantly, a GBM 43 resistance integrated TGI model structure based on the presence of innate resistance to TMZ did not result in

a superior model or improve the adaptive resistance alone model to TMZ treatment. Model runs were made that compared these various model structures of primary and/or acquired resistance Based on the principle of parsimony, the model with superior fit was selected. AIC values, residual errors and diagnostic plots indicated that the GBM 43 efficacy data was best described by an acquired resistance model. It is also important to note that all animals bearing GBM 43 xenografts initially responded to the TMZ treatment. Thus, although there may be an innate resistant component to these tumors, this initial response prevented estimation of this component. Accordingly, a population of cells with innate resistance were considered negligible at the start of treatment. [110].

Aim 3: *Perform simulations and derive Tumor Static Concentration curves that identify single concentration values or the pair of drug concentration combinations that would achieve tumor shrinkage*

5.3 Simulation Studies

The concept of tumor static concentration curves is not new [70, 111]. It is very similar to the concept of isobolograms [112, 113]. TSC comes from the exposure-growth model instead of dose-effect model. In the present studies, TSC curve analyses were based on the Simeoni growth model [63]. In this tumor growth model, growth occurs exponentially and switches to linear (constant, zero-order) growth as the tumor grows large. The relationship between tumor growth and tumor static concentrations was investigated. Weak synergy for RG7388 and TMZ in GBM 10 can be seen in the TSC curve (Figure 4.23). One of the assumptions made on deriving the TSC curve for the presently developed exponential/linear growth mixed tumor inhibition model was that the tumor maintains its exponential growth rate. This approximation is necessary in order to have concentration pairs of TMZ and small molecule inhibitors above the TSC curve to achieve tumor volume shrinkage. In this study, we only discussed the TSC graph for the base TGI model i.e; TGI model for mice bearing U87 and GBM 10 xenografts. However, TSC graphs could not be constructed for the TMZ acquired resistance integrated TGI model in mice bearing GBM 43 xenografts, as one of the main assumptions in deriving the TSC curve is that the net change in tumor volume over time in the cell proliferating compartment is zero, and this assumption does hold in the case of growth of resistant cells.

The tumor static concentration curves presented (Figure 4.22 (left), Figure 4.23) also provide insight regarding the efficacy of the compound and in-vivo sensitivity. We can leverage this graph to select the concentration pairs that require minimal exposure to achieve the tumor stasis. Similarly, concentration of a single agent required to produce stasis may be high and result in toxicity. In that scenario, we can utilize a TSC approach to optimize the combination regimen to lower the concentration of one drug and increase the concentration of other to achieve tumor shrinkage with minimal toxicity. The TSC cases in Figure 4.22 and Figure 4.23 represented scenarios involving two drug combinations. Using more sophisticated mathematical equations, the use of TSC concept can be explored further for three or more drug combinations to generate TSC surfaces.

The approach of developing TSC curves for combination drug therapy is based on the work of Gabrielsson, et al [67]. It is important to note that while the results in Figure 4.21 are based on a population PK model for TMZ developed from several published studies, the TSC curve could have been built from a single PK study of each agent and then linked to a single tumor growth study of the two agents administered individually or in combination. The combination dose could be the simple sum of the respective doses used in the individual treatment arms (as in the Raub, et al study), but that is not a requirement. Thus, this PKPD modeling approach is highly resource sparing. Its value lies in its ability to identify several dose scenarios for multiple drugs (two or more) given in combination to achieve tumor shrinkage, thereby enabling great flexibility in dose regimen selection for evaluation. This is an important finding in the context of identifying combination regimens that are both effective and well tolerated. The approach also provides qualitative information. The shape of the TSC curve identifies if a combination of agents achieves an additive (straight line), synergistic (concave line), or antagonistic (convex line) tumor volume effect.

5.4 Limitations of this research

There are several limitations and assumptions in this work. In designing rational drug combination treatments of TMZ with MDM2/AKT inhibitors for GBM, we are assuming that there is no PK-based drug interaction. In other words, we are considering that the pharmacokinetics of each drug does not influence the elimination of the other. However, there might be potential for a drug interaction in cases where PKPD model fit is poor in linking tumor volume response to

individual drug exposure profiles. Also, digitized data from the published source were limited to mean individual data, which means no estimation of inter-individual variability for digitized data and very few data points to base the PK Model. Secondly, linear drug action was assumed based on preliminary in vitro experiments (results not shown), in which in vitro IC50s (µM) >> in vivo drug concentrations (nM), which reduces the Hill equation to E_{max}/EC_{50} that we define as a constant 'b' (linear function of drug action) in our models. Another limitation is that in the resistance integrated TGI model, we assumed that the emergence of resistance is due to TMZ treatment. Specifically, the resistance integrated model is acquired resistance to TMZ treatment. For the specific set of available data, we were not able to justify the innate resistance mechanism. One of the assumptions in deriving the tumor static concentration is that the tumor growth rate is exponential. Deriving TSC assumes the condition that the tumor volume over time in cell proliferating compartment is zero to achieve tumor stasis. Because of this assumption that dV/dt = 0 for tumor to achieve the condition for stasis, resistance integrated TGI model for GBM 43 could not be used to generate the TSC curve.

CHAPTER 6. CONCLUSION

In summary, targeting specific pathways involved in the pro-survival response to TMZ exposure demonstrates statistically significantly reduced tumor growth relative to TMZ monotherapy when combining TMZ with targeted agent SMIs. Mathematical PKPD models describing the observed tumor growth according to simultaneous administration of TMZ with an MDM2 or AKT inhibitor or CDK4/6 kinase inhibitor have been developed. An integrated PKPD tumor growth inhibition model successfully described the growth inhibition activity of TMZ monotherapy and TMZ-small molecule inhibitors combination therapy in mouse flank xenograft tumors derived from three different types of GBMs (U87, GBM 10 and GBM 43). Plasma concentrations of TMZ and small molecule inhibitors were connected in a quantitative manner to model their inhibition of tumor growth. As a result, this modeling framework provides the quantitative characterization of tumor growth inhibition when TMZ was combined with select small molecule inhibitors.

In specific patient derived xenograft tumors (GBM 43), a model incorporating resistance development was used to characterize emergence of a sub-population of tumor cells resistant to TMZ treatment, which may not have been obvious by observing the data. The model evaluated the dynamic process of the onset of resistance to TMZ treatment. It predicted the growth of the tumor that is driven by the emergence of resistance and the PKPD TGI model framework evaluated why the tumors are growing aggressively or slowly. This enables exploration of hypotheses of tumor resistance development, and identification of novel dosing strategies to mitigate resistance development. Predictive PKPD modeling of tumor growth kinetics in xenograft models can be used to inform strategic combination treatment therapy design in combating primary and recurrent GBM, and readily supports translation of these therapies to the clinic.

Deriving tumor growth inhibition curves as an outcome of the integrated PKPD model provides prediction of exposures for multiple drug combinations required to inhibit tumor growth and, at a minimum, to maintain the tumor at stasis. Based on the exposure metrics, this approach provides an excellent graphical tool to determine the possibility of drug synergy and to optimize doses of targeted agents (AKT, MDM2, CDK4/6 kinase) in relation to TMZ dose. The next step is to validate model predictions in mice so that it can be used to translate and accurately identify efficacious dosing regimens in humans.

REFERENCES

1. Cardilin, T., et al., *Evaluation and translation of combination therapies in oncology–A quantitative approach.* European journal of pharmacology, 2018. **834**: p. 327-336.
2. Raub, T.J., et al., *Brain exposure of two selective dual CDK4 and CDK6 inhibitors and the antitumor activity of CDK4 and CDK6 inhibition in combination with temozolomide in an intracranial glioblastoma xenograft.* Drug Metabolism and Disposition, 2015. **43**(9): p. 1360-1371.
3. Lima, F.R., et al., *Glioblastoma: therapeutic challenges, what lies ahead.* Biochimica et Biophysica Acta (BBA)-Reviews on Cancer, 2012. **1826**(2): p. 338-349.
4. Davis, M.E., *Glioblastoma: overview of disease and treatment.* Clinical journal of oncology nursing, 2016. **20**(5): p. S2.
5. Ostrom, Q.T., et al., *CBTRUS statistical report: primary brain and other central nervous system tumors diagnosed in the United States in 2013–2017.* Neuro-oncology, 2020. **22**(Supplement_1): p. iv1-iv96.
6. Ghosh, D., S. Nandi, and S. Bhattacharjee, *Combination therapy to checkmate Glioblastoma: clinical challenges and advances.* Clinical and translational medicine, 2018. **7**(1): p. 33.
7. Goldwirt, L., et al., *Irinotecan and temozolomide brain distribution: a focus on ABCB1.* Cancer chemotherapy and pharmacology, 2014. **74**(1): p. 185-193.
8. Malkki, H., *Trial Watch: Glioblastoma vaccine therapy disappointment in Phase III trial.* Nature reviews Neurology, 2016. **12**(4): p. 190.
9. Safa, A.R., et al., *Emerging targets for glioblastoma stem cell therapy.* Journal of biomedical research, 2016. **30**(1): p. 19.
10. Stupp, R., et al., *Radiotherapy plus concomitant and adjuvant temozolomide for glioblastoma.* New England journal of medicine, 2005. **352**(10): p. 987-996.
11. Carter, T.C., R. Medina-Flores, and B.E. Lawler, *Glioblastoma treatment with temozolomide and bevacizumab and overall survival in a rural tertiary healthcare practice.* BioMed research international, 2018. **2018**.

12. Wei, W., et al., *The efficacy and safety of various dose-dense regimens of temozolomide for recurrent high-grade glioma: a systematic review with meta-analysis.* J Neurooncol, 2015. **125**(2): p. 339-49.
13. Gilbert, M.R., et al., *Dose-dense temozolomide for newly diagnosed glioblastoma: a randomized phase III clinical trial.* Journal of clinical oncology, 2013. **31**(32): p. 4085.
14. Rai, R., et al., *Temozolomide analogs with improved brain/plasma ratios–exploring the possibility of enhancing the therapeutic index of temozolomide.* Bioorganic & medicinal chemistry letters, 2016. **26**(20): p. 5103-5109.
15. Singh, N., et al., *Mechanisms of temozolomide resistance in glioblastoma-a comprehensive review.* Cancer Drug Resistance, 2021. **4**(1): p. 17-43.
16. Stupp, R., et al., *Maintenance therapy with tumor-treating fields plus temozolomide vs temozolomide alone for glioblastoma: a randomized clinical trial.* Jama, 2015. **314**(23): p. 2535-2543.
17. Lee, S.Y., *Temozolomide resistance in glioblastoma multiforme.* Genes & Diseases, 2016. **3**(3): p. 198-210.
18. Zhang, J., M. FG Stevens, and T. D Bradshaw, *Temozolomide: mechanisms of action, repair and resistance.* Current molecular pharmacology, 2012. **5**(1): p. 102-114.
19. van den Bent, M.J., et al., *Randomized phase II trial of erlotinib versus temozolomide or carmustine in recurrent glioblastoma: EORTC brain tumor group study 26034.* J Clin Oncol, 2009. **27**(8): p. 1268-74.
20. Thiessen, B., et al., *A phase I/II trial of GW572016 (lapatinib) in recurrent glioblastoma multiforme: clinical outcomes, pharmacokinetics and molecular correlation.* Cancer Chemother Pharmacol, 2010. **65**(2): p. 353-61.
21. de Groot, J.F., et al., *Phase II study of aflibercept in recurrent malignant glioma: a North American Brain Tumor Consortium study.* J Clin Oncol, 2011. **29**(19): p. 2689-95.
22. Muhic, A., et al., *Phase II open-label study of nintedanib in patients with recurrent glioblastoma multiforme.* J Neurooncol, 2013. **111**(2): p. 205-12.
23. Lassman, A.B., et al., *Phase 2 trial of dasatinib in target-selected patients with recurrent glioblastoma (RTOG 0627).* Neuro Oncol, 2015. **17**(7): p. 992-8.
24. Ghosh, D., S. Nandi, and S. Bhattacharjee, *Combination therapy to checkmate Glioblastoma: clinical challenges and advances.* Clin Transl Med, 2018. **7**(1): p. 33.

25. Chène, P., *Inhibiting the p53–MDM2 interaction: an important target for cancer therapy.* Nature reviews cancer, 2003. **3**(2): p. 102.
26. Momand, J., H.-H. Wu, and G. Dasgupta, *MDM2—master regulator of the p53 tumor suppressor protein.* Gene, 2000. **242**(1-2): p. 15-29.
27. Nag, S., et al., *The MDM2-p53 pathway revisited.* Journal of biomedical research, 2013. **27**(4): p. 254.
28. Wang, H., et al., *Combination therapy in a xenograft model of glioblastoma: enhancement of the antitumor activity of temozolomide by an MDM2 antagonist.* Journal of neurosurgery, 2017. **126**(2): p. 446-459.
29. Ogawara, Y., et al., *Akt enhances Mdm2-mediated ubiquitination and degradation of p53.* Journal of Biological Chemistry, 2002. **277**(24): p. 21843-21850.
30. Daniele, S., et al., *Combined inhibition of AKT/mTOR and MDM2 enhances Glioblastoma Multiforme cell apoptosis and differentiation of cancer stem cells.* Scientific reports, 2015. **5**(1): p. 1-14.
31. Rayburn, E., et al., *MDM2 and human malignancies: expression, clinical pathology, prognostic markers, and implications for chemotherapy.* Curr Cancer Drug Targets, 2005. **5**(1): p. 27-41.
32. Nag, S., et al., *Targeting MDM2-p53 interaction for cancer therapy: are we there yet?* Current medicinal chemistry, 2014. **21**(5): p. 553-574.
33. Vassilev, L.T., et al., *In vivo activation of the p53 pathway by small-molecule antagonists of MDM2.* Science, 2004. **303**(5659): p. 844-848.
34. Zhao, Y., et al., *Small-molecule inhibitors of the MDM2–p53 protein–protein interaction (MDM2 Inhibitors) in clinical trials for cancer treatment: miniperspective.* Journal of medicinal chemistry, 2015. **58**(3): p. 1038-1052.
35. Verreault, M., et al., *Preclinical efficacy of the MDM2 inhibitor RG7112 in MDM2-amplified and TP53 wild-type glioblastomas.* Clinical Cancer Research, 2016. **22**(5): p. 1185-1196.
36. Wang, H., et al., *Combination therapy in a xenograft model of glioblastoma: enhancement of the antitumor activity of temozolomide by an MDM2 antagonist.* J Neurosurg, 2017. **126**(2): p. 446-459.

37. Wang, H., et al., *Combination therapy in a xenograft model of glioblastoma: enhancement of the antitumor activity of temozolomide by an MDM2 antagonist.* Journal of neurosurgery, 2017. **126**(2): p. 446-459.
38. Daniele, S., et al., *Combined inhibition of AKT/mTOR and MDM2 enhances Glioblastoma Multiforme cell apoptosis and differentiation of cancer stem cells.* Sci Rep, 2015. **5**: p. 9956.
39. Saiki, A.Y., et al., *MDM2 antagonists synergize broadly and robustly with compounds targeting fundamental oncogenic signaling pathways.* Oncotarget, 2014. **5**(8): p. 2030-43.
40. Zhu, N., et al., *Inhibition of the Akt/survivin pathway synergizes the antileukemia effect of nutlin-3 in acute lymphoblastic leukemia cells.* Mol Cancer Ther, 2008. **7**(5): p. 1101-9.
41. Bellacosa, A., et al., *Activation of AKT kinases in cancer: implications for therapeutic targeting.* Advances in cancer research, 2005. **94**: p. 29-86.
42. Li, J., et al., *PTEN, a putative protein tyrosine phosphatase gene mutated in human brain, breast, and prostate cancer.* science, 1997. **275**(5308): p. 1943-1947.
43. Shayesteh, L., et al., *PIK3CA is implicated as an oncogene in ovarian cancer.* Nature genetics, 1999. **21**(1): p. 99-102.
44. Guha, A., et al., *Proliferation of human malignant astrocytomas is dependent on Ras activation.* Oncogene, 1997. **15**(23): p. 2755-65.
45. Holland, E.C., et al., *Combined activation of Ras and Akt in neural progenitors induces glioblastoma formation in mice.* Nat Genet, 2000. **25**(1): p. 55-7.
46. Clark, A.S., et al., *Constitutive and inducible Akt activity promotes resistance to chemotherapy, trastuzumab, or tamoxifen in breast cancer cells.* Molecular cancer therapeutics, 2002. **1**(9): p. 707-717.
47. Caporali, S., et al., *NF-kappaB is activated in response to temozolomide in an AKT-dependent manner and confers protection against the growth suppressive effect of the drug.* J Transl Med, 2012. **10**: p. 252.
48. Caporali, S., et al., *AKT is activated in an ataxia-telangiectasia and Rad3-related-dependent manner in response to temozolomide and confers protection against drug-induced cell growth inhibition.* Mol Pharmacol, 2008. **74**(1): p. 173-83.
49. Abbott, N.J., et al., *Structure and function of the blood–brain barrier.* Neurobiology of disease, 2010. **37**(1): p. 13-25.

50. Lyle, L.T., et al., *Alterations in Pericyte Subpopulations are Associated with Elevated Blood-Tumor Barrier Permeability in Experimental Brain Metastasis of Breast Cancer.* Clinical Cancer Research, 2016: p. clincanres. 1836.2015.
51. Lehmann, C., et al., *Superior anti-tumor activity of the MDM2 antagonist idasanutlin and the Bcl-2 inhibitor venetoclax in p53 wild-type acute myeloid leukemia models.* Journal of hematology & oncology, 2016. **9**(1): p. 50.
52. Huck, B.R. and I. Mochalkin, *Recent progress towards clinically relevant ATP-competitive Akt inhibitors.* Bioorganic & medicinal chemistry letters, 2017. **27**(13): p. 2838-2848.
53. Patnaik, A., et al., *Efficacy and safety of abemaciclib, an inhibitor of CDK4 and CDK6, for patients with breast cancer, non–small cell lung cancer, and other solid tumors.* Cancer discovery, 2016. **6**(7): p. 740-753.
54. Moreira, J., et al., *Chalcones as Promising Antitumor Agents by Targeting the p53 Pathway: An Overview and New Insights in Drug-Likeness.* Molecules, 2021. **26**(12): p. 3737.
55. Higgins, B., et al., *Preclinical optimization of MDM2 antagonist scheduling for cancer treatment by using a model-based approach.* Clinical Cancer Research, 2014. **20**(14): p. 3742-3752.
56. Lin, J., et al., *Targeting activated Akt with GDC-0068, a novel selective Akt inhibitor that is efficacious in multiple tumor models.* Clinical Cancer Research, 2013. **19**(7): p. 1760-1772.
57. Herrera-Perez, R.M., et al., *Presence of stromal cells in a bioengineered tumor microenvironment alters glioblastoma migration and response to STAT3 inhibition.* PloS one, 2018. **13**(3): p. e0194183.
58. Yu, S.-c., et al., *Isolation and characterization of cancer stem cells from a human glioblastoma cell line U87.* Cancer letters, 2008. **265**(1): p. 124-134.
59. Lakoma, A., et al., *The MDM2 small-molecule inhibitor RG7388 leads to potent tumor inhibition in p53 wild-type neuroblastoma.* Cell death discovery, 2015. **1**(1): p. 1-9.
60. Shangary, S., et al., *Temporal activation of p53 by a specific MDM2 inhibitor is selectively toxic to tumors and leads to complete tumor growth inhibition.* Proceedings of the National Academy of Sciences, 2008. **105**(10): p. 3933-3938.

61. Ray-Coquard, I., et al., *Effect of the MDM2 antagonist RG7112 on the P53 pathway in patients with MDM2-amplified, well-differentiated or dedifferentiated liposarcoma: an exploratory proof-of-mechanism study.* The lancet oncology, 2012. **13**(11): p. 1133-1140.
62. Yin, A., et al., *A review of mathematical models for tumor dynamics and treatment resistance evolution of solid tumors.* CPT: pharmacometrics & systems pharmacology, 2019. **8**(10): p. 720-737.
63. Simeoni, M., et al., *Predictive pharmacokinetic-pharmacodynamic modeling of tumor growth kinetics in xenograft models after administration of anticancer agents.* Cancer research, 2004. **64**(3): p. 1094-1101.
64. Ribba, B., et al., *A review of mixed-effects models of tumor growth and effects of anticancer drug treatment used in population analysis.* CPT: pharmacometrics & systems pharmacology, 2014. **3**(5): p. 1-10.
65. Akaike, H., *A new look at the statistical model identification.* IEEE transactions on automatic control, 1974. **19**(6): p. 716-723.
66. Bertrand, J., E. Comets, and F. Mentre, *Comparison of model-based tests and selection strategies to detect genetic polymorphisms influencing pharmacokinetic parameters.* Journal of biopharmaceutical statistics, 2008. **18**(6): p. 1084-1102.
67. Gabrielsson, J., F.D. Gibbons, and L.A. Peletier, *Mixture dynamics: combination therapy in oncology.* European Journal of Pharmaceutical Sciences, 2016. **88**: p. 132-146.
68. Park, B.J., Z.L. Whichard, and S.J. Corey, *Dasatinib synergizes with both cytotoxic and signal transduction inhibitors in heterogeneous breast cancer cell lines–lessons for design of combination targeted therapy.* Cancer letters, 2012. **320**(1): p. 104-110.
69. Tan, G.-R., S.-S. Feng, and D.T. Leong, *The reduction of anti-cancer drug antagonism by the spatial protection of drugs with PLA–TPGS nanoparticles.* Biomaterials, 2014. **35**(9): p. 3044-3051.
70. Cardilin, T., et al., *Tumor static concentration curves in combination therapy.* The AAPS journal, 2017. **19**(2): p. 456-467.
71. Ballesta, A., et al., *Multiscale design of cell-type-specific pharmacokinetic/pharmacodynamic models for personalized medicine: application to temozolomide in brain tumors.* CPT Pharmacometrics Syst Pharmacol, 2014. **3**: p. e112.

72. Zhou, Q., P. Guo, and J.M. Gallo, *Impact of angiogenesis inhibition by sunitinib on tumor distribution of temozolomide.* Clinical Cancer Research, 2008. **14**(5): p. 1540-1549.
73. Liu, H.-L., et al., *Pharmacodynamic and therapeutic investigation of focused ultrasound-induced blood-brain barrier opening for enhanced temozolomide delivery in glioma treatment.* PLoS One, 2014. **9**(12): p. e114311.
74. Goldwirt, L., et al., *Development of a new UPLC-MSMS method for the determination of temozolomide in mice: application to plasma pharmacokinetics and brain distribution study.* Biomedical Chromatography, 2013. **27**(7): p. 889-893.
75. Kumari, S., et al., *Overcoming blood brain barrier with a dual purpose Temozolomide loaded Lactoferrin nanoparticles for combating glioma (SERP-17-12433).* Scientific reports, 2017. **7**(1): p. 6602.
76. Vu, B., et al., *Discovery of RG7112: a small-molecule MDM2 inhibitor in clinical development.* ACS medicinal chemistry letters, 2013. **4**(5): p. 466-469.
77. Gebbia, V., et al., *Abemaciclib: safety and effectiveness of a unique cyclin-dependent kinase inhibitor.* Expert Opinion on Drug Safety, 2020. **19**(8): p. 945-954.
78. Yin, A., et al., *A Review of Mathematical Models for Tumor Dynamics and Treatment Resistance Evolution of Solid Tumors.* CPT: Pharmacometrics & Systems Pharmacology, 2019. **8**(10): p. 720-737.
79. Eigenmann, M.J., et al., *PKPD modeling of acquired resistance to anti-cancer drug treatment.* Journal of pharmacokinetics and pharmacodynamics, 2017. **44**(6): p. 617-630.
80. Bauer, R.J., *NONMEM Tutorial Part II: Estimation Methods and Advanced Examples.* CPT: pharmacometrics & systems pharmacology, 2019.
81. Xu, X.S., et al., *Shrinkage in nonlinear mixed-effects population models: quantification, influencing factors, and impact.* The AAPS journal, 2012. **14**(4): p. 927-936.
82. Mould, D. and R. Upton, *Basic concepts in population modeling, simulation, and model-based drug development.* CPT: pharmacometrics & systems pharmacology, 2012. **1**(9): p. 1-14.
83. Mould, D. and R.N. Upton, *Basic concepts in population modeling, simulation, and model-based drug development—part 2: introduction to pharmacokinetic modeling methods.* CPT: pharmacometrics & systems pharmacology, 2013. **2**(4): p. 1-14.

84. Zhu, A.Z., *Quantitative translational modeling to facilitate preclinical to clinical efficacy & toxicity translation in oncology.* Future science OA, 2018. **4**(5): p. FSO306.
85. Newlands, E., et al., *Phase i trial of temozolomide (CCRG 81045: M&B 39831: NSC 362856).* British journal of cancer, 1992. **65**(2): p. 287.
86. Brada, M., et al., *Phase I dose-escalation and pharmacokinetic study of temozolomide (SCH 52365) for refractory or relapsing malignancies.* British journal of cancer, 1999. **81**(6): p. 1022.
87. Plowman, J., et al., *Preclinical antitumor activity of temozolomide in mice: efficacy against human brain tumor xenografts and synergism with 1, 3-bis (2-chloroethyl)-1-nitrosourea.* Cancer research, 1994. **54**(14): p. 3793-3799.
88. Fisher, T., et al., *Mechanisms operative in the antitumor activity of temozolomide in glioblastoma multiforme.* The Cancer Journal, 2007. **13**(5): p. 335-344.
89. Berberich, A., et al., *Targeting resistance against the MDM2 inhibitor RG7388 in glioblastoma cells by the MEK inhibitor trametinib.* Clinical Cancer Research, 2019. **25**(1): p. 253-265.
90. Raub, T.J., et al., *Abemaciclib (LY2835219) is an oral inhibitor of the cyclin-dependent kinases 4/6 that crosses the blood-brain barrier and demonstrates in vivo activity against intracranial human brain tumor xenografts.* Drug Metabolism and Disposition, 2015.
91. Von Achenbach, C., et al., *Synergistic growth inhibition mediated by dual PI3K/mTOR pathway targeting and genetic or direct pharmacological AKT inhibition in human glioblastoma models.* Journal of neurochemistry, 2020. **153**(4): p. 510-524.
92. Oduola, W.O., et al., *Sequential therapeutic response modeling for tumor treatment using computational hybrid control systems approach.* IEEE Transactions on Biomedical Engineering, 2017. **65**(4): p. 866-874.
93. Wengner, A.M., et al., *Synergistic activity of the ATR inhibitor BAY1895344 in combination with immune checkpoint inhibitors in preclinical tumor models*. 2019, AACR.
94. Schneider, B.K., et al., *Optimal Scheduling of Bevacizumab and Pemetrexed/Cisplatin Dosing in Non-Small Cell Lung Cancer.* CPT: pharmacometrics & systems pharmacology, 2019. **8**(8): p. 577-586.
95. Laird, A.K., *Dynamics of tumour growth.* British journal of cancer, 1964. **18**(3): p. 490.

96. Jumbe, N.L., et al., *Modeling the efficacy of trastuzumab-DM1, an antibody drug conjugate, in mice.* Journal of pharmacokinetics and pharmacodynamics, 2010. **37**(3): p. 221-242.
97. Raub, T.J., et al., *Brain Exposure of Two Selective Dual CDK4 and CDK6 Inhibitors and the Antitumor Activity of CDK4 and CDK6 Inhibition in Combination with Temozolomide in an Intracranial Glioblastoma Xenograft.* Drug Metab Dispos, 2015. **43**(9): p. 1360-71.
98. Wang, H., et al., *Sensitization of temozolomide-mediated glioblastoma cell death by targeting MDM2: Assessment of PD biomarkers, brain penetration, and efficacy in humanized orthotopic xenograft models*. 2014, AACR.
99. Wong, H., et al., *Anti-tumor activity of targeted and cytotoxic agents in murine subcutaneous tumor models correlates with clinical response.* Clinical Cancer Research, 2012: p. clincanres. 0738.2012.
100. Tonsing-Carter, E., et al., *Potentiation of carboplatin-mediated DNA damage by the Mdm2 modulator Nutlin-3a in a humanized orthotopic breast-to-lung metastatic model.* Molecular cancer therapeutics, 2015. **14**(12): p. 2850-2863.
101. Choi, E.J., et al., *Enhanced cytotoxic effect of radiation and temozolomide in malignant glioma cells: targeting PI3K-AKT-mTOR signaling, HSP90 and histone deacetylases.* BMC cancer, 2014. **14**(1): p. 1-12.
102. Bernard, A., et al., *Mathematical modeling of tumor growth and tumor growth inhibition in oncology drug development.* Expert opinion on drug metabolism & toxicology, 2012. **8**(9): p. 1057-1069.
103. Lo, C., *Stochastic Gompertz model of tumour cell growth.* Journal of Theoretical Biology, 2007. **248**(2): p. 317-321.
104. Rowland, M. and T.N. Tozer, *Clinical pharmacokinetics/pharmacodynamics*. 2005: Lippincott Williams and Wilkins Philadelphia.
105. Oduola, W.O., et al., *Sequential Therapeutic Response Modeling for Tumor Treatment Using Computational Hybrid Control Systems Approach.* IEEE Trans Biomed Eng, 2018. **65**(4): p. 866-874.
106. Bottino, D.C., et al., *Dose Optimization for Anticancer Drug Combinations: Maximizing Therapeutic Index via Clinical Exposure-Toxicity/Preclinical Exposure-Efficacy Modeling.* Clin Cancer Res, 2019. **25**(22): p. 6633-6643.

107. Mazzocco, P., et al., *Increasing the Time Interval between PCV Chemotherapy Cycles as a Strategy to Improve Duration of Response in Low-Grade Gliomas: Results from a Model-Based Clinical Trial Simulation.* Comput Math Methods Med, 2015. **2015**: p. 297903.
108. Gallo, J.M., *Modulation of Cell State to Improve Drug Therapy.* CPT Pharmacometrics Syst Pharmacol, 2018. **7**(9): p. 539-542.
109. Rocchetti, M., et al., *Predicting the active doses in humans from animal studies: a novel approach in oncology.* European journal of cancer, 2007. **43**(12): p. 1862-1868.
110. Chmielecki, J., et al., *Optimization of dosing for EGFR-mutant non–small cell lung cancer with evolutionary cancer modeling.* Science translational medicine, 2011. **3**(90): p. 90ra59-90ra59.
111. Cardilin, T., et al., *Modeling long-term tumor growth and kill after combinations of radiation and radiosensitizing agents.* Cancer chemotherapy and pharmacology, 2019. **83**(6): p. 1159-1173.
112. Tallarida, R.J., *An overview of drug combination analysis with isobolograms.* Journal of Pharmacology and Experimental Therapeutics, 2006. **319**(1): p. 1-7.
113. Tallarida, R.J. and R.B. Raffa, *Testing for synergism over a range of fixed ratio drug combinations: replacing the isobologram.* Life sciences, 1995. **58**(2): p. PL23-PL28.

APPENDIX

Phoenix NLME Model codes for pharmacokinetic model with TMZ

```
test(){
deriv(A1 = - (Cl * C) + (Aapo * Kapo) + (Aaip * Kaip))
urinecpt(A0 = (Cl * C))
deriv(Aapo = - (Aapo * Kapo))
deriv(Aaip = - (Aaip * Kaip))
C = A1 / V
dosepoint(A1, idosevar = A1Dose, infdosevar = A1InfDose, infratevar = A1InfRate)
error(CEps = 0.1)
observe(CObs =C *(1 + CEps))
dosepoint(Aapo, bioavail = (Fpo), idosevar = AapoDose, infdosevar = AapoInfDose, infratevar =
AapoInfRate)
dosepoint(Aaip, bioavail = (Fip), idosevar = AaipDose, infdosevar = AaipInfDose, infratevar =
AaipInfRate)
fcovariate(flag1())
fcovariate(flag2())
fcovariate(flag23())
fcovariate(flag3())
fcovariate(flag4())
fcovariate(flag5())
fcovariate(flag6())
fcovariate(dose())
Kapo = Kapo1*flag1 + Kapo2*flag23 + Kapo3*flag4
Fpo = Fpo1*flag1 + Fpo2*flag2 + Fpo3*flag3 + Fpo4*flag4
Fip = Fip1*flag5 + Fip2*flag6
stparm(V = tvV * exp(nV))
stparm(Cl = tvCl * exp(nCl))
stparm(Kapo1 = tvKapo1 )
stparm(Kapo2 = tvKapo2 * exp(nKapo2) )
```

```
stparm(Kapo3 = tvKapo3 )
stparm(Fpo1 = tvFpo1 )
stparm(Fpo2 = tvFpo2)
stparm(Fpo3 = tvFpo3 )
stparm(Fpo4 = tvFpo4)
stparm(Kaip = tvKaip )
stparm(Fip1 = tvFip1 )
stparm(Fip2 = tvFip2 )
fixef(tvV = c(, 3,))
fixef(tvCl = c(, 2.5, ))
fixef(tvKapo1 = c(,15, ))
fixef(tvKapo2 = c(,0.4, ))
fixef(tvKapo3 = c(,1.5, ))
fixef(tvFpo1  = c(, 0.2, ))
fixef(tvFpo2 = c(, 0.2, ))
fixef(tvFpo3 = c(,0.06, ))
fixef(tvFpo4 = c(, 0.2, ))
fixef(tvKaip = c(, 7, ))
fixef(tvFip1 = c(, 0.08, ))
fixef(tvFip2 = c(,0.04, ))
ranef(block(nV, nCl) = c (0.1,0,0.1))
ranef(diag(nKapo2) = c(0.1))
}
```

Phoenix NLME Model codes for pharmacokinetic model with ACB

```
test(){
deriv(A1 = - (Cl_T  * C) + (Aapo * Kapo) + (Aaip * Kaip))
urinecpt(A0 = (Cl_T  * C))
deriv(Aapo = - (Aapo * Kapo))
deriv(Aaip = - (Aaip * Kaip))
deriv(A2 = - (CL_A * C1) + (Aa * Ka))
urinecpt(A3 = (CL_A * C1))
```

```
deriv(Aa = - (Aa * Ka))
C = A1 / V
C1 = A2 / V1
error(CEpsT = 0.405934)
observe(CObsT = C * (1 + CEpsT))
error(CEpsA = 0.398879)
observe(CObsA = C1 * (1 + CEpsA))
dosepoint(A1, idosevar = A1Dose, infdosevar = A1InfDose, infratevar = A1InfRate)
dosepoint(Aa, idosevar = AaDose, infdosevar = AaInfDose, infratevar = AaInfRate)
dosepoint(Aapo, bioavail = (Fpo), idosevar = AapoDose, infdosevar = AapoInfDose, infratevar =
AapoInfRate)
dosepoint(Aaip, bioavail = (Fip), idosevar = AaipDose, infdosevar = AaipInfDose, infratevar =
AaipInfRate)
fcovariate(flag2())
fcovariate(flag23())
fcovariate(flag3())
fcovariate(flag4())
fcovariate(flag5())
fcovariate(flag6())
fcovariate(dose())
Kapo = Kapo5*flag23 + Kapo50*flag4
Fpo =  Fpo5*flag2 + Fpo66*flag3 + Fpo50*flag4
Fip = Fip1*flag5 + Fip2*flag6
stparm(V = tvV * exp(nV))
stparm(V1 = tvV1)
stparm(Cl_T  = tvCl_T  * exp(nCl_T))
stparm(CL_A = tvCL_A )
stparm(Ka = tvKa)
stparm(Kapo5 = tvKapo5 )
stparm(Kapo50 = tvKapo50 )
stparm(Fpo5 = tvFpo5)
```

```
stparm(Fpo66 = tvFpo66)
stparm(Fpo50 = tvFpo50)
stparm(Kaip = tvKaip )
stparm(Fip1 = tvFip1 )
stparm(Fip2 = tvFip2 )
fixef(tvV = c(, 0.712368, ))
fixef(tvV1 = c(, 45, ))
fixef(tvCl_T  = c(, 0.719613, ))
fixef(tvCL_A (freeze)= c(, 9.96, ))
fixef(tvKa = c(, 0.7, ))
fixef(tvKapo5 = c(,0.364427, ))
fixef(tvKapo50 = c(,1.93786, ))
fixef(tvFpo5 = c(, 0.0540672, ))
fixef(tvFpo66= c(, 0.0109339, ))
fixef(tvFpo50 = c(, 0.0431629, ))
fixef(tvKaip= c(,33.7779, ))
fixef(tvFip1= c(, 0.02, ))
fixef(tvFip2 = c(,0.00561851, ))
ranef(block(nV, nCl_T) = c(0.1,0,0.1))
}
```

Phoenix NLME Model codes for pharmacokinetic model with RG7388

```
test(){
deriv(A1 = - (Cl * C) + (Aa * Ka))
urinecpt(A0 = (Cl * C))
deriv(Aa = - (Aa * Ka))
C = A1 / V
dosepoint(Aa, idosevar = AaDose, infdosevar = AaInfDose, infratevar = AaInfRate)
error(CEps = 0.243038657582547)
observe(CObs = C * (1 + CEps))
stparm(V = tvV * exp(nV))
stparm(Cl = tvCl)
```

```
stparm(Ka = tvKa )
fixef(tvV = c(, 316.829869950452, ))
fixef(tvCl = c(, 88.2884030330089, ))
fixef(tvKa = c(, 0.280104657919658, ))
ranef(diag(nV) = c(0.1))
}
```

Phoenix NLME Model codes for pharmacokinetic model with GDC0068

```
test(){
deriv(A1 = - (Cl * C) + (Aa * Ka))
urinecpt(A0 = (Cl * C))
deriv(Aa = - (Aa * Ka))
C = A1 / V
dosepoint(Aa, idosevar = AaDose, infdosevar = AaInfDose, infratevar = AaInfRate)
error(CEps = 0.279509563915144)
observe(CObs = C*(1 + CEps))
stparm(V = tvV )
stparm(Cl = tvCl )
stparm(Ka = tvKa * exp(nKa))
fixef(tvV = c(, 1040, ))
fixef(tvCl = c(, 386.724550365329, ))
fixef(tvKa = c(, 1.36657508072064, ))
ranef(diag( nKa) = c(0.047167401))
}
```

Phoenix NLME Model codes for pharmacodynamic model in mice bearing U87 xenografts

```
test(){
deriv(A1 = - (Cl_T  * C) + (Aapo * Kapo) + (Aaip * Kaip))
urinecpt(A0 = (Cl_T  * C))
deriv(Aapo = - (Aapo * Kapo))
deriv(Aaip = - (Aaip * Kaip))
deriv(A2 = - (CL_A * C1) + (Aa * Ka))
urinecpt(A3 = (CL_A * C1))
```

```
deriv(Aa = - (Aa * Ka))
C = A1 / Vt
C1 = A2 / Va
error(CEpsT = 0.265935)
observe(CObsT = C*(1 + CEpsT))
error(CEpsA = 0.307445)
observe(CObsA = C1*(1 + CEpsA))
dosepoint(A1, idosevar = A1Dose, infdosevar = A1InfDose, infratevar = A1InfRate)
dosepoint(Aa, idosevar = AaDose, infdosevar = AaInfDose, infratevar = AaInfRate)
dosepoint(Aapo, bioavail = (Fpo), idosevar = AapoDose, infdosevar = AapoInfDose, infratevar =
AapoInfRate)
dosepoint(Aaip, bioavail = (Fip), idosevar = AaipDose, infdosevar = AaipInfDose, infratevar =
AaipInfRate)
psi = 20
TV= V1+V2+V3+V4
Gwth = (1+ (kg0*TV/kg1)^psi)^(1/psi)
deriv(V1 = (kg0*V1/Gwth)*(1-ba*C1) - bt*C*V1)
deriv(V2 =   bt*C*V1 - kk*V2)
deriv(V3 =   kk*(V2-V3))
deriv(V4 =   kk*(V3-V4))
sequence {V1 = V0}
error(VEps = 0.328995)
observe(Vobs = TV*(1 + VEps))
fcovariate(dose())
fcovariate(flag1())
fcovariate(flag2())
fcovariate(flag23())
fcovariate(flag3())
fcovariate(flag4())
fcovariate(flag5())
fcovariate(flag6())
```

```
fcovariate(PD1())
fcovariate(U87A())
fcovariate(U87B())
Kapo = Kapo20*flag1 + Kapo5*flag23 + Kapo50*flag4
Fpo =  Fpo20*flag1 + Fpo5*flag2 + Fpo66*flag3 + Fpo50*flag4
Fip = Fip1*flag5 + Fip2*flag6  + Fip3*PD1
V0 = V0a*U87A + V0b*U87B
bt = bt5*U87A + bt3*U87B
kg0 = kg0a*U87A + kg0b*U87B
kg1 = kg1a*U87A + kg1b*U87B
kk = kka*U87A + kkb*U87B
stparm(Vt = tvVt * exp (nVt))
stparm(Va = tvVa )
stparm(Cl_T  = tvCl_T * exp (nCl_T))
stparm(CL_A = tvCL_A )
stparm(Ka = tvKa)
stparm(Kapo20 = tvKapo20 )
stparm(Kapo5 = tvKapo5 )
stparm(Kapo50 = tvKapo50 )
stparm(Fpo20 = tvFpo20)
stparm(Fpo5 = tvFpo5)
stparm(Fpo66 = tvFpo66)
stparm(Fpo50 = tvFpo50)
stparm(Kaip = tvKaip )
stparm(Fip1 = tvFip1 )
stparm(Fip2 = tvFip2 )
stparm(Fip3 = tvFip3 )
stparm(V0a = tvV0a)
stparm(V0b = tvV0b)
stparm(bt5 = tvbt5 )
stparm(bt3 = tvbt3 )
```

```
stparm(ba = tvba )
stparm(kg0a = tvkg0a * exp(nkg0a))
stparm(kg0b = tvkg0b )
stparm(kg1a = tvkg1a)
stparm(kg1b = tvkg1b )
stparm(kka = tvkka)
stparm(kkb = tvkkb)
fixef(tvVt   = c(, 3.28644, ))
fixef(tvVa  = c(, 43.0485, ))
fixef(tvCl_T  = c(, 3.43845, ))
fixef(tvCL_A (freeze)= c(, 9.96, ))
fixef(tvKa = c(, 0.888626, ))
fixef(tvKapo20 = c(,26.9957, ))
fixef(tvKapo5 = c(,0.353898, ))
fixef(tvKapo50 = c(,1.76784, ))
fixef(tvFpo20 = c(, 0.107651, ))
fixef(tvFpo5 = c(, 0.219065, ))
fixef(tvFpo66 = c(,0.0562632, ))
fixef(tvFpo50= c(, 0.217952, ))
fixef(tvKaip= c(,7.72404, ))
fixef(tvFip1= c(, 0.0638067, ))
fixef(tvFip2 = c(,0.0307382, ))
fixef(tvFip3  = c(,0.274869,))
fixef(tvV0a   = c(,106.637, ))
fixef(tvV0b   = c(,76.9909, ))
fixef(tvbt5 = c(,1.10722E-05, ))
fixef(tvbt3 = c(,3.04402E-05, ))
fixef(tvba = c(,0.000110648, ))
fixef(tvkg0a = c(,0.00450194, ))
fixef(tvkg0b = c(,0.00255944, ))
fixef(tvkg1a = c(,4.98307, ))
```

```
fixef(tvkg1b = c(,9.82464, ))
fixef(tvkka = c(, 0.0055191, ))
fixef(tvkkb = c(, 0.0181689, ))
ranef(block(nVt, nCl_T) = c(0.025456411,-0.019208448,0.068769879))
ranef(diag( nkg0a) = c(0.04394773))
}
```

Phoenix NLME Model codes for pharmacodynamic model in mice bearing GBM 10 xenografts

```
test(){
deriv(A1 = - (Cl_T  * C) + (Aapo * Kapo) + (Aaip * Kaip))
urinecpt(A0 = (Cl_T  * C))
deriv(Aapo = - (Aapo * Kapo))
deriv(Aaip = - (Aaip * Kaip))
deriv(A2 = - (CL_G * C1) + (AaG * KaG))
urinecpt(A3 = (CL_G * C1))
deriv(AaG = - (AaG * KaG))
deriv(A4 = - (CL_R * C2) + (AaR * KaR))
urinecpt(A5 = (CL_R * C2))
deriv(AaR = - (AaR * KaR))
C = A1 / Vt
C1 = A2 / Vg
C2 = A4/ Vr
error(CEpsT = 3.39973)
observe(CObsT = C*(1 + CEpsT))
error(CEpsG = 0.307122)
observe(CObsG = C1*(1 + CEpsG))
error(CEpsR = 0.259828)
observe(CObsR = C2*(1 + CEpsR))
dosepoint(A1, idosevar = A1Dose, infdosevar = A1InfDose, infratevar = A1InfRate)
dosepoint(AaG, idosevar = AaGDose, infdosevar = AaGInfDose, infratevar = AaGInfRate)
dosepoint(AaR, idosevar = AaRDose, infdosevar = AaRInfDose, infratevar = AaRInfRate)
```

```
dosepoint(Aapo, bioavail = (Fpo), idosevar = AapoDose, infdosevar = AapoInfDose, infratevar = AapoInfRate)
dosepoint(Aaip, bioavail = (Fip), idosevar = AaipDose, infdosevar = AaipInfDose, infratevar = AaipInfRate)
psi = 20
TV= V1+ V2 + V3 +V4
Gwth = (1+ (kg0*TV/kg1)^psi)^(1/psi)
deriv(V1 = (kg0*V1/Gwth) - V1*(bt*C+bg*C1+br*C2))
deriv(V2 =  V1*(bt*C+bg*C1+br*C2) - kk*V2)
deriv(V3 = kk*(V2-V3))
deriv(V4 = kk*(V3-V4))
sequence {V1 = V0}
error(VEps = 0.369656)
observe(Vobs = TV*(1 + VEps))
fcovariate(dose())
fcovariate(flag1())
fcovariate(flag2())
fcovariate(flag23())
fcovariate(flag3())
fcovariate(flag4())
fcovariate(flag5())
fcovariate(flag6())
Kapo = Kapo20*flag1 + Kapo5n66*flag23 + Kapo50*flag4
Fpo =  Fpo20* flag1 + Fpo5*flag2 + Fpo66*flag3 + Fpo50*flag4
Fip = Fip1*flag5 + Fip2*flag6
stparm(Vt = tvVt )
stparm(Vg = tvVg )
stparm(Vr = tvVr )
stparm(Cl_T  = tvCl_T )
stparm(CL_G = tvCL_G )
stparm(CL_R = tvCL_R )
```

```
stparm(KaG = tvKaG )
stparm(KaR = tvKaR )
stparm(Kapo20 = tvKapo20)
stparm(Kapo5n66 = tvKapo5n66 )
stparm(Kapo50 = tvKapo50 )
stparm(Fpo20 = tvFpo20)
stparm(Fpo5 = tvFpo5)
stparm(Fpo66 = tvFpo66)
stparm(Fpo50 = tvFpo50)
stparm(Kaip = tvKaip )
stparm(Fip1 = tvFip1 )
stparm(Fip2 = tvFip2 )
stparm(V0 = tvV0 * exp(nV0))
stparm(bt = tvbt )
stparm(bg = tvbg )
stparm(br = tvbr )
stparm(kg1 = tvkg1* exp(nkg1))
stparm(kg0 = tvkg0* exp(nkg0))
stparm(kk = tvkk * exp(nkk))
fixef(tvVt = c(, 3.7, ))
fixef(tvVg= c(, 1060.44, ))
fixef(tvVr= c(, 316.02, ))
fixef(tvCl_T= c(, 3.94, ))
fixef(tvCL_G= c(, 383.93, ))
fixef(tvCL_R= c(, 88.28, ))
fixef(tvKaG = c(, 1.32, ))
fixef(tvKaR = c(, 0.28, ))
fixef(tvKapo20 = c(,27.81,))
fixef(tvKapo5n66= c(,0.33, ))
fixef(tvKapo50= c(,1.86, ))
fixef(tvFpo20= c(, 0.107, ))
```

```
fixef(tvFpo5= c(, 0.177, ))
fixef(tvFpo66 = c(,0.074, ))
fixef(tvFpo50= c(, 0.247, ))
fixef(tvKaip= c(,7.59, ))
fixef(tvFip1= c(, 0.074, ))
fixef(tvFip2 = c(,0.036, ))
fixef(tvV0   = c(,87.4785, ))
fixef(tvbt = c(,3.41596E-07, ))
fixef(tvbg = c(,-1.39266E-06, ))
fixef(tvbr = c(,1.24096E-06, ))
fixef(tvkg1 = c(,1.40167, ))
fixef(tvkg0 = c(,0.00133024, ))
fixef(tvkk = c(, 0.799276, ))
ranef(diag( nkg0, nkg1, nV0, nkk) = c( 0.1,0.1,0.1,0.1))
}
```

Phoenix NLME Model codes for pharmacodynamic model in mice bearing GBM 43 xenografts

Base tumor growth inhibition model

```
test(){
deriv(A1 = - (Cl_T  * C) + (Aapo * Kapo) + (Aaip * Kaip))
urinecpt(A0 = (Cl_T  * C))
deriv(Aapo = - (Aapo * Kapo))
deriv(Aaip = - (Aaip * Kaip))
deriv(A2 = - (CL_G * C1) + (AaG * KaG))
urinecpt(A3 = (CL_G * C1))
deriv(AaG = - (AaG * KaG))
deriv(A4 = - (CL_R * C1) + (AaR * KaR))
urinecpt(A5 = (CL_R * C1))
deriv(AaR = - (AaR * KaR))
C = A1 / Vt
C1 = A2 / Vg
```

```
C2 = A4/ Vr
error(CEpsT = 3.4030149758783)
observe(CObsT = C*(1 + CEpsT))
error(CEpsG = 0.289781285242548)
observe(CObsG = C1*(1 + CEpsG))
dosepoint(A1, idosevar = A1Dose, infdosevar = A1InfDose, infratevar = A1InfRate)
dosepoint(AaG, idosevar = AaGDose, infdosevar = AaGInfDose, infratevar = AaGInfRate)
dosepoint(Aapo, bioavail = (Fpo), idosevar = AapoDose, infdosevar = AapoInfDose, infratevar =
AapoInfRate)
dosepoint(Aaip, bioavail = (Fip), idosevar = AaipDose, infdosevar = AaipInfDose, infratevar =
AaipInfRate)
psi = 20
TV= V1+V2+V3
Gwth = (1+ (kg0*TV/kg1)^psi)^(1/psi)
deriv(V1 = (kg0*V1/Gwth) - (bt*C )*V1)
deriv(V2 =   (bt*C )*V1 - kk*V2)
deriv(V3 = kk*V2-kk*V3)
sequence {V1 = V0}
error(VEps = 0.470416762648155)
observe(Vobs = TV*(1 + VEps))
fcovariate(dose())
fcovariate(flag1())
fcovariate(flag2())
fcovariate(flag23())
fcovariate(flag3())
fcovariate(flag4())
fcovariate(flag5())
fcovariate(flag6())
Kapo = Kapo20*flag1 + Kapo5n66*flag23 + Kapo50*flag4
Fpo =  Fpo20* flag1 + Fpo5*flag2 + Fpo66*flag3 + Fpo50*flag4
Fip = Fip1*flag5 + Fip2*flag6
```

```
stparm(Vt = tvVt )
stparm(Vg = tvVg )
stparm(Vr = tvVr )
stparm(Cl_T  = tvCl_T )
stparm(CL_G = tvCL_G )
stparm(CL_R = tvCL_R )
stparm(KaG = tvKaG )
stparm(KaR = tvKaR )
stparm(Kapo20 = tvKapo20)
stparm(Kapo5n66 = tvKapo5n66 )
stparm(Kapo50 = tvKapo50 )
stparm(Fpo20 = tvFpo20)
stparm(Fpo5 = tvFpo5)
stparm(Fpo66 = tvFpo66)
stparm(Fpo50 = tvFpo50)
stparm(Kaip = tvKaip )
stparm(Fip1 = tvFip1 )
stparm(Fip2 = tvFip2 )
stparm(V0 = tvV0 * exp(nV0))
stparm(bt = tvbt )
stparm(kg1 = tvkg1* exp(nkg1))
stparm(kg0 = tvkg0* exp(nkg0))
stparm(kk = tvkk * exp(nkk))
fixef(tvVt = c(, 3.70112, ))
fixef(tvVg= c(, 1094.03, ))
fixef(tvVr (freeze)  = c(, 17.53, ))
fixef(tvCl_T= c(, 3.94462, ))
fixef(tvCL_G= c(, 386.681, ))
fixef(tvCL_R(freeze) = c(, 4.5, ))
fixef(tvKaR (freeze)= c(, 0.9379, ))
fixef(tvKaG = c(, 1.33688, ))
```

```
fixef(tvKapo20 = c(,27.8147,))
fixef(tvKapo5n66 = c(,0.33544, ))
fixef(tvKapo50 = c(,1.85859, ))
fixef(tvFpo20 = c(, 0.107511, ))
fixef(tvFpo5 = c(, 0.17745, ))
fixef(tvFpo66 = c(,0.0741511, ))
fixef(tvFpo50 = c(, 0.247541, ))
fixef(tvKaip = c(,7.58814, ))
fixef(tvFip1 = c(, 0.0746719, ))
fixef(tvFip2 = c(,0.0364618, ))
fixef(tvV0  = c(,28.141410043245, ))
fixef(tvbt = c(,1.25120725664293E-06, ))
fixef(tvkg1 = c(,6.73586358205552, ))
fixef(tvkg0 = c(,0.00619399739386244, ))
fixef(tvkk = c(, 0.0284068780460615, ))
ranef(diag( nV0, nkg1, nkg0, nkk ) = c( 0.1,0.1,0.1,0.1))
}
```

Resistance integrated tumor growth inhibition model

```
test(){
deriv(A1 = - (Cl_T  * C) + (Aapo * Kapo) + (Aaip * Kaip))
urinecpt(A0 = (Cl_T  * C))
deriv(Aapo = - (Aapo * Kapo))
deriv(Aaip = - (Aaip * Kaip))
deriv(A2 = - (CL_G * C1) + (AaG * KaG))
urinecpt(A3 = (CL_G * C1))
deriv(AaG = - (AaG * KaG))
deriv(A4 = - (CL_R * C2) + (AaR * KaR))
urinecpt(A5 = (CL_R * C2))
deriv(AaR = - (AaR * KaR))
C = A1 / Vt
C1 = A2 / Vg
```

```
C2 = A4/ Vr
error(CEpsT = 3.40333153280212)
observe(CObsT = C*(1 + CEpsT))
error(CEpsG = 0.289804440411466)
observe(CObsG = C1*(1 + CEpsG))
dosepoint(A1, idosevar = A1Dose, infdosevar = A1InfDose, infratevar = A1InfRate)
dosepoint(AaG, idosevar = AaGDose, infdosevar = AaGInfDose, infratevar = AaGInfRate)
dosepoint(Aapo, bioavail = (Fpo), idosevar = AapoDose, infdosevar = AapoInfDose, infratevar =
AapoInfRate)
dosepoint(Aaip, bioavail = (Fip), idosevar = AaipDose, infdosevar = AaipInfDose, infratevar =
AaipInfRate)
psi = 20
TV= V1+V2+V3+R
Gwth = (1+ ((kg0/kg1)*TV)^psi)^(1/psi)
Gwthres = (1+ ((kgr0/kgr1)*TV)^psi)^(1/psi)
deriv(V1 = (kg0*V1/Gwth) - bt*C*V1)
deriv(V2 =   (bt*C*V1) - kk*V2)
deriv(V3 = kk*V2-kk*V3-kstor*V3)
deriv(R = (kgr0*R/Gwthres)+ kstor*V3)
sequence {V1 = V0}
error(VEps = 0.463461929262836)
observe(Vobs = TV*(1 + VEps))
fcovariate(dose())
fcovariate(flag1())
fcovariate(flag2())
fcovariate(flag23())
fcovariate(flag3())
fcovariate(flag4())
fcovariate(flag5())
fcovariate(flag6())
Kapo = Kapo20*flag1 + Kapo5n66*flag23 + Kapo50*flag4
```

```
Fpo =  Fpo20* flag1 + Fpo5*flag2 + Fpo66*flag3 + Fpo50*flag4
Fip = Fip1*flag5 + Fip2*flag6
stparm(Vt = tvVt )
stparm(Vg = tvVg )
stparm(Vr = tvVr )
stparm(Cl_T  = tvCl_T )
stparm(CL_G = tvCL_G )
stparm(CL_R = tvCL_R )
stparm(KaG = tvKaG )
stparm(KaR = tvKaR )
stparm(Kapo20 = tvKapo20)
stparm(Kapo5n66 = tvKapo5n66 )
stparm(Kapo50 = tvKapo50 )
stparm(Fpo20 = tvFpo20)
stparm(Fpo5 = tvFpo5)
stparm(Fpo66 = tvFpo66)
stparm(Fpo50 = tvFpo50)
stparm(Kaip = tvKaip )
stparm(Fip1 = tvFip1 )
stparm(Fip2 = tvFip2 )
stparm(V0 = tvV0 * exp(nV0))
stparm(bt = tvbt )
stparm(kg1 = tvkg1* exp(nkg1))
stparm(kg0 = tvkg0* exp(nkg0))
stparm(kk = tvkk * exp(nkk))
stparm(kstor = tvkstor * exp(nkstor))
stparm(kgr0 = tvkgr0 * exp(nkgr0))
stparm(kgr1 = tvkgr1 * exp(nkgr1))
fixef(tvVt  = c(, 3.70112, ))
fixef(tvVg = c(, 1094.03, ))
fixef(tvVr (freeze)  = c(, 17.53, ))
```

```
fixef(tvCl_T  = c(, 3.94462, ))
fixef(tvCL_G = c(, 386.681, ))
fixef(tvCL_R(freeze) = c(, 4.5, ))
fixef(tvKaR (freeze)= c(, 0.9379, ))
fixef(tvKaG = c(, 1.33688, ))
fixef(tvKapo20  = c(,27.8147,))
fixef(tvKapo5n66 = c(,0.33544, ))
fixef(tvKapo50  = c(,1.85859, ))
fixef(tvFpo20  = c(, 0.107511, ))
fixef(tvFpo5  = c(, 0.17745, ))
fixef(tvFpo66 = c(,0.0741511, ))
fixef(tvFpo50 = c(, 0.247541, ))
fixef(tvKaip = c(,7.58814, ))
fixef(tvFip1 = c(, 0.0746719, ))
fixef(tvFip2  = c(,0.0364618, ))
fixef(tvV0   = c(,35, ))
fixef(tvbt = c(,1.53169942696361E-06, ))
fixef(tvkg1  = c(,7.33442766137454, ))
fixef(tvkgr1 = c(,2.71348405057203, ))
fixef(tvkg0  = c(,0.0064036936583605, ))
fixef(tvkgr0 = c(,0.00246299328089874, ))
fixef(tvkk = c(, 0.0381723384346736, ))
fixef(tvkstor = c(,0.00729794476879764, ))
ranef(diag( nkg0, nkgr0, nkg1, nkgr1, nV0, nkk, nkstor ) = c( 0.1,0.1,0.1,0.1,0.1,0.1,0.1))
}
```